

https://dspace.org/

Determination of the pressures within an injector: Experimentation and model validation.

Sprich, Thomas Karl.

2011-10-12
http://hdl.handle.net/10539/10545

Downloaded from a DSpace repository. https://dspace.org/

DETERMINATION OF THE PRESSURES WITHIN AN INJECTOR - EXPERIMENTATION AND MODEL VALIDATION

Thomas Karl Sprich

A dissertation submitted to the Faulty of Engineering and the Built Environment, University of the Witwatersrand, Johannesburg, in fulfillment of the requirements for the degree of Master of Science in Engineering.

Johannesburg, 2011

Declaration

I declare that this dissertation is my own unaided work. It is being submitted for the Degree of Master of Science in Engineering in the University of the Witwatersrand, Johannesburg. It has not been submitted before for any degree or examination in any other University.

_____

(Signature of Candidate)

On this _____day of_____2011

Acknowledgements

I would like to thank my supervisor Prof D Cipolat for the opportunity to part take in this project and the time, guidance and patience that he had for me and this project, without which this work would not be possible.

Thank you to Prof Moss for his assistance creating the model that was used in this work.

Thank you to my family and friends whose patience and support throughout this project has been invaluable.

The financial assistance of the South African National Energy Research Institute (SANERI) towards this research is hereby acknowledged. Opinions expressed and conclusions arrived at, are those of the author and are not necessarily to be attributed to SANERI.

Abstract

Amid concerns of global warming, it has become necessary to reduce the emissions produced by engines. One method of achieving this is by controlling the air/fuel mixture formed by the spray of the injector within the combustion chamber. In comparing previous experimental results and the equations which describe the spray structure disagreement was found, which is expected to be caused by having insufficient information of the injection pressure; a required input of the equation. The aim of this research is to predict this injection pressure by modelling a mechanical injector, and testing and modelling a common rail injector. The mechanical injector simulations show that the injection pressure is lower than the line and opening pressure and is dependent on the number of discharge orifices, throttling condition and opening pressure of the injector. Consequently, the line and opening pressures are not sufficient approximations of the injection pressure and must not be used to predict spray properties. The simulations showed the injected flow rate is higher for a three hole injector at high engine loads and higher opening pressures, resulting in a more atomised and penetrating spray. The common rail injector model agrees with the experimental results and both show the injection pressure being about 90% of the rail pressure. The rail pressure is therefore suitable for use in the penetration equations. A sensitivity analysis of the common rail model showed that it could be used to diagnose injector problems because each varied parameter changed the injected flow rate differently, allowing the source of the problem to be easily identified.

Contents

Declaration i

Acknowledgements ii

Abstract iii

Contents iv

List of Figures xi

List of Tables xviii

Nomenclature xx

1 Introduction 1

1.1 Background 1

1.1.1 Vehicle design 2

1.1.2 Fuels 3

1.1.3 Engine improvements 3

1.2 Project scope 4

1.3 Project outline 4

2 Literature review **6**

2.1 Spray characteristics 6

2.1.1 Atomisation 6

2.1.2 Spray penetration 10

2.1.3 Drop dispersion 13

2.2 Parameters that affect spray 14

2.2.1 The effect of fuel properties 15

2.2.2 The effect of the chamber gas 15

2.2.3 The effect of injector conditions 16

2.3 Mathematical modelling of injectors 19

2.3.1 Investigated model components 19

2.3.2 Volumetric fuel property variation 23

3 Motivation and objectives **26**

3.1 Motivation 26

3.1.1 Set up and results 26

3.1.2 Processing of the results 28

3.1.3 Penetration results and discussion 30

3.2 Objectives 32

4 The mechanical injector model **34**

4.1 Model construction 34

4.1.1 Scicos 35

4.1.2 The injector system 35

4.1.3 Assumptions 37

4.1.4 Governing equations 38

4.1.5 Boundary conditions 44

4.2 Model inputs 44

4.2.1 Inlet flow rate 44

4.2.2 The line and chamber pressure 48

4.2.3 Volumes and areas 49

4.2.4 Bulk modulus and density 50

4.2.5 The spring constant 50

4.2.6 The selection of empirical constants 51

4.2.7 The initial opening pressure 52

4.3 Proposed simulations 52

5 The mechanical injector simulations **54**

5.1 The effect of reverse flow 54

5.2 Pressure 55

5.3 Flow rate 61

5.3.1 Total flow rate 62

5.3.2 Flow rate through a single orifice 63

5.3.3 Injected and supplied flow rate comparison 65

5.4 Needle lift 65

6 The common rail model **70**

6.1 Injector behaviour 70

6.1.1 Common rail system 70

6.1.2 Assumptions 74

6.2 Injector geometry 75

6.3 Scicos model 77

6.3.1 Scicos equations 77

6.4 Conversion to C++ 81

6.4.1 Numerical integration method 81

6.4.2 Program flow 87

6.4.3 C++ common rail injector equations 88

6.4.4 Akribis 90

6.4.5 Bulk modulus and density 92

6.4.6 Discharge coefficients 93

7 The common rail equipment **94**

7.1 The injection Test Stand 94

7.1.1 Injection system 94

7.1.2 Test fuel 97

7.1.3 Pressure measurement 97

7.1.4 Fuel delivery measurement 97

7.2 Uncertainty analysis 99

7.3 Methodology 99

7.3.1 Precautions 99

7.3.2 Procedure 101

7.3.3 Capturing data 103

7.3.4 Proposed tests 103

8 Common rail experimental results **105**

8.1 Data averaging 105

8.2 Delivery 106

8.3 Rail pressure 107

8.4 Flow rate 110

8.5 Pressure and flow rate 113

8.6 Orifice pressure calculation 116

9 Common rail model validation **119**

9.1 Discharge coefficients 120

9.2 Sensitivity analysis 126

9.3 Scilab vs. C++ model 138

9.4 Injector pressures 139

9.5 Test pressure input 145

9.6 Needle lift 147

10 Conclusion and Recommendations **149**

10.1 Conclusion 149

10.1.1 The mechanical model 149

10.1.2 The common rail experimental tests 150

10.1.3 The common rail model 151

10.2 Recommendations 152

10.2.1 The mechanical model 152

10.2.2 The common rail experimental tests 153

10.2.3 The common rail model 154

References **156**

A Image processing code **160**

A.1 Main program 160

A.2 Additional functions 164

A.2.1 Spray_area 164

A.2.2 Rotated 165

A.2.3 GetLine 165

A.2.4 Cut 165

A.2.5 Image_FixA 166

A.2.6 Rem_Noise 166

A.2.7 Find_Breakup 167

B Area change derivation **168**

C Injector models **171**

C.1 Mechanical model 171

C.2 Common rail model 173

C.3 Common rail model program source code 176

D Testscope output file sorting program **207**

E Sample output files **212**

F Discharge coefficient approximation **217**

F.1 Analysis 217

List of Figures

2.1 The flow regimes for nozzles of different l/D_o ratios. 18

2.2 The different components of the mechanical injection system used in the pressure release valve model. 20

2.3 Bulk modulus for ISO 4113 and diesel versus pressure. 24

2.4 Density for ISO 4113 and diesel versus pressure. 25

3.1 Diesel spray images injected at 15 MPa opening pressure for a three orifice injector. 27

3.2 A three column by one row matrix. 28

3.3 Images at 10 MPa opening pressure for a three orifice injector with diesel fuel. 30

3.4 Figure showing the injection axis of the spray along which the penetration is measured. 30

3.5 The intensity versus pixels for spray penetration for a three orifice, 10 MPa injection. 31

3.6 Penetration versus time from image processing for a three orifice diesel injector. 31

3.7 Penetration versus time for 10 MPa opening pressure, three orifice diesel injector and the predicted penetration using the equations by Hiroyasu and Dent. 32

4.1 Simplified system circuit for the injector 35

4.2 The mechanical injector 38

4.3 Two volumes separated by a constriction. 39

4.4 A schematic showing a volume changing size due to the motion of one (or more) walls. 40

4.5 Free body diagram of the all forces acting on the needle. 43

4.6 Line pressure versus time for engine tests at low and medium load. . . . 45

4.7 Flow rate from the line to the injector versus time for the engine tests simulations. 46

4.8 The flow rate provided by the pump into the line versus time as calculated from the engine simulation. 46

4.9 Flow rate versus time provided the pump used in the simulations for both low and medium load. 48

4.10 Cross-section indicating the different radii upon which pressure acts. . . 50

5.1 Line pressure versus time for the three orifice injector simulations at low engine load conditions. 56

5.2 Line pressure versus time for the three orifice injector simulations at medium engine load conditions. 56

5.3 Line pressure versus time for the four orifice injector simulations at low engine load conditions. 57

5.4 Line pressure versus time for the four orifice injector simulations at medium engine load conditions. 57

5.5 Line and sac pressure for three orifice injector, low engine load and 10 MPa opening pressure. 59

5.6 Line and sac pressure for three orifice injector, low engine load and 25 MPa opening pressure. 59

5.7 Line and sac pressure for three orifice, medium engine load and 10 MPa opening pressure. 60

5.8 Line and sac pressure for three orifice, medium engine load and 25 MPa opening pressure. 60

5.9 The average sac pressure versus the opening pressure for different engine loads and number of nozzle orifices. 61

5.10 Comparison of the flow rate versus time for the three orifice injector at low engine load for different opening pressures. 62

5.11 Comparison of the flow rate versus time for the three orifice injector at medium engine load for different opening pressures. 63

5.12 Comparison of the flow rate versus time for the four orifice injector at low engine load for different opening pressures. 63

5.13 Comparison of the flow rate versus time for the four orifice injector at medium engine load for different opening pressures. 64

5.14 Comparison of the flow rate through a single orifice of a three and four orifice injector at low and medium engine loading conditions for an injector opening pressure of 10 MPa. 64

5.15 Comparison of the flow rate through a single orifice of a three and four orifice injector at low and medium engine loading conditions for an injector opening pressure of 25 MPa. 65

5.16 Line and sac pressure with the needle lift versus time for a three orifice injector, low engine load and 10 MPa opening pressure. 66

5.17 Line and sac pressure with the needle lift versus time for a three orifice injector, low engine load and 25 MPa opening pressure. 66

5.18 Line and sac pressure with the needle lift versus time for three orifice, medium engine load and 10 MPa opening pressure. 67

5.19 Line and sac pressure with the needle lift versus time for a three orifice injector, medium engine load and 25 MPa opening pressure. 67

5.20 Time derivative of line and sac pressure versus time for a three orifice injector under medium engine load conditions for a 25 MPa opening pressure. 68

6.1 Electronically actuated common rail injector showing the different components and internal volumes that are needed for the model. 71

6.2 Photograph of the sectioned body of the injector showing the passageway of the fuel to the nozzle. 76

6.3 Photograph of the control volume component showing the control volume, the bore for the plunger, and the feed and bleed orifices 77

6.4 Photograph of the nozzle of the injector showing the fuel passageway and an internal fuel volume. 78

6.5 Photograph of the injector needle showing the shoulders and the needle tip. 78

6.6 Euler's approximation of numerical integration. 83

6.7 The slope at the beginning and end of Heun's approximation. 84

6.8 The flow of the program for the C++ solution. 87

6.9 Akribis schematic showing the piston, chamber and nitrogen volume. . 91

7.1 Photograph showing the injector, rail, Akribis and fuel lines for the test stand. 95

7.2 The common rail test stand system circuit. 96

8.1 Comparison between the average and individual values for volume versus time for the injection events. 106

8.2 Injected volume versus injection duration. 106

8.3 Rail pressure versus time for various injection durations. 108

8.4 A schematic of rail pressure versus time illustrating the pressure features that are visible in the pressure profiles. 109

8.5 Flow rate versus time for 500 μs to 900 μs injection durations. 111

8.6 Flow rate versus time for 500 μs to 900 μs injection durations through one of the six injector orifices. 112

8.7 Rail pressure and flow rate versus time for the 500 μs injection. 114

8.8 Rail pressure and flow rate versus time for a 2000 μs injection. 115

8.9 Calculated pressure just before the discharge orifice versus time for a 500 μs injection event. 117

9.1 Flow rate versus time for experimental and simulated results. 120

9.2 Values of the bleed orifice discharge coefficient $c_{d,b}$, versus the injection duration and the best fit equation through the data. 121

9.3 Values of the feed orifice discharge coefficient $c_{d,f}$, versus the injection duration and the best fit equation through the data. 122

9.4 Simulated and experimental flow rate versus time for a 500 μs injection with varying discharge coefficients. 122

9.5 Delivered volume change versus parameter variation for the 500 μs injection. 126

9.6 The schematic of the flow rate profile versus time from the simulations showing the opening and closing time definitions. 127

9.7 Flow rate versus time for the sensitivity analysis performed on $c_{d,b}$ for a 500μs injection. 128

9.8 Flow rate versus time for the sensitivity analysis performed on $c_{d,f}$ for a 500μs injection. 129

9.9 Flow rate versus time for the sensitivity analysis performed on the overall discharge coefficient, c_d for a 500μs injection. 130

9.10 The pressure versus time for a 500 μs injection for the rail, line and volume 1 and volume 2. 132

9.11 Flow rate versus time for the sensitivity analysis on the needle lift limit for a 500μs injection. 135

9.12 Percentage variation in volume and mass delivered for the sensitivity analysis performed on density for a 500μs injection. 136

9.13 Volumetric flow rate versus time for the sensitivity analysis performed on density for a 500μs injection. 137

9.14 Flow rate versus time for Scilab, C++ and the experimental results. . . . 138

9.15 Electronically actuated common rail injector showing the different components and internal volumes that are needed for the model. 139

9.16 Pressure versus time for a 500 μs injection for the rail, line, volume 1 and volume 2. 140

9.17 The pressure versus time for a 500 μs injection for the sac and control volumes. 140

9.18 A schematic of the control volume pressure versus time. 141

9.19 Sac pressure versus time for a 500 μs injection. 144

9.20 Pressure versus time for a 500 μs injection for the sac and control volumes using the experimental rail pressure as the input pressure. . . . 146

9.21 Pressure versus time for a 500 μs injection for the rail, line and volume 1 and volume 2 using the experimental rail pressure as the input pressure. 146

9.22 Flow rate versus time for a 500 μs injection showing measured results and simulated results for both constant rail pressure and measured rail pressure inputs. 147

9.23 Needle lift versus time for the 500 μs injection. 147

B.1 Schematic used for calculating the change of area caused by the needle lifting of the injector seat 169

C.1 The Scilab model 172

F.1 Discharge coefficient versus Reynolds number for flow through an orifice in a pipe. 218

List of Tables

1.1 Euro emission standards schedule for compression ignition passenger vehicles. 2

4.1 List of control volumes for the injector tested. 49

4.2 List of radii and corresponding areas for the injector tested. 50

4.3 Injector opening pressure and corresponding spring force. 52

7.1 Measured delivery and pressure uncertainty. 99

9.1 Comparison of the features of the C++ and Scilab models. 138

C.1 Common rail injector model geometric inputs. 174

C.2 Additional common rail injector model inputs for the Scilab model and the C++ program. 174

C.3 Akribis related inputs used only in the C++ program. 175

E.1 A sample of the data from the output file from the Scilab program. . . . 213

E.2 A sample of the data from the output file from the C++ program for the common rail model. Only the first seven columns have been shown. . . 214

E.3 A sample of the data from the output file from the C++ program for the common rail model. The next seven columns have been shown. 215

E.4 A sample of the data from the output file from the C++ program for the common rail model. The last seven columns have been shown. 216

Nomenclature

Abreviations

CFD	Computational fluid dynamics
DME	Dimethyl ether
EEA	European Environment Agency
EGR	Exhaust gas recirculation
EPA	Environmental Protection Agency
KH	Kelvin-Helmholtz
LVDT	Linear variable differential transformer
ODE	Ordinary differential equation
PM	Particulate matter
RK	Runge-Kutta (normally 4^{th} order)
RT	Rayleigh-Taylor
SMD	Sauter mean diameter
SOI	Start of injection
VCO	Valve covered orifice

Greek symbols

α	The ratio of volume fraction of spray in the air	-
β	Bulk modulus	Pa

ρ	Density	kg/m^3
σ	Surface tension	mN/m
υ	Kinematic viscosity	m^2/s
θ	Cone half angle	degrees

Variables

A	Area	m^2
a	Flow constriction area	m^2
c	Damping constant	m/s
c	Speed of sound in a fluid	m/s
c_d	Discharge coefficient	-
c_{df}/c_{db}	Discharge coefficient for the feed/bleed orifice	-
D	diameter	m
D_S	The Sauter mean diameter	m
F	Force	N
h	Interval size	-
k	Runge Kutta integration constant	-
k	Spring constant	N/m
l	Length	m
m	Mass	kg
n	Number of injector nozzle orifices	-
P	Pressure	Pa
Q	Volumetric flow rate	m^3/s
Re	Reynolds number	

r	Radius	m
S	Spray tip penetration	m
T	Temperature	K
t	Time	s
V	Velocity	m/s
v	Volume	m^3
We	Weber number	
x	Displacement	m

Subscripts

fic	Associated with the ficticous spray
orig	Associated with the original spray
s	Spray
a	Atomosphere
b	Bleed orifice
break	Point associated with the jet break up time
cv	Control volume
d	Drop
F	Fuel
f	Feed orifice
g	Gas
in	Into a volume
inj	Injection
limit	limit

l	Line
N	Needle
o	Orifice
out	Out of a volume
p	Piston
r	Rail
sac	Sac

Chapter 1

Introduction

New political policies and shifts in consumer thinking that have stimulated research in energy efficiency and emission reduction in engines. Some of the potential solutions that can be used to improve engines are mentioned, but the injection process is ultimately chosen as the topic of this research. The exact scope of this project is discussed before an outline of the project is given.

1.1 Background

Amid fears of global warming, governments and consumers have put pressure on vehicle manufacturers to reduce the emissions. In the United States, the Environmental Protection Agency (EPA) introduced the Tier 1 to Tier 4 emission standards which specify allowable engine emission levels for new non-road diesel engines [1, 2]. Each 'Tier' introduces more stringent allowable emission levels for vehicle producers to adhere to. The Tier 1 standards were introduced in 1994, Tier 2 and Tier 3 in 1998, while Tier 4 will only be phased in 2011. The European Union's European Environment Agency (EEA), has introduced similar legislation called Euro 1 to Euro 6 [3]. An example of the Euro standards for compression ignition engines for passenger vehicles is shown in Table 1.1 [4]. In Table 1.1 it can be seen that all the emissions are being reduced with each new standard. Both the EPA and EEA's standards provide unique schedules and emissions levels for different types of vehicles, as well as the required testing procedures that need to be performed when evaluating the emissions of engines.

Additionally, consumers now demand more environmentally friendly vehicles as they too become more environmentally conscious.

Table 1.1: Euro emission standards schedule for compression ignition passenger vehicles.

Tier	Date	CO	HC	HC+NOx	NOx	PM
Euro 1	1992.07	2.72 (3.16)	-	0.97 (1.13)	-	0.14 (0.18)
Euro 2, IDI	1996.01	1	-	0.7	-	0.08
Euro 2, DI	1996.01	1	-	0.9	-	0.1
Euro 3	2000.01	0.64	-	0.56	0.5	0.05
Euro 4	2005.01	0.5	-	0.3	0.25	0.03
Euro 5	2009.09	0.5	-	0.23	0.18	0.01
Euro 6	2014.09	0.5	-	0.17	0.08	0.01

Besides the obvious greenhouse gases, carbon monoxide and carbon dioxide, other emissions such as NO_x, particulate matter (PM) and unburned hydrocarbons must also be reduced. The American and European standards aim to address all of these emissions. Vehicle manufacturers have many options open to them in order to achieve these new lower emission levels, but it all comes down to changing the vehicle design, fuels and the combustion process.

1.1.1 Vehicle design

Changing the vehicles to reduce emissions can be done in a variety of ways. Firstly, the size and weight of the vehicle can be reduced which will reduce the fuel consumption and thereby, the emissions. Secondly, hybrid vehicles capable of storing and recovering energy also reduce the amount of fossil fuels required and thereby reduce the overall emissions. Caution must be taken when considering purely electric cars that appear attractive due to their apparent zero emission levels, as they require electricity which may still be produced by burning fossil fuels. Thus, the emission problem has not been solved, merely moved away from the vehicle.

1.1.2 Fuels

Different fuels with better combustion properties such as Dimethyl Ether (DME) or biodiesel could aid in reducing emissions [5, 6]. DME has oxygen as part of its chemical make-up [7], which aids in the combustion process, while the production of Biodiesel offsets the carbon emissions produced in the engine by absorbing some carbon while the plant material grows [8]. Interestingly, the first diesel engine demonstrated by Rudolf Diesel used peanut oil and not a petroleum based diesel [6]. However, due to some differences between the properties of diesel and biodiesel used today, some modifications to a diesel engine need to be made before biodiesel can be a suitable alternative fuel [6, 9].

Research is being carried out into converting existing diesel engines so that they are capable of running other more efficient fuels such as DME or biodiesel. The cost and availability of these alternate fuels is however another hindrance to this technology, but this could change if the technology can be proven.

High quality diesel fuels containing less impurities such as sulphur and lead [10] also reduce engine emissions because these impurities are no longer present in the combustion process. Thus, it is necessary that fuel manufacturers produce higher quality fuels and thereby contribute to lowering the emissions of vehicles.

1.1.3 Engine improvements

Initially when the Tier 3 standards were set, it was thought that exhaust gas recirculation (EGR) would provide the primary means of reducing emissions [2]. Since then however, it has been shown the EGR is only a part of the combustion process that needs to be considered in reducing emissions. Technologies such as Caterpillar's ACERT or Volvo's V-ACT systems also use multiple precision injections, air management and after-treatment measures to reduce the emissions of their engines [11, 12].

One aspect of this combustion process is the injection of fuel into the chamber. The emissions are highly dependent on injection because its sets up the air/fuel mixing in the combustion chamber upon which combustion is reliant. The development of

the common rail system has aided in reducing the emissions of newer diesel vehicles by improving the spray structure, the air/fuel mixture in the combustion chamber and quantity of fuel delivered during injection.

1.2 Project scope

This project focuses on studying the injection process of mechanical and common rail injectors. The project developed from attempting to use existing spray penetration equations to predict the spray structure for a mechanical injector, but finding this difficult due to a lack of knowledge of the actual injection pressure. Thus a way of predicting this pressure is required. This is done by modelling a mechanical injector, extending it to model a common rail injector, and testing a common rail injector. From these models and tests, insight into what injection pressure can be used for these equations can be gained.

1.3 Project outline

A literature review is presented where the important characteristics in the spray structure can be identified and related to the injection conditions. The empirical equations for estimating the spray characteristics are presented. A literature review of the different injector models is then carried out. In this, the considerations of different authors as well as the different methods are shown.

It will be shown that when the results of the penetration equations and previous experimental results were compared, disagreement was found. Because the equations are well established and accepted as being reasonably accurate, the only source of error is in their application. Finding the source of this error and rectifying it, motivates the need for modelling the injector and ultimately, the need for this research. With the problems that this research attempts to solve, the objectives can be stated.

The mechanical injector is modelled first, as it is for this type of injector that the differences between the experimental results and the penetration equations were identified. A common rail injection system will be tested and the results will be compared to the

simulated results of a common rail model that will be constructed.

Finally the conclusions from each of these tests can then be presented and recommendations made.

Chapter 2

Literature review

In this chapter, important spray characteristics and how they change according to the varying injection conditions is discussed. These characteristics are important to the combustion process and understanding how they vary is important in improving the combustion in the engine and thereby reducing emissions. Following this, a review of the literature pertaining to the modelling of an injector is presented.

2.1 Spray characteristics

In a direct injection engine, the injector delivers fuel into the combustion chamber in such a way as to mix the fuel with the air in the chamber. This is achieved by injecting the fuel so that it forms a spray when coming into contact with the air. How well the spray has formed is defined by how well the air and fuel are mixed before they combust.

The fuel mixes with the air in three ways when it forms a spray, namely fuel atomisation, dispersion and penetration. None of the mechanisms work in isolation to improve mixing, making it necessary to understand their interactions as well.

2.1.1 Atomisation

When fuel is injected into the combustion chamber, it leaves the nozzle as a stream or jet of fuel due to large driving pressures. Because of this high pressure, the fuel leaves

the nozzle at a high velocity and breaks down into smaller drops. This process is called atomisation. Atomisation improves the air/fuel mixing by increasing the amount of fuel surface area in contact with air. Furthermore, increasing the surface area promotes the rapid evaporation of the fuel which promotes air/fuel mixing through vapour diffusion.

The injected fuel atomises into fine drops which, provided the conditions are correct, can atomise again. This continues until the mechanisms that prevent this atomisation dominate. Initially the drops form as spheres, but gradually they distort and form disks due to the drag forces [13]. As the drop tends to a disk, the drag acting on it increases.

Surface tension of the fuel resists the breakup which needs to be overcome before atomisation will occur. The theoretical minimum amount of energy required for atomisation is the surface tension of the fuel multiplied by the liquid surface area of the drop or jet [13]. This energy is provided by the drag forces acting on the drop as it travels through the air.

During the evolution of the spray, the jet exiting the nozzle must first atomise. The drops that form off the jet are then atomised further. The jet and drop breakup have different atomisation mechanisms and must be described separately.

Jet breakup

When the fuel is traveling through the orifice of the injector, it cannot atomise because the walls suppress any radial force arising due to turbulence in the jet [13]. When the fuel leaves the orifice and the walls no longer support the jet, it is only the fuel's surface tension that maintains its shape. Because the fuel jet is now traveling through air, it experiences drag forces dependent on the relative velocities between the jet and the air. The jet breaks when the drag forces exceed the restoring forces of the surface tension of the fuel [14]. Therefore, higher relative velocities between the jet and the air will cause the jet to break up sooner and the spray to atomise better.

Jet breakup is described by the Plateau instability. It shows that the jet becomes unstable when the perturbation wavelength caused by the drag forces exceeds the circumference of the jet [14, 15]. These wavelengths are dependent on the fuel properties, initial conditions of the jet and the relative velocities.

Drop breakup

Like jet breakup, drop breakup is prevented by the surface tension of the fuel and is caused by drag. For drops, the ratio of these two forces is taken into account in the Weber number, which has been found to be useful for predicting when breakup will occur [16]. The Weber number is constructed as follows [14, 16, 17]:

$$We = \rho_g \frac{V^2 r_d}{\sigma} \tag{2.1}$$

where V is the relative velocity between the drop and the surrounding air, r_d is the drop radius, σ is the surface tension of the fuel and ρ_g is the density of the air.

It has been found that the critical value of the Weber number for breakup is about 10, but this reduces when the flow is turbulent [14, 16]. Fuel viscosity acts to delay breakup by damping the magnitude of the disturbances (the effect of fuel properties is discussed more fully in Section 2.2.1).

Two breakup regimes have been identified as being important in diesel sprays. They are bag and stripping breakup [18].

'Bag' breakup occurs when two fluids of different densities approach causing interference at the meeting plane. A surface wave develops, which upon exceeding a critical value causes the drop to become unstable and break down further [14, 15]. The behaviour of the drop is well described by the Rayleigh-Taylor (RT) instability [18]. The Rayleigh-Taylor model is used to describe inviscid flow. In applying this theory to viscous fluids, it is understood that viscosity acts to dampen the destabilising mechanisms [15], causing delayed atomisation. Bag breakup is said to occur when $We > 6$ [18].

'Stripping' breakup is when a region of interference occurs where the heavy fluid is 'stripped' away from the bulk of the fluid [15]. This drop breakup regime is well described by the Kelvin-Helmholtz (KH) instability. A property of Kelvin-Helmholtz instability is that instability occurs no matter how small the difference in fluid relative motions may be. The surface tension of the fluids acts to dampen the Kelvin-Helmholtz

instability. Stripping breakup is said to occur when

$$Z = \frac{We}{\sqrt{Re}} > 0.5 \tag{2.2}$$

which represents the internal viscosity to the interfacial surface tension forces [13]. Re is the Reynolds number.

Although this knowledge of atomisation looks promising, its application in predicting atomisation of a diesel spray is difficult. Any spray consists of many thousands of drops that are all atomising, colliding, bouncing or joining. Additionally, it is seen above that breakup is highly dependent on the relative velocities between the drops and the air. Each drop however, is passing energy to the air, changing these relative velocities. These velocity flow fields are difficult to measure non-intrusively and any models that attempt to predict this and the resulting atomisation must make gross simplifications in order to obtain a solution. The most important factor to understand about atomisation is that it is improved by very large drop and jet velocities or any other external factors that may cause destabilisation of the fuel.

Measuring atomisation

The size of drops throughout the spray indicates the systems efficacy to atomise the spray. Drop sizes vary within a spray from about 5 μm to about 200 μm [17].

Drop sizes are estimated from spray photographs by measuring the drop diameter and approximating the drop as sphere. Clearly this is impractical when analysing many photographs as the amount of required measurements would be enormous. One approach is to estimate the drop size distribution statistically. In industrial sprays, the distribution shape is defined about the mean drop size with an exponential decrease for other drop sizes [16].

Another method of describing the drop size distribution in the spray is to define a fictitious spray of equal volume that has the same total drop surface area made up entirely of drops of equal diameter [10]. This is called the Sauter Mean Diameter (SMD) [10, 16, 17] and is calculated as follows:

$$D_S = \frac{6v_{orig}}{A_{orig}} = \frac{6v_{fic}}{A_1} \tag{2.3}$$

where v is the spray volume and A is the surface area of the spray. The subscript $orig$ represents the actual spray and fic is the fictitious spray.

Finer or more 'misty' sprays have smaller SMDs. The SMD has been accepted because it takes into account area and volume which are considered important in the combustion process [14].

Methods of calculating the SMD are given by Lichty [19], conversely Giffen and Musaszew [14] state that no satisfactory formula has been presented that allows the mean drop size to be calculated under any injection condition.

Another average diameter that is also used is the mean mass diameter where the average diameter is based on the mass of the drops. This mean diameter is approximately 15-25% larger than the Sauter mean diameter [13].

2.1.2 Spray penetration

Spray penetration is the perpendicular distance that the spray travels from the orifice into the chamber [10, 17]. As with atomisation, penetration facilitates air/fuel mixing. Under-penetration of the fuel causes under-utilisation of the available air while over-penetration will cause spray impingement on the (normally) cooler chamber wall. In both cases air/fuel mixing and evaporation is decreased. The spray penetration needs to be such that as much air as possible is entrained into the spray without impinging on the chamber wall before combustion has occurred.

Attempts at understanding penetration by analysing the breakup of a single drop underestimate the penetration of a spray. This is because momentum is imparted to the air by the leading drops, making the passage of later drops through the air easier, allowing them to travel further [14].

Many empirical equations exist that predict spray penetration. These equations have similarities in their form, providing information about how the spray penetration can be changed. These equations will be discussed in the following sections.

Two stage penetration equation

Hiroyasu provided the following equation for the penetration of a spray, S [10, 20];

$$S = \begin{cases} 0.39\sqrt{\left(\frac{2\Delta P}{\rho_F}\right)}t & t < t_{break} \\ \\ 2.95\left(\frac{\Delta P}{\rho_g}\right)^{1/4}\sqrt{(D_o t)} & t > t_{break} \end{cases} \tag{2.4}$$

where

$$t_{break} = \frac{29\rho_F D_o}{\sqrt{(\rho_g \Delta P)}}. \tag{2.5}$$

In the above equations, ΔP is the difference between the pressure within the injector and the pressure in the combustion chamber, ρ_F is the density of the fuel and ρ_g is the density of the chamber gas. The equation also shows the evolution of the penetration with time, t.

Equation (2.4) shows two stages in the penetration of the spray separated by t_{break}, which is the jet break up time. The jet breakup time is the time required for the jet exiting the nozzle to atomise into a spray.

Two phase model

Another empirical equation was derived by Sazhin et al. [18] for spray far away from the nozzle using a two phase model:

$$S = 1.189\sqrt{\left(\frac{1}{\sqrt{1-\alpha}}\right)\left(\frac{c_d D_o t}{\tan(\theta)}\right)}\left(\frac{\Delta P}{\rho_g}\right)^{1/4} \times \left[1 - \frac{\sqrt{D_o}}{4\sqrt{V_{in}}(1-\alpha)^{1/4}\tilde{\rho_g}^{1/4}\sqrt{\tan(\theta)t}}\right] \tag{2.6}$$

where the velocity $V_{in} = c_d\sqrt{\frac{2\Delta P}{\rho_F}}$ and $\tilde{\rho_g} = \frac{\rho_g}{\rho_F}$. Equation 2.6 takes into account the discharge coefficient, c_d, of the orifice, the cone angle of the spray, θ and the volume

fraction of the spray in the air, α. In this model α is usually $\ll 1$ [18]. In diesel engines $\tilde{\rho_g}$, the ratio of the gas density and liquid density lies typically between 10×10^{-3} and 30×10^{-3} [10]. Sazhin et al. suggest ignoring the second part of Equation (2.6) to yield Equation (2.7):

$$S = 1.189\sqrt{\left(\frac{1}{\sqrt{1-\alpha}}\right)\left(\frac{c_d D_o t}{\tan(\theta)}\right)}\left(\frac{\Delta P}{\rho_g}\right)^{1/4} \tag{2.7}$$

Equation (2.7) is derived using the conservation of momentum and incorporates the gaseous fuel. The model assumes that as the drop distance from the nozzle increases, the relative velocity between the drops and the gas decrease and that the spray cone angle is sufficiently large that turbulent air entrainment can be ignored [18].

Sazhin et al. performed a comparison of their derived equations with two experimental results and found good agreement. Equation (2.6) followed the trend of the data well, but over estimated the penetration distance, whereas Equation (2.7) followed the data accurately.

It can be seen in Equation (2.7) that the cone angle is required. In their evaluation of their model, Sazhin et al. obtained it from experimental results, but it is possible to estimate the cone angle using empirical equations [18]. Suh and Lee [20] showed that the empirical equation by Sazhin et al. does not agree well at the early stages of the spray development. It is suggested that transient conditions in the early stages of the spray formation make measurement of the cone angle difficult which leads to these inaccuracies.

Chamber temperature sensitive penetration

An equation provided by Dent [20] takes into account the effects of pressure on the formation of the spray and used jet-mixing theory [13]:

$$S = 3.36\sqrt{c_d\left(D_o t\right)}\left[\left(\frac{\Delta P}{\rho_g}\right)\left(\frac{294}{T_g}\right)\right]^{1/4} \tag{2.8}$$

where D_o is the diameter of the discharge orifice. This equation also takes into account

the temperature of the chamber gas, T_g. It is found that Equation (2.8) overestimates the penetration for injection pressures greater than 10 MPa.

A comparison between equations (2.4), (2.7) and (2.8) was carried out by Suh and Lee [20] for diesel and DME. All the equations agreed adequately with the experimental results for distances far from the nozzle i.e. at later time intervals.

Empirical equation similarities

Despite the different derivation of the penetration equations, it can be seen that equations (2.4) to (2.8) are dependent on the same injection parameters. For example: the penetration is dependent on the fourth root of the injection pressure. This similarity gives confidence in the accuracy of these models. Penetration is also dependent on density of the fuel and the spray cone angle.

2.1.3 Drop dispersion

Drop dispersion describes how drops are dispersed from the central injection axis. In a well dispersed spray, the drops are evenly distributed throughout a cross-section of a spray volume [10]. Another definition of spray dispersion is the volume of liquid to the volume of air contained within the spray volume [13]. Drop dispersion can be described statistically by the Rosin-Rammler distribution. This distribution will not be presented because it requires the mass fraction and average drop sizes which are very difficult to measure in well atomised diesel sprays. Another property of the spray that is more easily measured is the cone angle. This angle gives an indication of how widely the drops are distributed.

Cone angle

The cone angle is the angle that the spray edge makes with the injection axis. Typically it is measured at a point $60D_o$ downstream of the nozzle exit [13], so that comparison can be made between different injectors. A study by Yu and Bae [21] revealed that measuring the cone angle for DME at $60D_o$ is not appropriate due to the rapid

evaporation of the fuel. In their study, the cone angle was then measured near the nozzle. Consequently, where fuels with significantly different properties are concerned, measuring the cone angle at $60D_o$ may not be reasonable.

A large cone angle means that the spray is dispersing as it travels into the chamber and not only penetrating forward. This means that the overall volume of air encompassed by the fuel is larger which results in a better air/fuel mixture.

An empirical equation which allows the cone angle to be estimated is given by Heywood [10]:

$$\tan(\theta) = \frac{1}{A} 4\pi \sqrt{\left(\frac{\rho_g}{\rho_F}\right)} \frac{\sqrt{3}}{6} \tag{2.9}$$

where ρ_F is the density of the fuel and A is a constant dependent on the model geometry which can be calculated with the following empirical Equation [10]:

$$A = 3.0 + 0.28 \left(\frac{l_o}{D_o}\right). \tag{2.10}$$

Thus, it can be seen that the cone angle θ is dependent on the length and diameter of the orifice, l_o and D_o respectively. This dependence will be explained more fully in Section 2.2.3.

2.2 Parameters that affect spray

The properties that affect the spray structure can be divided into three groups. These are fuel properties, injection properties and the ambient chamber gas properties. In each section that follows, the spray structure will be discussed in terms of the atomisation, penetration and cone angle.

It must be noted that changing some variables that affect the spray structure can alter other variables simultaneously. For example: changing the fuel will vary density, bulk modulus and viscosity. This makes studying a single parameter in isolation difficult, even meaningless, in some cases [14, 22].

2.2.1 The effect of fuel properties

It was discussed above that the minimum theoretical energy required to atomise a jet or drop was determined by the surface tension multiplied by the area. Therefore, an increase in the surface tension of the fuel results in a less atomised spray.

Viscosity of the fuel dampens out the effect of turbulence and any surface oscillations that arise due to aerodynamic forces. Atomisation therefore tends to occur further downstream, by which point the aerodynamic drag has slowed the jet down. The relative velocities are then lower and so jet breakup is delayed and the spray that is formed is not as well atomised [13, 14].

For an increase in both the surface tension and the viscosity, the overall atomisation of the spray is reduced. The larger drops that result can penetrate further due to their larger momentum and consequently a narrower cone angle forms [14]. A denser fuel will also have more momentum, and therefore will penetrate further into the chamber, and a decrease in the cone angle should also be expected.

2.2.2 The effect of the chamber gas

The combustion chamber gas density can be varied in three ways: by increasing the chamber pressure, increasing the chamber temperature and by changing the gas. Inert or incombustible gases such as nitrogen or argon could be used [14], but changing the gas in this way is only useful in research and not in a real engine. The temperature of the gas could be varied, but this often leads to additional evaporation of the fuel. Thus, the most common method of varying the gas density is to increase the chamber pressure. Varying the density in this way also results in only a small change in the viscosity as its variation with pressure is small [14], meaning that the effect of the chamber gas density can be studied in relative isolation of changes in viscosity.

The air density affects the resistance that the drop experiences as it travels through the chamber. Thus, the drop experiences greater drag and atomises better [13]. Specifically, an increase in density improves the fineness of the spray making it more ‘misty’. Smaller drops occur, as they are more easily broken up. Even though the average drop

size of the spray is smaller, the minimum drop size remains unchanged [13].

It is found that the penetration decreases for increasing chamber pressure [14]. Intuitively this makes sense as denser gaseous mediums offer greater resistance to the passage of the spray. Consequently, the drag experienced by the droplets increases, resulting in a more atomised spray with a larger cone angle [13, 14].

2.2.3 The effect of injector conditions

The injector conditions affect the initial conditions of the jet and therefore have a strong influence on the rest of the spray development. The spray evolution is affected by the injection pressure, turbulence and the orifice geometry.

Injection pressure

The injection pressure is the pressure over the nozzle orifice that drives the fuel into the chamber. This pressure affects the initial velocity of the injected fuel. A simple relation derived from the Bernoulli's equation shows that the fluid velocity leaving the nozzle is equal to:

$$v = c_d A \sqrt{\frac{2\Delta P}{\rho}}. \tag{2.11}$$

An increase in the initial velocity will result in a larger pressure difference between the drops and air. The drops will therefore experience greater drag forces and a more atomised spray will develop.

The greater initial velocity also means that the fluid will have more initial momentum, and will consequently be able to penetrate further into the domain. This is confirmed when considering equations (2.4) to (2.8), where it can be seen that the penetration is proportional to the pressure.

Turbulence

The flow regime, be it laminar, transitional or turbulent, is indicated by the Reynolds number [23] given by:

$$Re = \frac{VD_n}{\upsilon}. \tag{2.12}$$

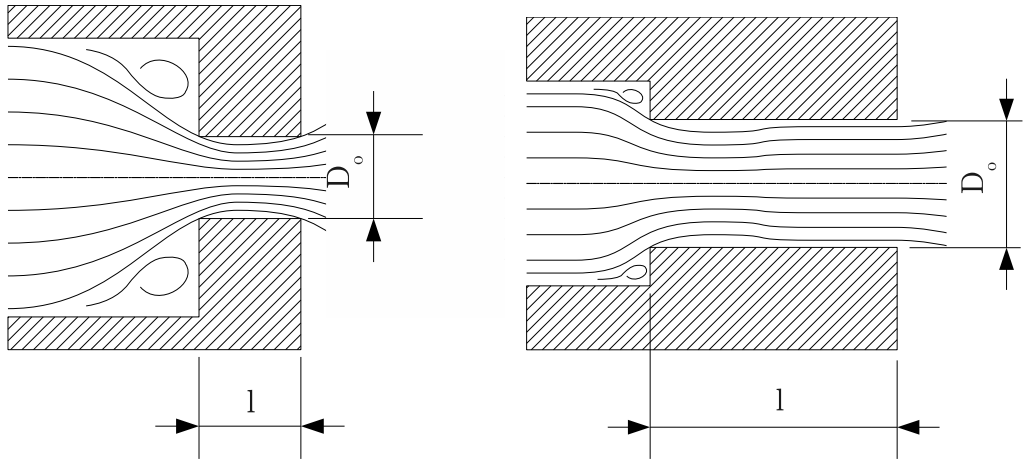
Flow with Reynolds numbers larger than 2500 are considered to be turbulent. Turbulence introduces radial forces into the jet that when unrestrained by a wall, overcome the restoring effects of the surface tension allowing the jet to atomise. The greater the degree of turbulence in the initial jet, the better atomised the overall spray and as a result the cone angle of the spray increases, while the penetration decreases. It can be seen that the Reynolds number is dependent on the flow stream velocity, which is in turn affected by the pressure. Therefore, the injection pressure also plays a role in the turbulence of the jet. A larger source of turbulence is any vibration that the system suffers while operating [14], once again resulting in better atomisation of the fuel.

Orifice geometry

The orifice geometry is described as the ratio of the length of the orifice to its diameter. Figure 2.1 shows a long and short orifice and how they affect the flow stream of the fuel as it passes through.

If the diameter of the orifice is increased, then a more penetrating spray results. This is because the volume delivered increases with D_o^2 whereas the surface area of the jet increases with D_o [14]. Therefore, there is more mass and therefore more momentum in the jet that allows it to penetrate into the chamber. Conversely, a less penetrating spray results from a smaller orifice. In this situation, the atomisation is improved, resulting in more droplets that experience more air resistance and therefore, also have a wider cone angle.

The length of the orifice affects the degree of turbulence of the jet as it leaves the nozzle. This can be seen in Figure 2.1, where a longer orifice has allowed the streamlines of the flow to stabilise and become laminar.



(a) Flow through a short orifice. (b) Flow through a long orifice.

Figure 2.1: The flow regimes for nozzles of different l/D_o ratios.

A longer orifice tends to form a narrower, more penetrating spray for two reasons. The turbulence is decreased by the longer orifice and therefore breakup does not occur as readily. By decreasing this turbulence and therefore the radial force components in the spray, the axial velocity dominates and the spray can penetrate further.

As the fuel is injected, it is constricted as is passes through the orifice. To account for this reduced effective flow area, the discharge coefficient, c_d is introduced [14, 23]. If the discharge coefficient is unity then the flow area is the same as the orifice area, which means the flow is unrestricted. A coefficient less than unity implies that a constriction (or vena contracta) is present, as shown in Figure 2.1.

Short orifices (orifices with low l/D_o ratios) do not allow for laminar flow to form within the orifice [13, 14], resulting in a low discharge coefficient, high turbulence and a less penetrating spray. As the l/D_o ratio increases, so too does the discharge coefficient. The penetration is largest when the discharge coefficient is closest to unity which occurs when the l/D_o ratio is between four and six [10, 14]. Further increases in the l/D_o ratio yield no improvement in the penetration of the spray [10].

Localised disturbances to the discharge coefficient can also be caused by cavitation. Cavitation occurs when the pressure of the fluid drops below the vapour pressure and causes localised pockets of boiling fluid with large pressure differentials [23]. Typically this occurs on any sharp edges, where the flow needs to change abruptly. These bubbles then expand or collapse and aid in the fluid breakup. Although this causes disturbances

in the fuel which aid in forming a well atomised spray, cavitation damages the injector. Cavitation increases the cone angle of the spray by introducing disturbances to the injection event [24].

2.3 Mathematical modelling of injectors

This section is a result of the inability to predict the pressure at the orifice which is discussed more fully in Chapter 3. One method of attempting to predict this pressure is through the modelling of an injector. A literature review of modelling mechanical and common rail injectors is therefore conducted. It is expected that many of the approaches used in the mechanical injector could be used with the common rail injector due to some similarities that exist and so they are discussed here together.

The ability to accurately and rapidly model is advantageous because it provides insight into the system without the need for expensive hardware. A sensitivity analysis to any of its inputs is useful during the research or design stages of an injector [25].

2.3.1 Investigated model components

Both the mechanical and common rail injection systems comprise of many components. The components presented below provide insight into what is important to take into account in the model that will be constructed.

Pressure release valve

Rakopoulos and Hountalas [26] created a model to simulate the behaviour of a mechanical injector. The fluid component of the model was derived from the relationship between the bulk modulus, pressure and volume, while the injector was modelled as a mass spring system. Common rail system models based on similar equations to Rakopoulos and Hountalas have been used by Seykens et al. [27]. The equations need to be adapted to include the additional volume that controls the common rail injector and the constant rail pressure.

A simplified schematic of the mechanical injection system and its components that was modelled by Rakopoulos and Hountalas is shown in Figure 2.2. In this setup, the rotation of the cam causes translation of the piston which results in a pressure wave in the line that opens the injector (a more detailed explanation of the mechanical injection system will be included in Chapter 4).

The model by Rakopoulos and Hountalas took into account pipe flow friction, the cam profile of the pump and the relief valve. Pipe friction acts to dampen out oscillations caused by the spring and needle bounce. Including the cam profile of the pump means that the inlet flow rates delivered to the injector are accurately accounted for.

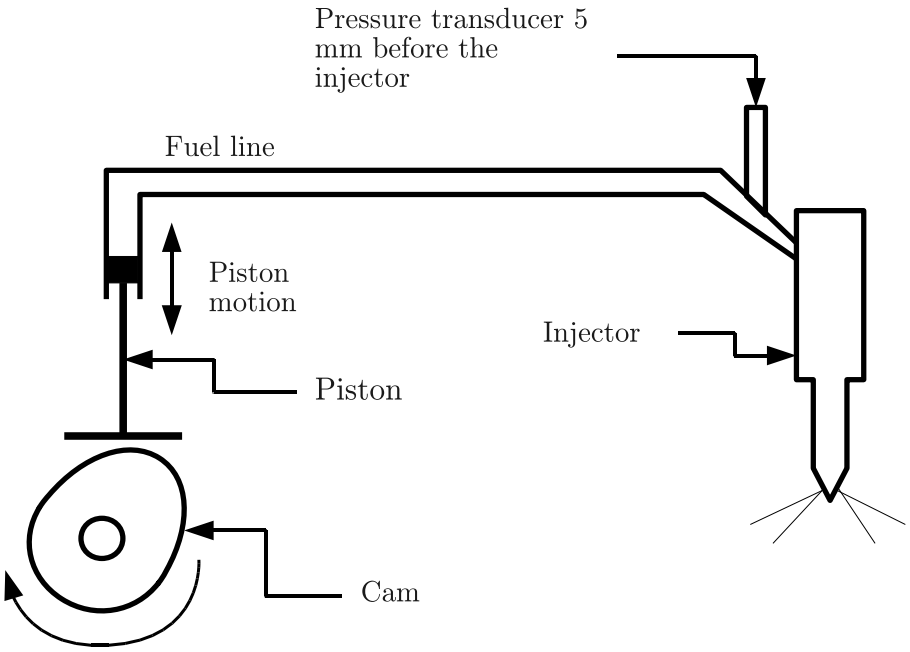


Figure 2.2: The different components of the mechanical injection system used in the pressure release valve model.

The model investigated the injector behaviour with and without a constant pressure valve. The simulation results were compared with experimental results for the pressure measured five millimetres before the injector as shown in Figure 2.2. Measurements were taken at this point to be as close to the injector as possible and would therefore also be close to the injection pressure at the orifice. It was found that the model predicted the experimental results well and the pressure relief valve removed any secondary pressure waves that were in the system before its implementation.

Cavitation

Cavitation occurs when the fuel pressure drops below its vapour pressure and vaporises. Although the injection pressures for both the mechanical and common rail injectors are well above the vapour pressures of the fuel, a localised drop in pressure can occur around sharp geometric changes. As the bubbles move into regions of higher pressure, they collapse resulting in high pressure waves that emanate from that point [23]. The collapsing bubbles can cause pressure waves, resulting in surface damage such a pitting that may alter the injector's behaviour. The bubbles can also restrict the flow through the injector if they form in orifices, thereby lowering the discharge coefficients.

Cavitation is taken into account by determining when it occurs and adjusting the discharge coefficient accordingly. Seykens et al. found large variation in the recommended values of the discharge coefficients for an injector where it is known that cavitation occurs. Seykens et al. evaluated the sensitivity of their model to the coefficient of discharge by varying it between 0.7 and 0.75.

The results for the injected fuel were measured and compared to the simulation results, but the deviation was less than 4% of the measured results. This shows that the sensitivity to variation in the discharge coefficient does not greatly affect the results of the model. Seykens et al. concluded that better knowledge of the discharge coefficient would allow for more accurate modelling of injection.

Lee et al. [28] created a model that took the effects of cavitation into account. It is claimed that attempts at modelling the injector can result in serious errors if cavitation is ignored. This model uses CFD which breaks the system into cells and calculates the injector behaviour by conservation of momentum and energy principles. The cavitation is included by ascertaining whether it would occur, and altering the continuity equation and the states of the cells to fit in with a two phase liquid-vapour model.

Modelling the injector in a CFD package allows cavitation and pressure waves to be taken into account accurately. The drawback of modelling the injector with CFD is that it requires precise knowledge of the injector geometry.

Injection duration

Lee et al. investigated the injector behaviour under high and low loads, which in a common rail model translates into longer and shorter injection durations. The need for this investigation was justified by different needle lifts as short injections may not have enough time to open the injector fully. This suggests that there is a maximum value to which the needle can lift, and it is constrained by the interior geometry of the injector.

A non-rigid needle

The models discussed thus far used a rigid needle assumption, but this was abandoned by Payri et al. [25] and Seykens et al. [27]. It is claimed that a rigid needle quickened the opening response time of the injector in the simulation. Seykens et al. modelled long injection durations over which time the slight increase in injection time makes little difference to the fuel injected. For pilot injections, this time may become significant. The injection flow rate however, was unaffected by taking into account the elasticity of the needle and plunger of the injector.

Volumetric fuel properties

Seykens et al. [27] took into account the fuel density and bulk modulus as it varied with pressure and temperature in the model. The effect in taking into account the variation of these properties was not investigated.

Discharge coefficients

For all models, determining the state of the injector was necessary to determine a discharge coefficient for the injector. An approach to finding the coefficient of discharge of the injector was presented by Payri et al. [25]. The flow rate through a modified injector was measured at steady state conditions where the pressure at the orifice would be equal to the rail pressure. Using Bernoulli's equation in conjunction with the mass flow rate, a discharge coefficient could be calculated.

The assumption of this test is that the discharge coefficient for transient conditions

would be the same as those in steady state. The injector is a highly transient system with enormous momentum changes in both the needle and the fluid and the interaction between these components. Thus, the steady state assumption is invalid.

Maximum needle lift

The model by Lee et al. limits the motion of the needle to 0.2 mm. This implies there is a limitation on the maximum height that the needle can achieve. This is important because it means that an extra boundary condition must be imposed on the model. Excessive needle lift would result in no additional injected flow, thus this boundary condition is justified. The main constriction that the flow experiences is due to the discharge orifice. Extra needle lift would only delay the closing time of the injector due to the extra distance that it would have to travel.

2.3.2 Volumetric fuel property variation

The variation of the bulk modulus and density with pressure for diesel and ISO 4113 test fluid is presented as it will be required in the model that is to be constructed. ISO 4113 is an accepted test fuel for injectors [29] and is the fuel that will be used for tests on the common rail injector. Besides being useful for modelling the injector, the properties of ISO 4113 are presented to show its similarity with diesel.

Bulk modulus

The properties for diesel are provided by Boehman et al. [30] for 0 MPa to 30 MPa and up to 450 MPa by Rodriguez-Anton et al. [31]. The results of Boehman et al. and Rodriguez-Anton et al. coincide well with each other, showing that the bulk modulus is linear with pressure across the entire pressure range. The properties of ISO 4113 are provided by Catania et al. [32]. The bulk modulus with pressure data obtained from the work of Boehman et al., Rodriguez-Anton et al. and Catania et al. for the different fuels has been combined and shown in Figure 2.3. A simple linear regression equation was fitted to the data of the bulk modulus of ISO 4113 against pressure so that the data could be used in the model in equation form. This equation is given as:

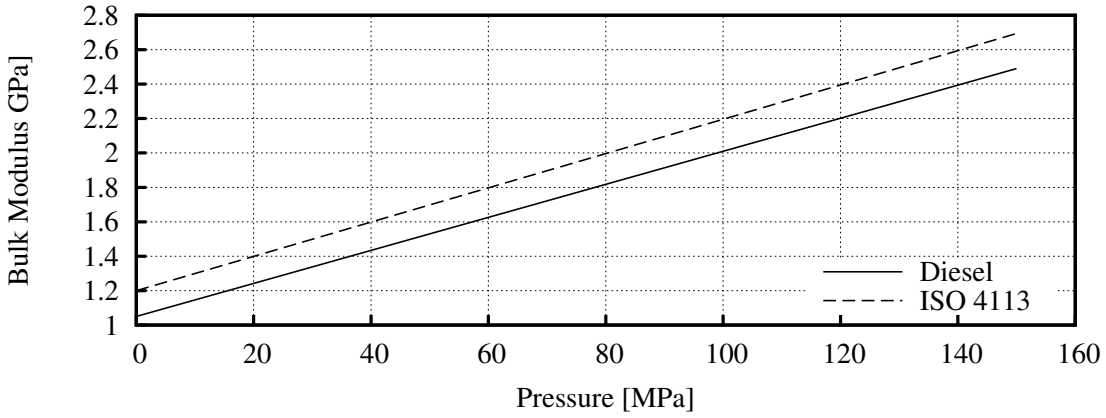


Figure 2.3: Bulk modulus for ISO 4113 and diesel versus pressure.

$$\beta(P) = 11.667P + 1.4 \times 10^9 \tag{2.13}$$

where P and β are pressure in pascals. A comparison of the bulk modulus of diesel and ISO 4113 shows that these properties are indeed similar. The bulk modulus of ISO 4113 is about 15% larger than that of diesel.

This equation is a best fit through the data with no physical meaning of the dependency of the bulk modulus on any other parameters such as temperature. It is only presented here because it will be used when modelling the injector, where the physical significance is not required. Rodriguez-Anton et al. also provided the bulk modulus values at three temperatures, 15°C, 35°C and 55°C, and little variation in the value of the bulk modulus was reported.

Density

The variation of density with pressure is also investigated by Rodriguez-Anton et al. [31] and is expressed as a specific volume, the inverse of density. Figure 2.4 shows the variation of density with pressure for diesel and ISO 4113 extracted from the work Rodriguez-Anton et al. and Catania et al. respectively. It can be seen that as with the bulk modulus, the density of these fuels is similar. The best fit equation for the density of ISO 4113 is given by:

$$\rho = (7.61905e - 19 \times P^2 - 6.78571e - 10 \times P + 1.22167)^{-1} \tag{2.14}$$

where P is in pascals and ρ is in kg/m. Like the bulk modulus, this equation also has no physical meaning, and is used later when modelling the injector.

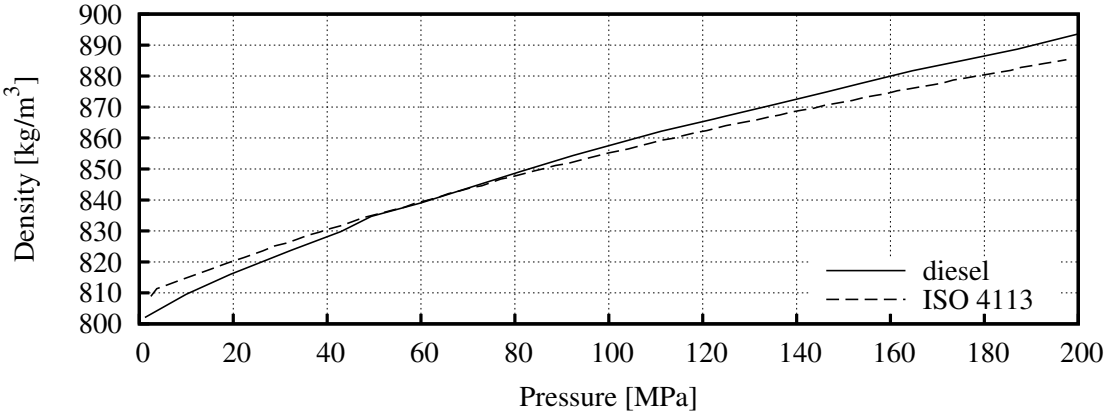


Figure 2.4: Density for ISO 4113 and diesel versus pressure.

Chapter 3

Motivation and objectives

The motivation for this project is presented below and from this the objectives of the research project can be developed.

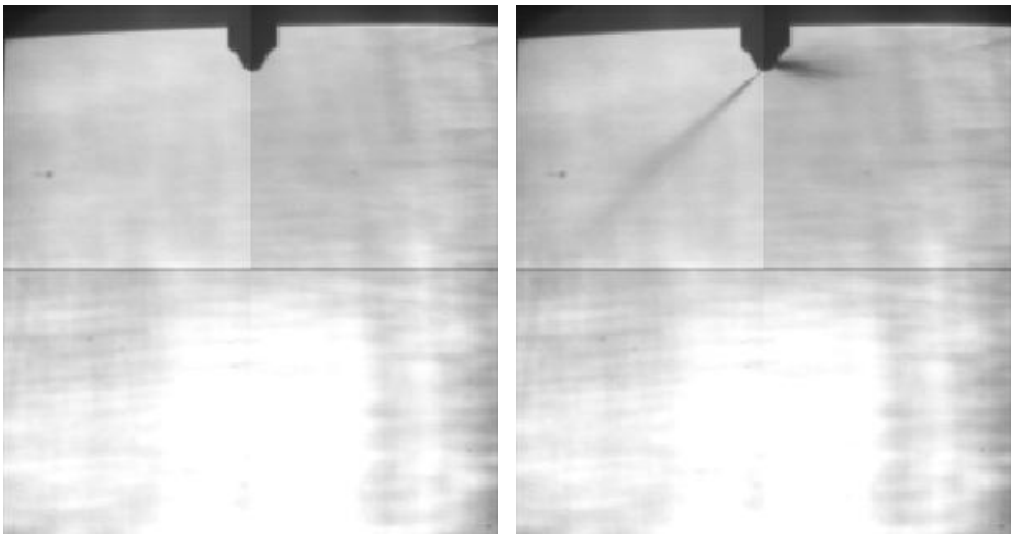
3.1 Motivation

The motivation for the research is based off previous experimental results carried out in the School. The exact details and discussion can be found in the report titled "Study of fuel injection spray patterns" by Rice [33]. A brief summary of the work by Rice is presented here, as well as the additional work that was done as part of this research that made Rice's work more quantitative in nature, and which forms the basis of the motivation of this work.

3.1.1 Set up and results

Tests were done on a mechanical injector setup for both DME and diesel fuels by Rice [33]. The injector was tested at various ranges of opening pressures, from 5 MPa to 22.5 MPa for DME and 10 MPa to 25 MPa for diesel. Tests were performed on three orifice and four orifice injectors.

The results were in the form of digital images, captured using schlieren photography which show the spray evolution with time. An example of the results is shown in



(a) The image captured just prior to injection. (b) The image captured for a fully developed spray.

Figure 3.1: Diesel spray images injected at 15 MPa opening pressure for a three orifice injector.

Figure 3.1 for a three orifice diesel injection with an injector opening pressure of 15 MPa. The images have a resolution of 320×300 pixels that translates into a resolution of 0.3 mm per pixel. The camera captures images at 1000 frames per second. Due to the injection angle and the container size, the maximum penetration for the three orifice diesel injector is just over 60 mm.

In the Figure 3.1(b), two sprays are visible. The left spray is of interest only as the right spray is not in the same plane as the page. The spray is seen to penetrate the volume as a black shadow due the spray being denser than the air. It can be seen that the spray is initially very dense (being very dark) close to the nozzle, but gradually approaches the intensity of the background.

This series of tests allowed for the evaluation of the effect of nozzle geometry, injection pressure and fuel properties on the spray structure. The fuel properties that are important in this case are the bulk modulus and the density. Tests showed that the vapour pressure was important with DME injections, which was shown to vaporise very quickly which is similar to what Yu and Bae [21] observed.

Rice discussed these results and found that the experimental results agreed with the theory. Penetration did indeed increase with pressure, but no measurements of the spray penetration were taken. Other conclusions were drawn by Rice, but only the

penetration is relevant here.

3.1.2 Processing of the results

It was attempted to obtain agreement between the penetration measured in the experiment and the penetration equations presented in Section 2.1.2 to make the data more quantitative in nature and to relate the work done back to penetration theory. Difficulties arise in measuring the spray tip penetration because the boundary of the spray is not well defined due to atomisation and evaporation. To solve this problem, image processing code was written by the author to track the penetration of the spray. This image processing code is presented in Appendix A.

The image as a matrix

The first step in processing the images is to understand how a computer treats an image. All image files are broken down into a matrix of numbers, where each number in the matrix represents a pixel in the total image. For a grey scale image, each number represents a value between 0 and 1, where 0 represents black and 1 represents white. Values in between 0 and 1 represent different intensities of grey. In Figure 3.2 there are three differently coloured blocks, each one representing a pixel. Thus the image represents a 3×1 matrix. The first block is white, the second is 40% grey intensity and the last block is black. The resulting matrix is

$$[1; 0.4; 0]. \tag{3.1}$$



Figure 3.2: A three column by one row matrix.

As the spray enters the chamber, it casts a shadow. This is the shadow that can be seen in Figure 3.1(b). An image with no spray still contains levels of grey due to noise, seen in Figure 3.1(a).

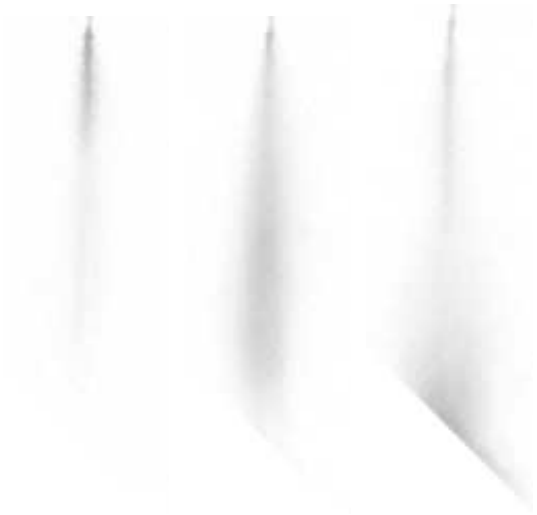
Part of the problem of measuring the spray penetration by hand is to determine where the tip of the spray is located because the shadow of the spray lightens as the drops become smaller and more dispersed. This is especially a problem when the background of the image is noisy. Therefore the noise in the images must be removed first.

Noise removal

Noise is introduced by the camera which measures light intensity within a range, and therefore images of the same subject can vary. Additionally, reflections, flaws or dust on mirrors also introduce noise. Fortunately, most of the noise that is present in the images is common throughout the sequence of photographs. To remove noise that is common in a sequence, subtraction of a reference image will be used. A reference image is a photograph of the system before the injector has injected and therefore contains no spray. All parts of the image that are constant, such borders and the injector nozzle would be removed and only the spray would remain. The results of the noise removal can be seen in Figure 3.3. The images have also been rotated and cropped so that the spray is vertical and the images are smaller. Figures 3.3(a) to 3.3(c) show different stages of the spray evolution for 10 MPa opening pressure diesel injection with a three orifice injector. The simple method of removing the noise can be seen in the images to be very effective. Since the position of the injector and the axis of the spray to be analysed are known, the program will not attempt to locate these and are instead inputted into the program.

Penetration measurement method

Once the noise is removed, the next step is to track the penetration. In Figure 3.4 the injection axis is shown. The penetration is found by comparing the grey levels of the image for each point along the injection axis to a reference level provided by the reference image. For any point along the axis, if the intensity is different from that of the reference image for the same point, then the spray has at least penetrated that far and the next point should be compared. This continues for all points along the injection axis until the intensities are approximately the same signifying that the spray has not reached that point. Once this has occurred then the checks can stop.



(a) (b) (c)

Figure 3.3: Images at 10 MPa opening pressure for a three orifice injector with diesel fuel.

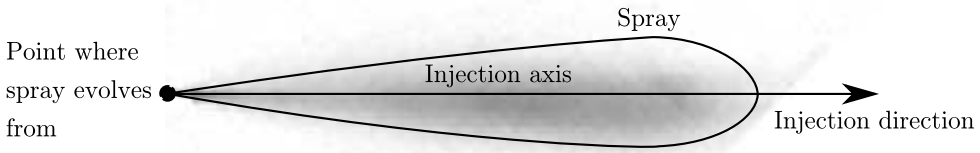


Figure 3.4: Figure showing the injection axis of the spray along which the penetration is measured.

A sample of the grey intensities along the injection axis for a 10 MPa, three orifice injector is shown in Figure 3.5. This shows how the grey levels vary when the spray is in the domain. All the images reach an intensity of 1 at the end of the injection axis. This occurs because this is the edge of the visible area of the images.

3.1.3 Penetration results and discussion

Threshold values had to be set to account for any deviation that was still present in the intensity measurements. For the jet breakup point, differences of 15% were used. The spray tip was defined as where the level of grey after jet breakup approached 99% of the reference value.

Figure 3.6 shows the penetration for the low pressure injections only. At higher

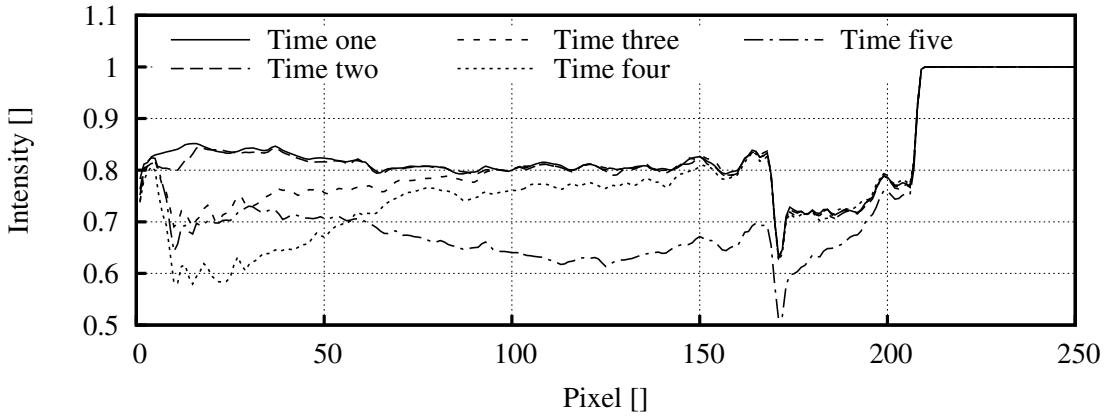


Figure 3.5: The intensity versus pixels for spray penetration for a three orifice, 10 MPa injection.

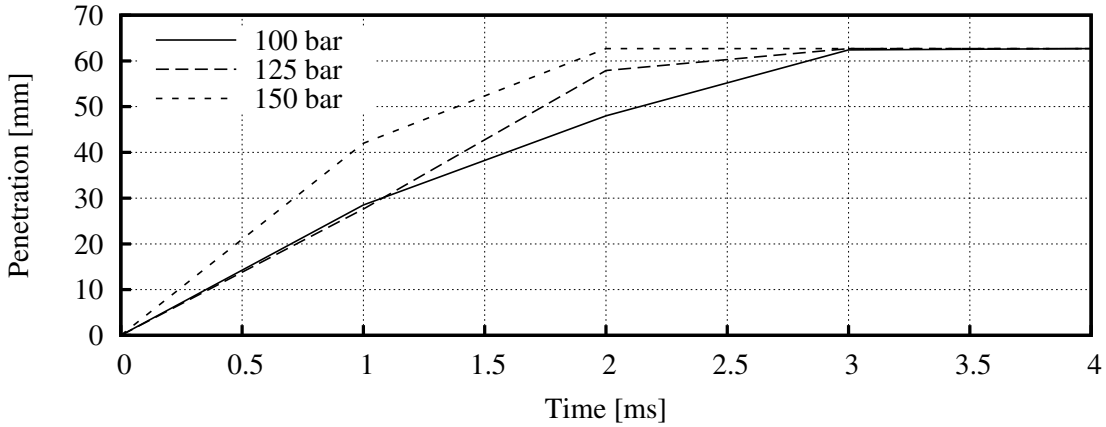


Figure 3.6: Penetration versus time from image processing for a three orifice diesel injector.

pressures, only one point could be obtained from the images before the spray had penetrated past the visible area and no trends could be observed.

The empirical equations by Hiroyasu and Dent were compared to the experimental results for a three orifice injector, where more than one data point was observed. For the empirical equations, the injection pressure will be taken as the pressure at which the injector opens. Figure 3.7 shows the result of these equations and the measured data from the image processing for comparison.

It is seen here, that the penetration equations over predict the penetration. Similar disagreement was shown between the four orifice penetration results and the empirical equations. However, it should be mentioned, that the images and the penetration results show the spray penetrating into the chamber more slowly when injected by a four orifice injector as opposed to a three orifice injector. This difference in spray structure is discussed more fully by Rice [33].

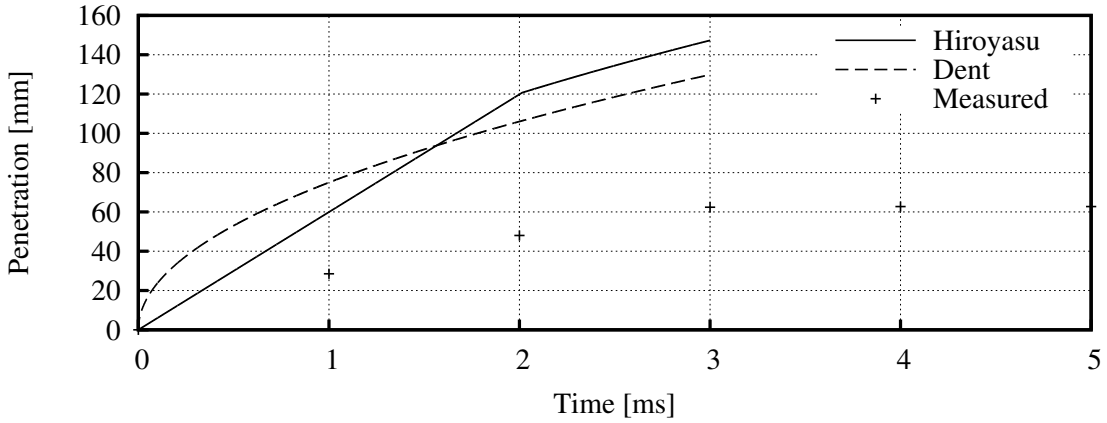


Figure 3.7: Penetration versus time for 10 MPa opening pressure, three orifice diesel injector and the predicted penetration using the equations by Hiroyasu and Dent.

The disagreement between the empirical equations and the experimental results is unexpected as the equations have been shown to fit the data well in the literature [10, 13, 20]. It is thought that the differences arise here because the pressure causing the injector to open (the opening pressure) and not the pressure at the orifice is used in the equations. The pressure at the orifice was not recorded during the experiment, but is also very difficult to measure. The correct pressure could be estimated from a mass flow rate, but as it was not recorded during the tests, this is not possible. It is anticipated that a similar problem may occur in the common rail injector, making this an area of interest as well, especially since this is the later technology. One way of predicting the pressure and the mass flow rate for both the mechanical and common rail injectors, is through modelling techniques.

3.2 Objectives

The objectives evolved out of the problems that were discovered in Section 3.1. It was shown that with the mechanical injector, the actual injection pressure just before the discharge orifice is different from the line pressure and opening pressure. This would justify why discrepancies between the penetration equations with the experimental results exist.

A method of predicting this injection pressure for mechanical injectors is therefore required. From there, it would be a simple process to adapt the model to predict the

injection pressure in a common rail injector. The objectives are thus to:

1. Model a mechanical injector and compare the simulated injection pressure to the line and opening pressures.
2. Model a common rail injector to analyse how the injection pressure varies in the common rail injection system.
3. Perform tests on a common rail injection system, to ascertain how the injection pressure varies with time.
4. Validate the common rail model with the experimental results.
5. Perform an analysis on the common rail model to determine how sensitive it is to its inputs.
6. Determine the injection pressure using the simulation results at the nozzle of the injector and compare this to the rail and injection pressure determined from the experimental results.

Chapter 4

The mechanical injector model

The injection flow rates of a mechanical injector are highly dependent upon transient fluid behaviour, making their prediction very difficult. Thus, the need for a model that can predict the flow rate of an injector exists. Such a model must take into account the needle and fluid dynamics. An estimate of the injected flow rate would be useful for predicting the spray penetration either using empirical equations or CFD modelling.

The injector is a complex system whose operation is dependent on many parameters. To accurately model the injector, a thorough understanding of the entire system is required. Only then can an accurate model be constructed. A result of constructing a detailed model is that the effect of different parameters on the injection can also be evaluated.

This chapter describes how the model was constructed and what inputs were used for the model.

4.1 Model construction

This section details the approach used to construct a model for a mechanical injector. Firstly the software used to solve the equations that governs the behaviour of the injector is presented. Following that, the operation of the injector can be explained, from which point simplifying assumptions, governing equations and boundary conditions can be developed. An example of how the Scicos program is constructed is shown in Appendix C.

4.1.1 Scicos

The model was constructed and solved in Scicos, a toolbox of Scilab which is an open source program that can be used to solve mathematical problems in science and engineering. Scilab is used for rapidly constructing models without the need of hard coding mathematical functions like integration or data representation as all of these tools are already included in the software. Thus, Scilab is very effective at quickly inputting the equations that govern a model and solving them.

4.1.2 The injector system

Figure 4.1 shows the fuel circuit for the injection system from the tank to the injector. This figure shows how the injector is placed relative to the pump and the tank. Only the high pressure line and the injector will be modelled. This decision will be explained in Section 4.2.

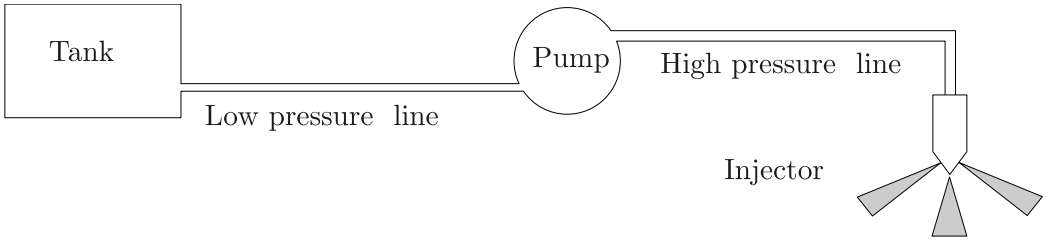


Figure 4.1: Simplified system circuit for the injector

The injector opens when the pump supplies sufficient fuel to raise the pressure and lift the injector needle. The fuel is sprayed into the chamber, at a pressure that is dependent on the opening pressure of the injector and the pressure supplied by the pump. The control and actuation of this process with reference to the engine requirements will be described below.

The timing of injection

In an engine, it is important that injection occurs at the correct time to ensure that the engine can operate properly and smoothly [10]. The pressure signal that opens the injector is created by the injector pump. The injector pump operates at half the engine

speed to ensure that injection coincides with the expansion/combustion stroke. Only injection is modelled and therfore only the pressure profile that opens the injector is important, and not the time where injection begins and ends.

The pressure signal

In the system being modelled, each injector has its own pump. The signal is generated by a piston in the pump that rests on a rotating cam. A pressure wave is produced that is dependent on the cam profile and the piston speed [26]. The pressure wave can vary according to the engine load so that more or less fuel can be delivered when necessary.

The fuel delivery system is designed to reduce secondary injections and cavitation. Preventing secondary injections is achieved by allowing flow retraction by the injector pump. Cavitation is reduced by allowing excess fuel to bleed off once it is delivered [17, 26].

The injector opening pressure

The injector pump provides a rapid increase in pressure so that high injection rates and good atomisation are achieved. It is therefore necessary to be able to set the injector to remain closed while the pressure builds to the required critical opening pressure. A typical opening pressure for mechanical injectors is 22.5 MPa. The opening pressure of the injector is set by the initial compression of the spring that pushes down on the injector needle. The injector opens due to a buildup of pressure on the needle faces that cause opening upward forces that eventually overcome the initial downward spring force. When the needle lifts, injection begins.

As the fuel discharges, it causes the pressure acting on the needle to decrease and so the spring begins decompressing and the injector closes. Being a highly dynamic system, the needle may oscillate before finally closing, causing oscillating pressures and discharge flow rates. This oscillation is undesirable as it results in secondary injections that are unpredictable. Pressure release valves attempt to remove these secondary injections by releasing excess line pressure [26].

The injected volume

The amount of fuel delivered under constant engine load and speed should be the same for every injection. Additionally, the fuel line pressure should also be the same for every injection so that the line pressure is at the same initial condition for each injection. When the load on the engine changes however, the injection system compensates so that the required power is still produced. This is achieved by a throttle which varies the amount of fuel supplied to the injector pump according to the engine load.

4.1.3 Assumptions

These assumptions simplify the solution by eliminating complexities or assuming values for unknowns that are difficult to ascertain experimentally.

1. The system is rigid and so deformation within the injector does not occur. Deformation would cause increases to the internal volumes which would cause slight reductions in pressure. This assumption applies specifically to the expansion and contraction of the internal volumes, and does not apply to the deformation that occurs when the needle impacts against any part of the injector.
2. Acceleration due to gravity is negligible in comparison to accelerations due to any forces acting on the system.
3. Cavitation is ignored.
4. The discharge coefficients of the flow through changing areas are set at 0.6, which is typical for flows through an orifice [23].
5. There is no leakage of fuel out of the system.
6. Variations in bulk modulus and density of the fuel with pressure are ignored. This assumption is justified by the low range of pressures expected in the mechanical injector (8 MPa - maximum 40 MPa).
7. The fuel temperature remains constant.
8. There is always enough fuel to fill all the volumes within the injector.

9. There is no reverse flow within the system.

4.1.4 Governing equations

The system is broken down into a fluid and needle component. Each component is defined by its own set of equations.

Fluid equations

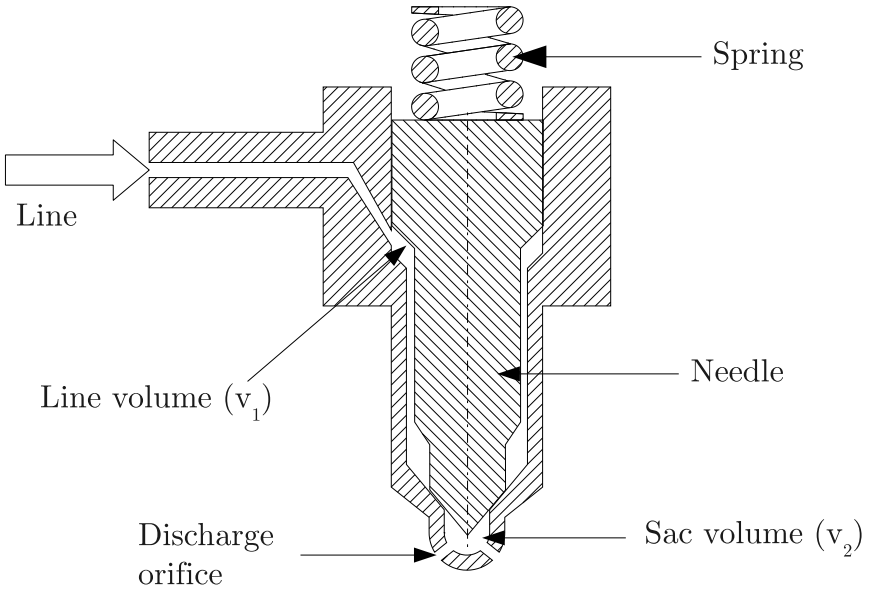


Figure 4.2: The mechanical injector

To begin with, the fuel volume within the injector is divided into smaller volumes. These volumes can be seen in Figure 4.2, labeled as v_1 and v_2. Volume v_1 represents the line volume and the volume within the injector up to the sac volume v_2. A pressure difference between two volumes causes flow between them that occurs until the pressures equalise. In the injection system disturbances to the pressure are provided by the pump.

Figure 4.3 shows a simplified system that illustrates how the flow rates and pressures are defined. Here two volumes exist, volume A and volume B, each with its own unique pressure, P_A and P_B respectively. If P_A is larger than P_B then the flow occurs from volume A to volume B. Thus, there is a flow rate $Q_{A,B}$. The constriction has its own discharge coefficient based on its geometry and flow conditions.

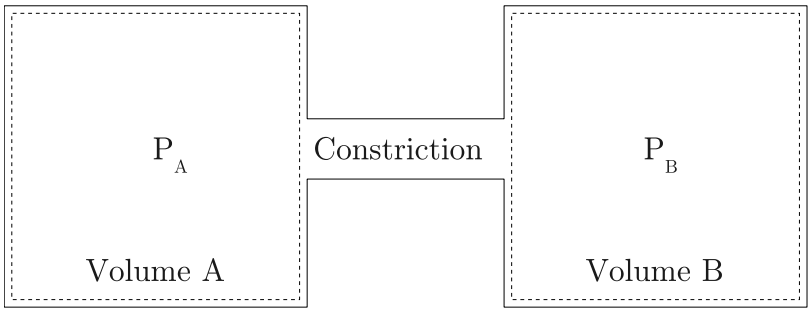


Figure 4.3: Two volumes separated by a constriction.

The subscript convention used henceforth will be the same as the convention used above, thus for the flow rate, the subscript A, B denotes the direction of the flow, from volume A to volume B. The area of the constriction is designated in a similar manner, as $a_{A,B}$.

The equation governing the fluid motion within the volumes can be found from the definition of the bulk modulus β of a fluid [23] and is similar to the model used by Rakopoulos and Hountalas [26]:

$$\beta = -\frac{\partial P}{\partial v/v}. \tag{4.1}$$

Writing Equation (4.1) in terms of pressure, P, and differentiating with respect to time yields (4.2):

$$\frac{dP}{dt} = \frac{\beta}{v}\left(\frac{dv}{dt}\right). \tag{4.2}$$

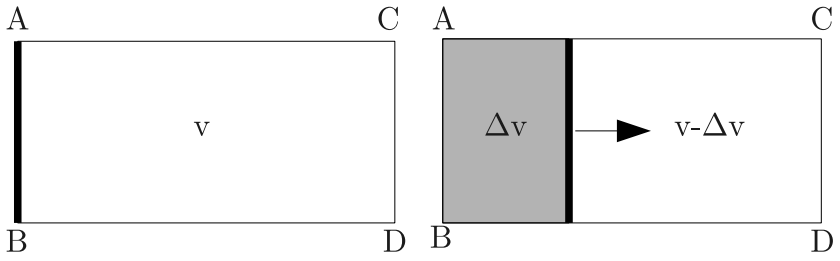
Equation (4.2) assumes that P varies only with time. This assumption is reasonable as the pressure disturbance provided by the pump is a function of time only. The needle motion, which also affects the pressure, is a function of the needle displacement, which will be shown in Section 4.1.4 also to be a function of time. Thus, normal differentiation can be used.

The term dv/dt represents the rate of change of volume v. This change of volume is made up of two components: the flow rate into and out of the volume. A change in size of the volume can be included as one of these two components as well, but must also be included in v. Expanding the dv/dt term and including the change of volumes:

$$\frac{dP}{dt} = \frac{\beta}{v - \Delta v}\left(Q_{in} + \dot{\Delta v} - Q_{out}\right).$$

The Δv term results from a volume changing size due to motion of one of its walls. Figure 4.4 shows a volume defined by the points $ABDC$ with a unit depth. The wall AB can move, changing the size of the initial volume v. In Figure 4.4(b) the wall decreases the initial volume by Δv to leave $v - \Delta v$.

Similarly, the $\dot{\Delta v}$ term is the rate at which the initial volume changes. This can be thought of as an artificial flow rate into or out of the volume. This flow rate is dependent on the velocity of the wall and the wall area.



(a) Initial volume. (b) Final volume.

Figure 4.4: A schematic showing a volume changing size due to the motion of one (or more) walls.

In the injector, the needle acts as the moving wall in some of the internal volumes, causing artificial flow rates that are dependent on its motion. Thus, Δv can be represented as the area A of the needle multiplied by its displacement x. Similarly, $\dot{\Delta v}$ is the rate at which the volume changes due to the needle motion and can be written as the needle area multiplied by its velocity $\dot{x}$. Thus:

$$\frac{dP}{dt} = \frac{\beta}{v - A_N x}\left(Q_{in} + A_N \dot{x} - Q_{out}\right). \tag{4.3}$$

Equation (4.3) describes the variation of pressure with time in the volume based on the bulk modulus, the size of the volume and the flow rate into and out of the volume. Thus, the fluid behaviour is adequately described to be able to predict the flow rate between two volumes.

Because the injector is divided into multiple volumes and the needle has step changes in

its diameter along its length, Equation (4.2) needs to be written for each volume using only the area of the needle that enters that volume. The different volumes are shown in Figure 4.2 while the different diameters and areas of the needle are discussed in greater detail in Section 4.2.3. Thus:

$$\begin{aligned} \frac{dP_1}{dt} &= \frac{\beta}{v_1 - A_{1,2}x}\left[Q_{in}(t) + A_{1,2}\dot{x} - Q_{1,2}(t)\right] \\ \frac{dP_2}{dt} &= \frac{\beta}{v_2 - A_2 x}\left[Q_{1,2}(t) + A_2\dot{x} - Q_{2,a}(t)\right]. \end{aligned} \tag{4.4}$$

The subscripts of area A are defined as follows. For two arbitrary areas A_a and A_b, area $A_{a,b}$ is the difference between A_a and A_b. The pressures are named after the volumes in which they occur. So a pressure P_i occurs in volume i. Therefore, pressure P_1, is the pressure in the line from the pump to the injector. Given that this distance is short, the effects of friction can be ignored. A similar approach and assumptions were adopted by Lino et al. [34] for a common rail injector model. The flow rate out of the volume is calculated from the pressure difference across the outlet to the next volume. This is shown in Equation (4.5).

$$\begin{aligned} Q_{1,2}(t) &= c_d a_{1,2}(x)\sqrt{\frac{2(P_1 - P_2)}{\rho_f}} \\ Q_{2,a}(t) &= c_d a_{2,a}\sqrt{\frac{2(P_2 - P_a)}{\rho_f}}. \end{aligned} \tag{4.5}$$

The area $a_{1,s}(x)$ is created by the needle lifting and is therefore dependent on the needle displacement x, which is a function of time. This displacement allows the fuel to flow from volume 1 into the volume 2. Two solutions exist for this area, because the area only opens for negative displacements of x where x is positive downward. The equation to calculate this area is:

$$a_{2,a}(x) = \begin{cases} \sqrt{2}\pi \left[\dfrac{\left(\dfrac{4r_4 - x}{2}\right)^2}{2} - r_4 \dfrac{4r_4 - x}{2} \right] & (x < 0) \\ \\ 0 & (x \geq 0) \end{cases} \tag{4.6}$$

where r_4 is the radius of the sac of the injector shown in Figure 4.10 and Figure B.1 where Equation 4.6 has been derived. The area $a_{2,a}$ is the total area of the orifices through which the fuel is injected into the chamber and thus is independent of time or needle lift.

A drawback of this model is that the system responds to a change in pressure in a volume immediately, whereas as there should be a delay as this pressure signal travels through the volumes. The flow rates that are predicted are still correct, even though they are predicted to occur sooner than they would in reality. These equations therefore assume that the pressure disturbances travel throughout the system immediately, or that the speed of sound in the fluid is infinite.

Needle dynamics

Needle motion arises due to the fluid pressure on the shoulders of the needle. These forces, when large enough, cause the needle to lift and the injection to start. The equation of motion of the needle is derived from Figure 4.5 using simple balancing of forces and can be seen in Equation (4.7).

$$\ddot{x} = \frac{1}{m} \left(P_1 A_{1,2} + P_2 A_{2,3} - P_a A_0 + F - c_1 \dot{x} + k_1 x \right) \tag{4.7}$$

where $\ddot{x}$ is the second derivative of the needle displacement x with respect to time (i.e. acceleration), k_1 is the spring constant, P_i is the pressure in volume i acting on the needle area A that is in that volume. F is a force that has two possible solutions depending on the position of the needle.

The force F varies because while x is positive, the needle experiences a reaction force from the injector whereas when x is negative the needle experiences a force from the

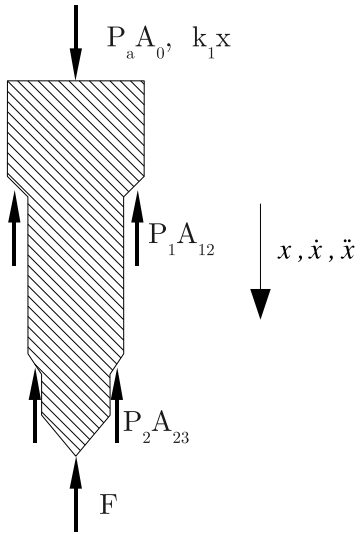


Figure 4.5: Free body diagram of the all forces acting on the needle.

fluid as it discharges out of the injector. The two solutions for F are given in (4.8).

$$F = \begin{cases} k_2 x + c_2 \dot{x} & (x > 0) \\ \\ \dfrac{P_2 + P_a}{2} A_3 & (x \leq 0). \end{cases} \tag{4.8}$$

The force that acts when the needle has lifted represents the average pressure that acts on the needle. The tip of the needle is open to the chamber pressure, whereas the pressure P_2 acts at the corner of the shoulder. This tip however, is so small that the magnitude of this force is inconsequential. This average pressure is just a simple approximation of what may occur between these two points.

When the needle is in contact with the injector, it experience contact force due to the elasticity and possible damping of the material or friction. The constant k_2 represents the elasticity of the injector material as it deforms and c_2 represents the losses associated with deformation and friction. The values of k_2 and c_2 are chosen empirically so that the results fit the available engine test data, but remain fixed for the remaining simulations. How these constant are chosen is described in more detail in Section 4.2.6.

4.1.5 Boundary conditions

The boundary conditions are limitations within which the system operates. Two boundary conditions exist that restrict the needle motion. They are:

1. The maximum compression of the spring is 2.5 mm, after which the spring compresses like a solid bar and the spring constant is significantly larger. This value is obtained by estimating the distance between the coils of the spring.
2. Extension of the spring is restricted by the needle interacting with the injector tip.

4.2 Model inputs

This section defines the inputs that are required for the model. The accuracy of the model is obviously dependent upon the accuracy of the inputs.

4.2.1 Inlet flow rate

The most important input into the system is the flow rate into the line volume as this causes the pressure rise that actuates the injector. The best way to model the injector would be to also model the pump system and thereby calculate the inlet flow rate. This was used by Rakopoulos and Hountalas [26] in their model of a mechanical injector. However, without detailed knowledge of the pump available, an alternative method needs to be found.

Engine test data for the line pressure and needle lift during injection are available. From the pressure data, the inlet flow rate can be calculated. This process will be detailed below.

Engine test data

The line pressure versus time for a low (25 Nm) and medium load (45 Nm) test are shown in Figure 4.6. This data was extracted from the Masters dissertation submitted by Lopes [35]. The figure shows a sudden pressure rise at about 10.5 ms which is caused by the injector pump and opens the injector. At about 11.5 ms there is a decrease in the pressure gradient, which indicates that the injector opened and that fuel is being injected. The pump continues to supply fuel until the line pressure peaks at about 12.5 ms. Injection continues until the pressure in the injector no longer overcomes the closing spring force. After the main pressure wave at about 14 ms, there are many smaller waves that are a result of the water hammer caused by the needle as it closes suddenly to terminate injection and not by smaller, secondary injections.

Because the line pressures in Figure 4.6 are only appropriate to a 22.5 MPa opening pressure injection, they cannot be used as the pressure rise provided by the pump for any other opening pressure. This is because the line pressure is dependent on the downstream conditions of the fluid flow which in turn is dependent on the opening pressure.

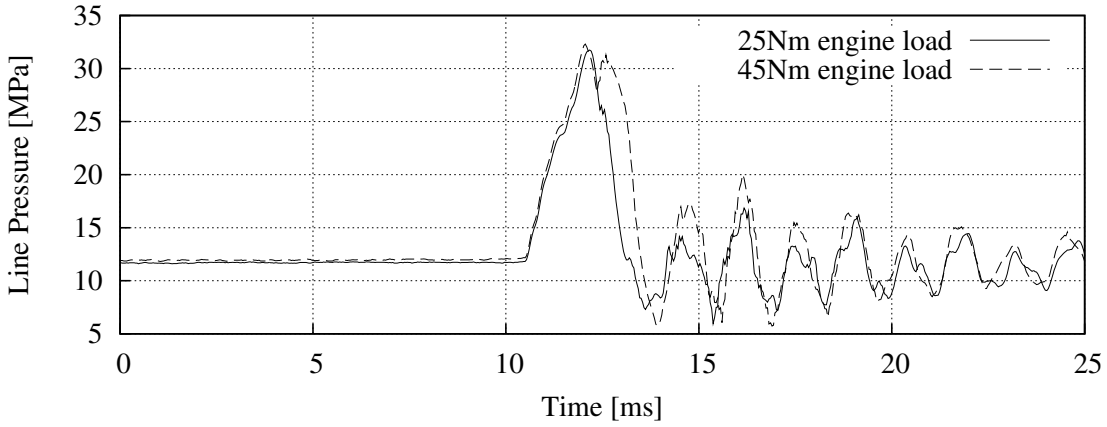


Figure 4.6: Line pressure versus time for engine tests at low and medium load.

A model can be constructed to simulate the injection for the engine test conditions. Instead of using an inlet flow rate into volume 1, the line pressure from the engine test (shown in Figure 4.6) can be used as an input to the model. By doing this, the flow rate out of v_1 is now known and is shown in Figure 4.7. This figure shows the fuel flow rate from the line into the injector for a low and high engine load. It can be seen in the figure that the high engine load flow rate proceeds for longer because more fuel needs

to be injected. For the duration where both the low and high load cases supply fuel to the injector, both flow rates are similar. This implies that the flow rate provided by the pump during this time is similar and independent of the throttling of the engine. Using the flow rates in Figure 4.7 and

$$\frac{dP_1}{dt} = \frac{\beta}{v_1 - A_{1,2}x} \left[Q_{in}(t) + A_{1,2}\dot{x} - Q_{1,2}(t) \right],$$

from Equation (4.4), the only unknown Q_{in}, representing the flow rate provided by the pump, can be solved for. The resulting flow rates provided by the pump for both loading conditions are shown in Figure 4.8.

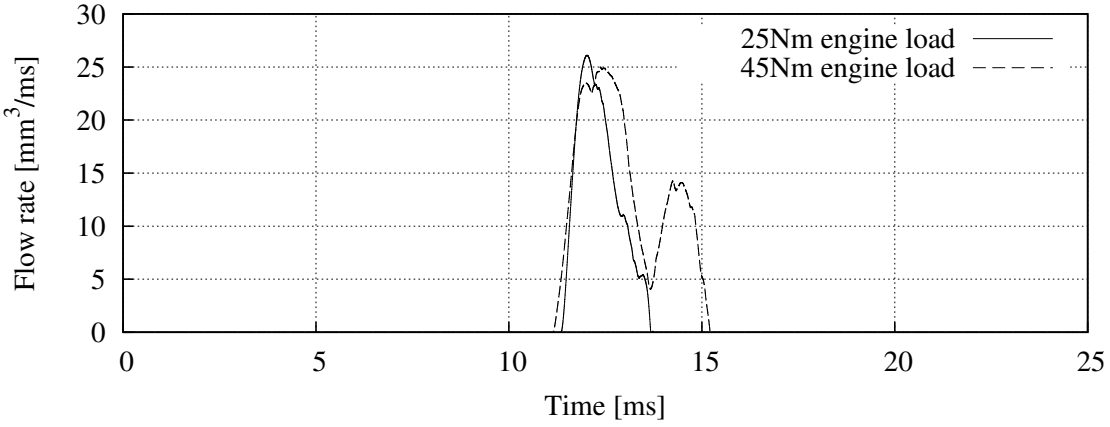


Figure 4.7: Flow rate from the line to the injector versus time for the engine tests simulations.

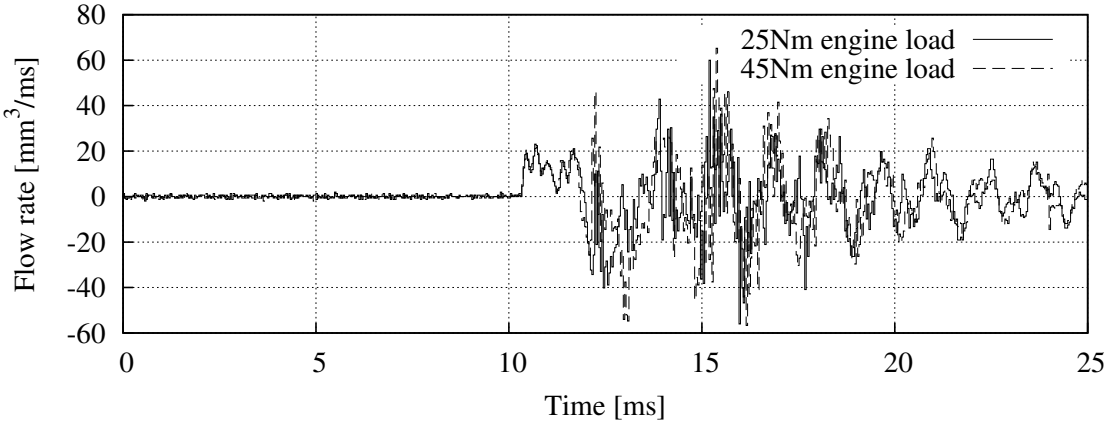


Figure 4.8: The flow rate provided by the pump into the line versus time as calculated from the engine simulation.

Simulated inlet flow rate provided by the pump

Figure 4.8 shows the inlet flow appearing to be quite random due to the sensitivity of the solution to dP/dt. Positive values indicate that the pump is supplying fuel. Between 10 ms and 12.5 ms, where the pump is supplying fuel, the flow rate for both loads is similar. Then, the pump stops supplying fuel for the low load condition. The medium load also briefly stops receiving fuel, but then has a second peak causes an additional peak pressure in the main delivery that occurs at 12.5 ms in Figure 4.6. This additional peak is important as it causes the additional pressure rise seen in figure 4.7, and therefore must also be considered.

These flow rate profiles imply that the rate at which fuel is delivered by the pump is similar in magnitude but differs in duration for each throttling condition. The pump supplies fuel for a longer duration for the medium load condition than for the low load, as expected. The pump varies only the amount of fuel that is delivered by varying the throttle. If the engine speed remains constant however, then the rate at which this fuel is delivered must also remain constant. Thus, the flow rate provided by the pump is essentially a square wave.

After this delivery period, the inlet flow rate becomes negative. This indicates that the flow leaves the line or the inlet flow has now become an outlet flow. Although this seems unreasonable, this feature may indeed occur. Reverse flow could act to dampen out secondary injections in the system [36]. Also, the pump, being a piston pump, may draw fluid back when the piston is not pumping. It is reasonable that some fuel may not be injected even though it is pumped to a high pressure so that the fuel that is injected, does so at a much higher pressure.

Following this reverse flow phase, there are fluctuations in the inlet flow rate. These flow rates occur to accommodate the pressure fluctuations that arise due to a water hammer effect from the injection event. Although the pressure fluctuations that occur are large in magnitude in comparison to the original supplied fuel pressure, they should be ignored as they occur after the pump has already drawn fuel back in, which means it has already stopped pumping.

This approach for determining the pump flow rate assumes that a pressure wave that is

experienced at some point in the line, is the same as the pressure wave that the injector will experience at some point later in time.

The supplied flow rate used for in the model

For the model, a square wave with a magnitude of 15 mm^3/ms will be used to represent the flow rate supplied by the pump as it simplifies the input. The magnitude of the low and medium load conditions will be equal, but the durations for each, will be 2 ms and 2.5 ms respectively as was observed above. In the engine test, the pump consisted of a drop cam and piston arrangement. In this case, it is reasonable to expect the pumping cycle to be a square wave, justifying the decision to use a square wave in the model. Reverse flow will not be included because it is dependent on how much fuel is injected which is unknown. The flow rate supplied by the pump that will be used in the model is shown in Figure 4.9.

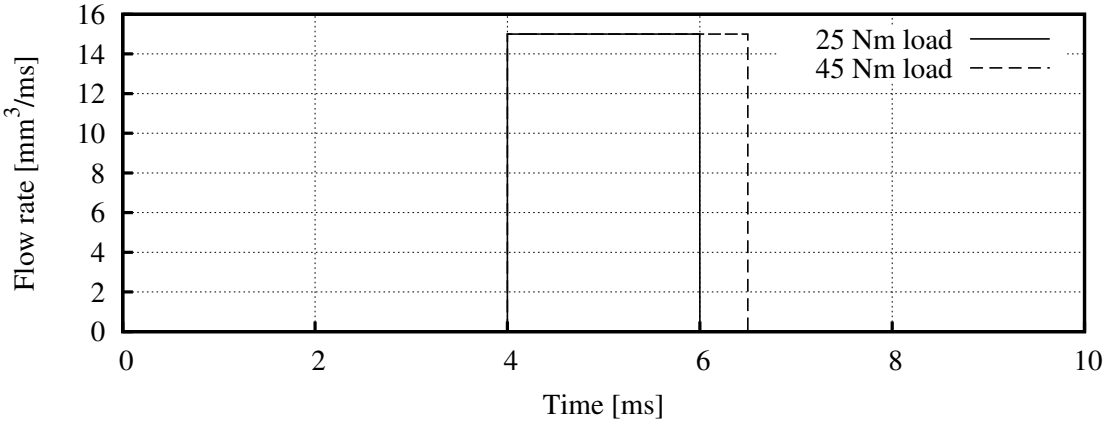


Figure 4.9: Flow rate versus time provided the pump used in the simulations for both low and medium load.

The time where the pump is delivering fuel has also been changed from what was represented in Figure 4.8. This decision has been taken to shorten the solution time and will have no affect on the nature of the solution that will be obtained.

4.2.2 The line and chamber pressure

In Figure 4.6, the line pressure is non zero at the start of injection. This value is called the residual line pressure and is the pressure to which it stabilises to after the preceding

injection. This residual pressure needs to be included in the model as an initial value for the line pressure and in Figure 4.6 this value is 12 MPa. A problem arises however, where one of the proposed simulations has an opening pressure of 10 MPa since the injector would always be open and would not open only for the pressure signal provided by the pump. Thus, a lower residual line pressure of 8 MPa has been used instead.

The model has to account for different combustion chamber pressures. The engine test simulations in Section 4.2.1 used a combustion chamber pressure of 4 MPa, whereas atmospheric pressure is used when attempting to replicate the results of Rice [33]. Regardless of this difference, the engine test data may still be used because the downstream chamber pressure is seperated from the line by the needle and therefore has no influence on the amount of fuel supplied by the pump during injection. In the model, a chamber pressure of 0.1 MPa is used so that the model is solved with respect to the results of Rice.

4.2.3 Volumes and areas

The internal volumes and areas of the injector are difficult to measure and detailed drawings of the injector are not available. Some measurements could be taken from a cut-away of an injector, and the internal volumes and areas are based off these values. The values used for the line and sac volume are shown in Table 4.1. The location of these volumes within the injector can be seen in Figure 4.2. The needle areas could be measured more accurately. The different radii are defined in Figure 4.10, their values and the corresponding areas are shown in Table 4.2.

Table 4.1: List of control volumes for the injector tested.

Region	Volume [mm^3]
1	235.6
2	1.8

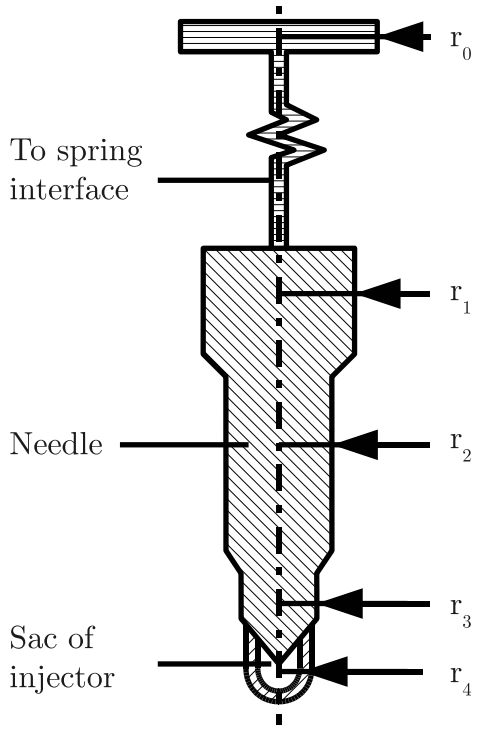


Figure 4.10: Cross-section indicating the different radii upon which pressure acts.

Table 4.2: List of radii and corresponding areas for the injector tested.

Region	Radius [mm]	Area [mm^2]
r_0	5.00	78.54
r_1	2.00	12.56
r_2	1.50	7.07
r_3	1.00	3.14
r_4	0.75	N/A

4.2.4 Bulk modulus and density

The bulk modulus is a measure of the compressibility of a fluid. In the model, a constant bulk modulus of 1.4 GPa and density of 825 kg/m^3 are used for diesel, which is reasonable considering the expected range of pressure shown in Figure 2.3 and 2.4.

4.2.5 The spring constant

The spring constant was obtained experimentally using the Lloyd MX100K, which is capable of loading the spring in compression and measuring the change in length. Using

Hooke's law, the spring constant was calculated as 0.11 kN/mm.

4.2.6 The selection of empirical constants

Two constants, k_2 and c_2 were introduced into Equation (4.8). These constants represent the deformation of the injector and the damping respectively. The deformation constant behaves like a spring constant. It arises when the needle interacts with the injector, causing a contact force to act. The damping constant arises due to losses in the system such as friction as the needle moves.

These values are difficult to measure and assign, but play an important role in the behaviour of the injector. The values chosen for k_2 and c_2 need to be weighed up against each other. A value of k_2 that is too large, results in rapid deceleration and nullifies the effect of the damper. A value that is too low, results in unrealistic deformation of the needle and injector. A value of c_2 that is too large also dampens out low amplitude phenomena which may be of interest. Thus, ideally the damping coefficient should be as small as possible, while still dissipating energy adequately.

Because these constants are difficult to measure, they have to be selected empirically to match known engine test results. Thus, the values are chosen so that they give the correct needle lift for the engine test simulations. Obtaining similar traces for the model and test data would suggest a degree of accuracy. Once the constants are chosen for the engine tests, they are left unchanged for all the other simulations conducted.

Another solution that is similar to damping and used by Kiijarvi [36], is to make the needle velocity after an impact with the injector body a fraction of the velocity before impact, but in the opposite direction. Thus, the kinetic energy of the needle is reduced and the direction of the needle's motion is changed and the motion will eventually dampen out. This method would still require a value for k_2 to be chosen. Both methods have the same affect on the system.

4.2.7 The initial opening pressure

The initial opening pressure is the pressure in the line that will cause the injector to open and inject. It must be noted that the opening pressure of the injector is not necessarily the peak pressure of the injector. In the engine tests, the opening pressure is set to 22.5 MPa.

Physically, this pressure is set by adjusting the spring force that maintains the injector in a closed position by varying the spring's initial compression. The pressure in the line that overcomes this spring force is the opening pressure of the injector. This force is varied by altering the initial spring compression.

In the model, the initial opening pressure is chosen by setting the closing spring force. This force can be calculated by taking a force balance on the needle and considering the instant that the needle is just about to move. At this point in time, the spring force will balance the pressure forces on the needle. The spring force can then be calculated from Equation (4.9).

$$F_{spring} = k_1 x = P_1 A_{13} + P_2 A_3 - P_a A_0. \tag{4.9}$$

For each injector opening pressure that will be simulated, a different spring force is required. These forces are shown in Table 4.3.

Table 4.3: Injector opening pressure and corresponding spring force.

Pressure [MPa]	Initial force [N]
10	79.5
15	126.6
20	173.7
25	220.9

4.3 Proposed simulations

The following inputs into the model will be varied and their change will be simulated:

- the injector opening pressure,

- the number of injector discharge orifices, and
- the amount of fuel delivered by the pump.

The above will be investigated in terms of how they affect the injected flow rate. The flow rate is chosen for investigation because it has a direct relation to exit velocity and therefore the spray evolution within the combustion chamber. The simulations will also indicate how different the sac pressure is from the line pressure. This was a problem that was encountered in Chapter 3 and resulted in the spray penetration being over predicted.

The injection system will be simulated for a three and four hole injector. The throttling conditions will be modelled as described in Section 4.2.1. The average flow rate will be 15 mm^3/s. The low load and medium load conditions will have durations of 2 ms and 2.5 ms respectively. These values are based on the results shown in Figure 4.9.

Chapter 5

The mechanical injector simulations

The injector was simulated for a three and four orifice nozzle at low and medium engine conditions and opening pressures of 10 MPa, 15 MPa 20 MPa and 25 MPa. The results from the simulations are discussed below. The reverse flow on the model is discussed first as it affects how the results can be interpreted. Following that, the results for the system pressures, injected flow rate and needle lift are discussed. A sample of the data obtained from the Scilab model has been presented in Appendix E.

5.1 The effect of reverse flow

The simulated inlet flow rate from the pump is only an approximation of the actual supply and excludes all reverse flow. Consequently, the simulation will produce different results to those of an experiment. Understanding how this reverse flow in the pump would alter the simulation allows for meaningful conclusions to be obtained.

Figure 4.8 shows how the calculated flow rate into the line from the pump varies. The figure shows reverse flow when the flow rate is less than zero. If this is not taken into account, then the injector will behave differently because excess pressure remains in the system. This reverse flow was excluded from the model as it could not be predicted, thus the simplified flow rate profile shown in Figure 4.9 was used.

The absence of reverse flow in the model decreases the rate of injector shut off. This is because the pressure that lifts the needle remains higher for longer thereby maintaining

the injection. More fuel is therefore delivered and the residual pressure in the line is lower after injection.

The simulations are all carried out with the same assumption that no reverse flow occurs and will consequently show results that are meaningful relative to each other. Because the behaviour of the injector is accurately captured in the model, the response of the injector to different test conditions will show the same trends as in any experiment. These valid trends and commonality between the simulations therefore mean that the objectives of the investigation can be met.

5.2 Pressure

The pressure features are discussed with special reference to the type of spray that would evolve. The line and opening pressures are compared to the sac pressure to see which gives a better approximation of the injection pressure.

Line pressure

Figures 5.1 to 5.4 show the line pressure P_1, for low and medium load conditions at the opening pressures shown. The figures show that the pressures tend to different values after injection for each opening pressure. Because there is no reverse flow in the model, it is likely that these residual pressures shown do not represent what would occur in the respective engine tests. This is important when considering the flow rate and pressure plots.

For the same loading conditions, number of orifices or opening pressures, it can be seen that the line pressure is affected in three ways. These are the duration of injection, the peak line pressure and the final pressure that the line pressure tends towards.

The duration of injection can be seen in the pressure plot by noting the time when injection starts and ends. The start of injection is when the line pressure reaches the opening pressure of the injector. As the injector opens, the gradient of the pressure decreases because fuel is being injected and the pressure in the line cannot increase as rapidly as before.

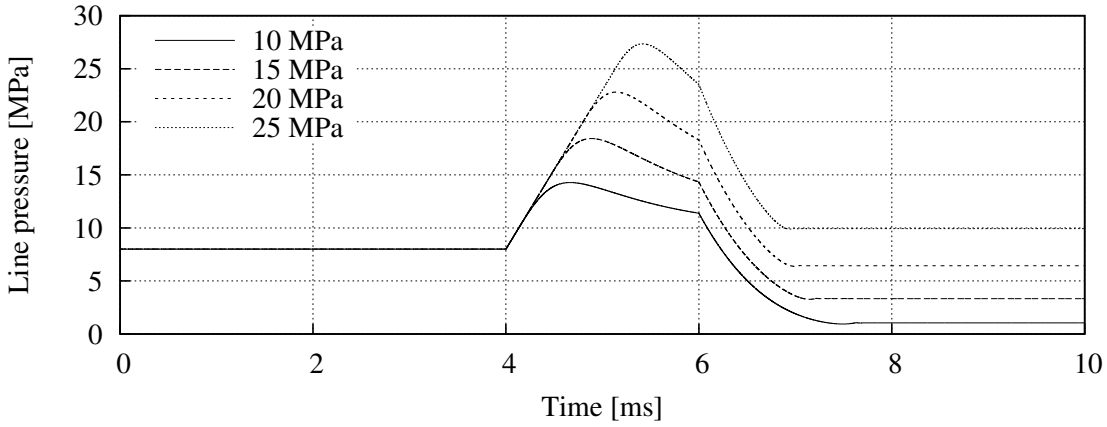


Figure 5.1: Line pressure versus time for the three orifice injector simulations at low engine load conditions.

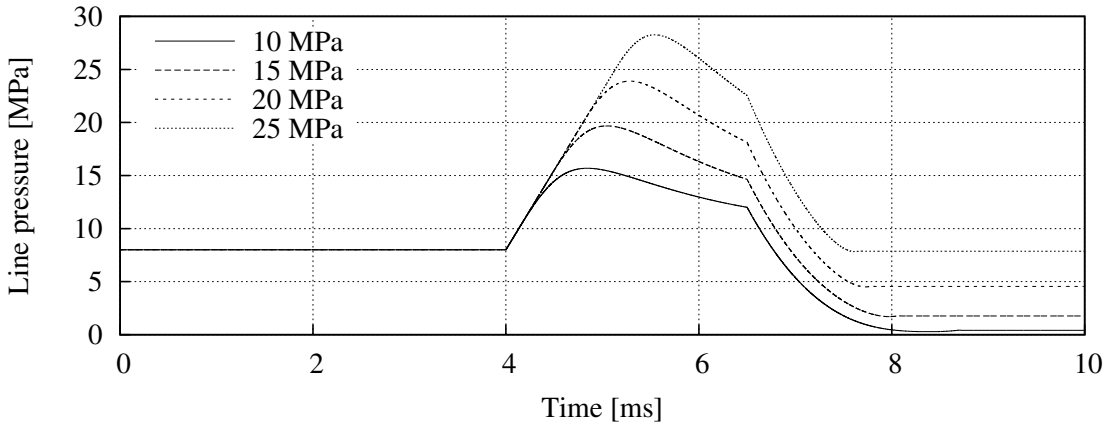


Figure 5.2: Line pressure versus time for the three orifice injector simulations at medium engine load conditions.

The end of injection is when the line pressure becomes constant. At this point, the pump is no longer supplying fuel to the line and injection has stopped. The point where injection stops and therefore the duration of the event, is affected by the needle motion which will be discussed in Section 5.4.

Now that the duration of injection has been defined in Figures 5.1 to 5.4, the effect of the engine load, opening pressure and number of orifices can be discussed. A comparison of the different loading conditions shows that the duration of the injection is longer for medium load throttling conditions, which is expected since the pump supplies fuel for a longer duration.

A comparison of Figures 5.1 and 5.3 for low throttling conditions and Figures 5.2 and 5.4 for medium throttling conditions show shorter injections for four orifice injectors

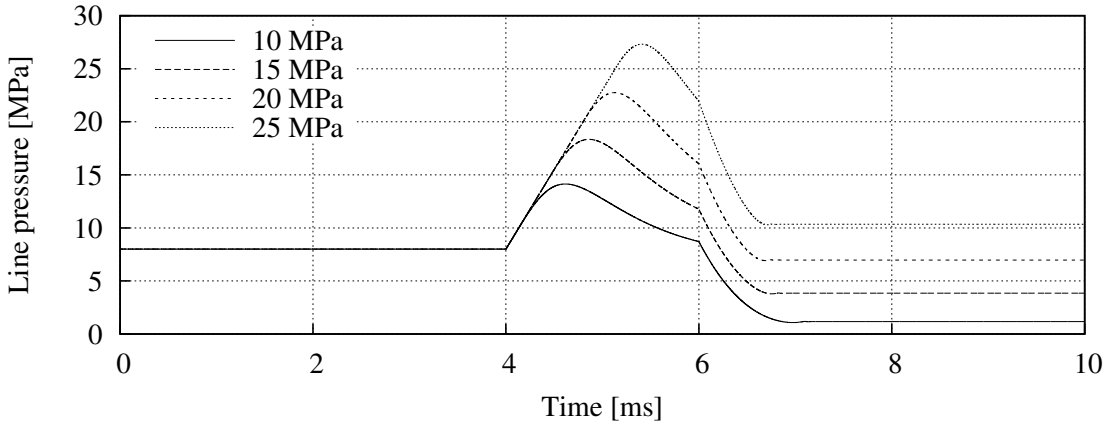


Figure 5.3: Line pressure versus time for the four orifice injector simulations at low engine load conditions.

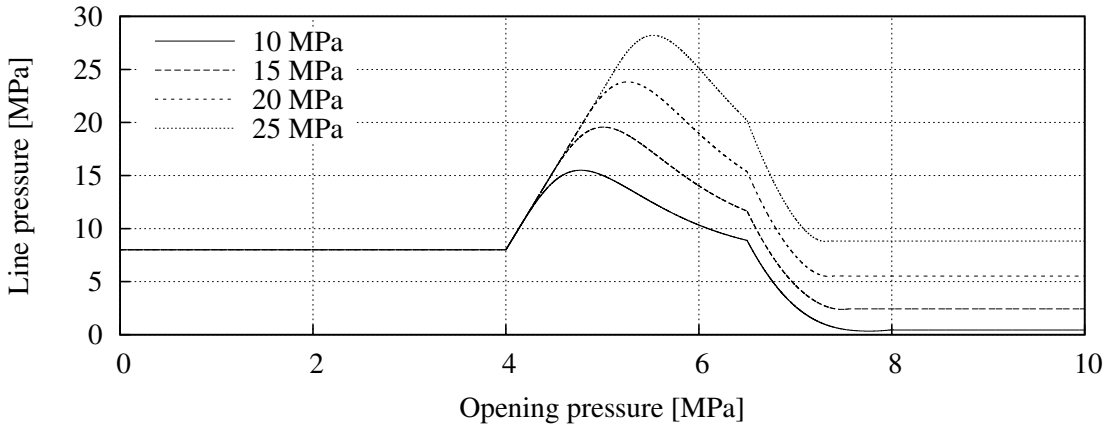


Figure 5.4: Line pressure versus time for the four orifice injector simulations at medium engine load conditions.

for both loads. The four orifice injector offers less restriction to the flow, so the fuel is injected into the chamber quicker. It will be shown below that this does not imply that the initial injected velocity of the jet into the chamber is higher, so the spray is not necessarily better atomised.

Simulations with high opening pressures also have high peak line pressures because the pressure is allowed to build more before injection can begin. High line pressures are desirable because the overall pressure in the system is higher, resulting in faster needle responses, higher mass flow rates and therefore a more atomised, dispersed and penetrating spray.

Figures 5.1 to 5.4 suggest that the final line pressure after injection would be different for every opening pressure of the injector. This value however, is also affected by any

reverse flow that would occur in the system. Thus, the line pressures after injection shown in Figures 5.1 to 5.4 do not represent what would occur in an engine.

Because the line pressures have different final values to the initial 8 MPa set in the model, the amount of fuel delivered in each simulation cannot be compared. Some fuel is 'stored' in the line under pressure, so for example: the 10 MPa opening pressure has final pressure lower than 8 MPa. Thus, fuel that was stored in the line before injection has also been injected in addition to the fuel supplied by the pump.

The duration of the injection, peak and the final line pressure after injection all affect the volume and rate of fuel delivered. Thus, these parameters are all important in predicting the quality of spray that will form during injection.

The line pressure is measured far from the orifice. A better indication of what occurs during injection is to analyse the sac pressure. The line pressure is still used for comparison because it can be easily measured and therefore is useful to compare to the experimental results. From the comparison of the line pressure and the sac pressure, the difference between them can be better understood.

Line and sac pressure

Figures 5.5 to 5.8 show the line and sac pressures for a three orifice injector at an opening pressure of 10 MPa and 25 MPa at low and medium engine load conditions. The 15 MPa and 20 MPa opening pressures and the four orifice injector results show no extra information and therefore have not been presented.

The most noticeable differences are that the line pressure is always larger than the sac pressure for a particular opening pressure. Consequently, the line pressure cannot be used to approximate the sac pressure in an attempt to predict the penetration for a mechanical injector. A comparison of engine loading cases for the different injectors shows that the difference between the line and sac pressures is also dependent on these parameters. Thus, there is no simple relationship that can be given that would predict this difference.

The sac pressure is important to the spray that develops as it influences the exit velocity of the fuel. So far, only the sac pressure has been shown to be a function of time. For

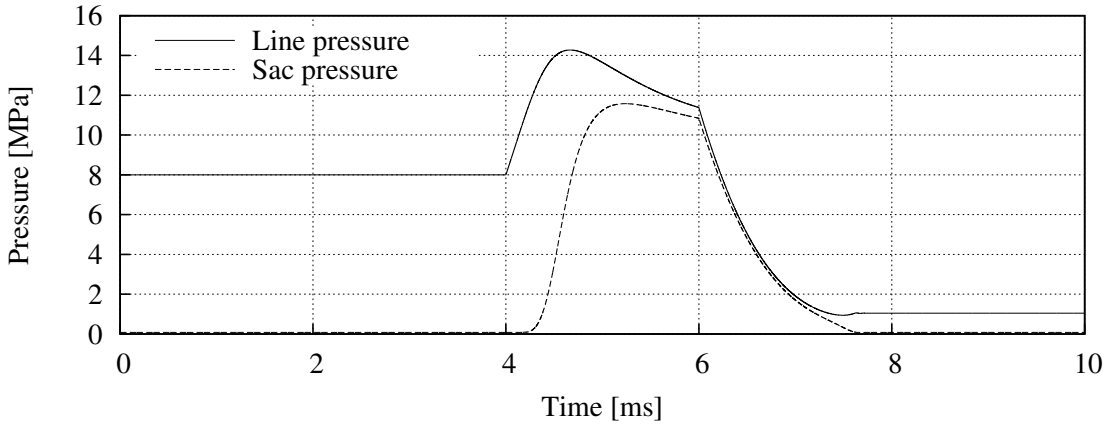


Figure 5.5: Line and sac pressure for three orifice injector, low engine load and 10 MPa opening pressure.

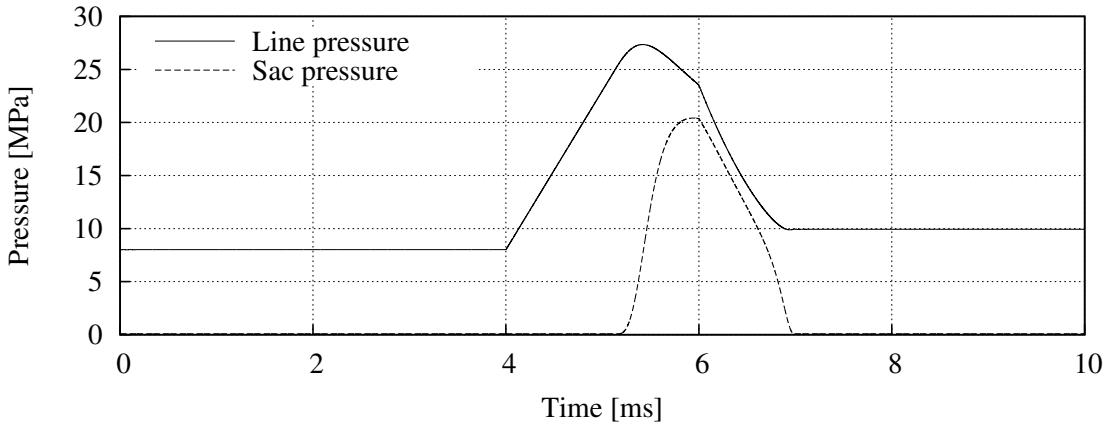


Figure 5.6: Line and sac pressure for three orifice injector, low engine load and 25 MPa opening pressure.

the penetration equations, an average injection pressure is more useful. This average sac pressure is shown in Figure 5.9.

Average sac pressure

The average sac pressure was calculated for the duration of injection and not over the whole duration simulated. The results of this can be seen in Figure 5.9. The figure shows that the low and medium load average sac pressures are similar for their respective nozzles. The three orifice nozzle average pressures are higher than the four orifice nozzle. The reasons for this have been discussed above.

For both the three and four orifice nozzles, the average pressures are significantly lower

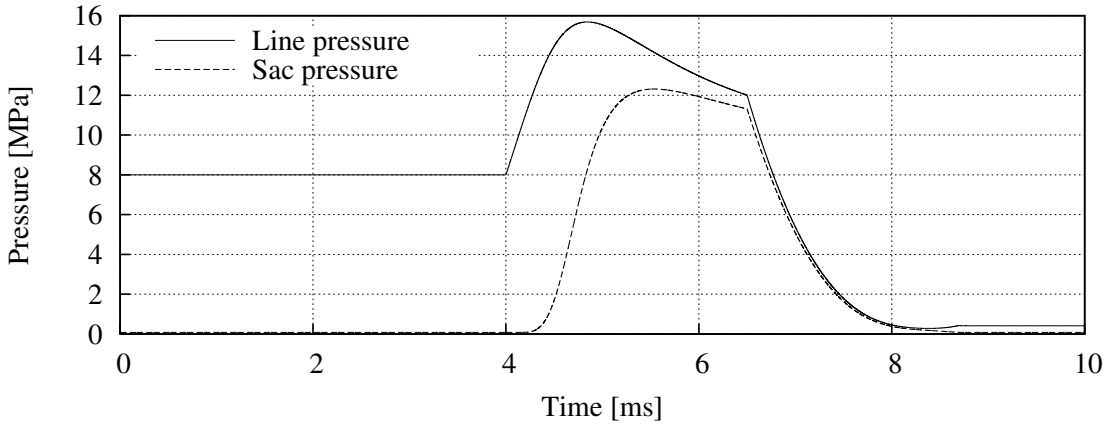


Figure 5.7: Line and sac pressure for three orifice, medium engine load and 10 MPa opening pressure.

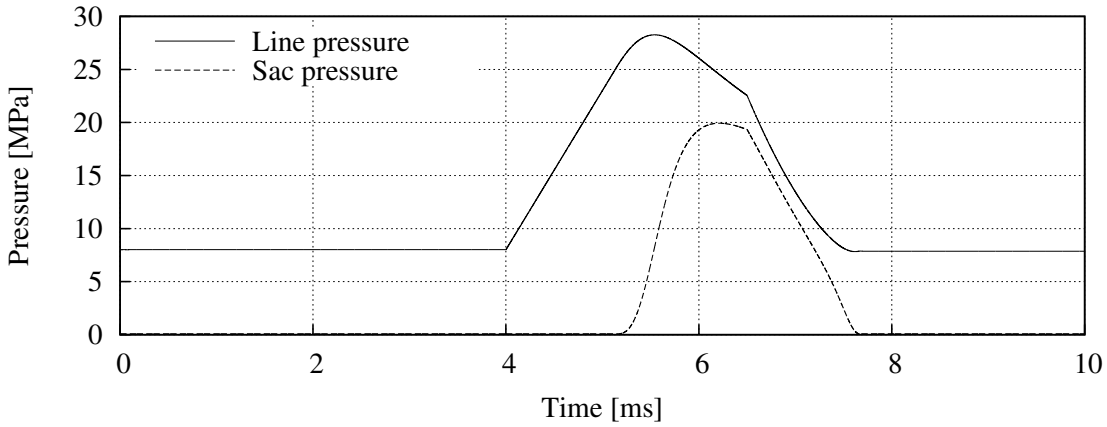


Figure 5.8: Line and sac pressure for three orifice, medium engine load and 25 MPa opening pressure.

than the opening pressures. The three orifice nozzle has an average sac pressure of 6 MPa at an opening pressure of 10 MPa and 11.8 MPa at 25 MPa opening pressure. The four orifice has an average sac pressure of 4 MPa and 8.5 MPa for an opening pressure of 10 MPa and 25 MPa respectively. The injection pressure therefore lies between 30% and 60% of the opening pressure, depending on the test condition. Therefore increasing the amount of nozzle orifices has a negative impact on atomisation, dispersion and penetration.

Figure 5.9 shows that the average pressure is therefore affected strongly by both the opening pressure and number of orifices. The average pressures are very different to the opening pressures and therefore the opening pressure is completely unsuitable as an approximation of the sac pressure and should not be used in the penetration equations.

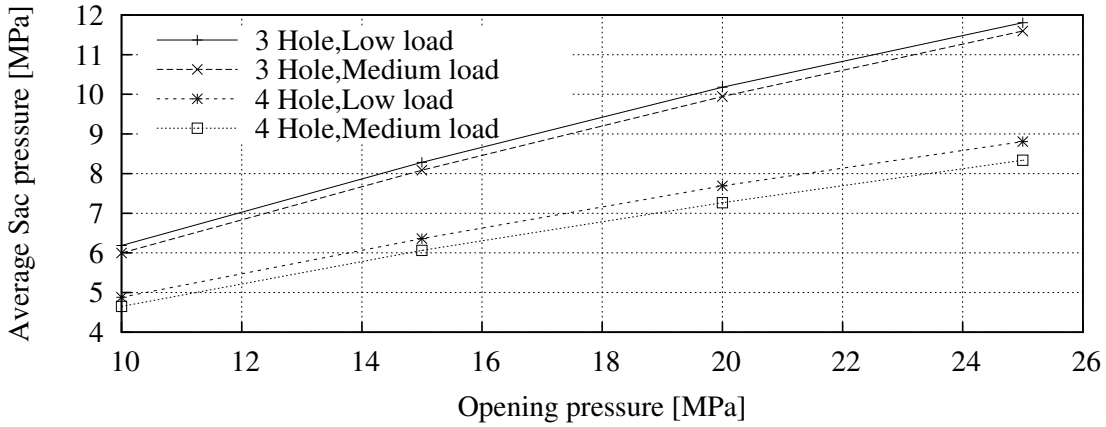


Figure 5.9: The average sac pressure versus the opening pressure for different engine loads and number of nozzle orifices.

Furthermore, the figure shows that the average pressure is significantly lower than the opening pressure of the injector, and this may explain why there was over-prediction of the penetration in Figure 3.7.

The question therefore arises that if the spray properties are degraded by increasing the number of orifices in the injector, then why is it done? It must be remembered that an engine requires a certain amount of fuel to be delivered to output the required power. The amount of fuel that is delivered is dependent on the number of orifices on the injector. This relationship will be shown by considering the injected flow rate.

5.3 Flow rate

The injected flow rate is obviously important in determining the type of spray that is formed during injection. The flow rate can therefore be analysed in terms of its peak, duration and its profile with time for the different conditions that are simulated. Another interesting aspect of the flow rate is the comparison between the injected rate and the rate supplied by the pump.

The total flow rate delivered by a three and four orifice injector gives an indication of how fuel is delivered into the chamber and from the volume of fuel delivered, predictions about the power produced by the engine can be made. To compare these two injectors in terms of the spray that will develop, the flow rate through a single orifice should be compared instead. Thus, the total flow rate and the flow rate through

a single orifice of the injector will be discussed. A comparison of the two rates will be made, and then the injected rate will be discussed in relation to the supplied flow rate from the pump.

5.3.1 Total flow rate

The injected flow rate is important in describing the spray evolution because of the dependence between it and the exit velocity of the fuel from the injector. This flow rate is strongly related to the sac pressure, and thus, they can be easily compared. The flow rate for the three orifice injector for the low and medium engine loading conditions are shown in Figures 5.10 and 5.11 respectively, while the four orifice results are presented in Figures 5.12 and 5.13 respectively. In these plots, the flow rate is shown for the different injector opening pressures.

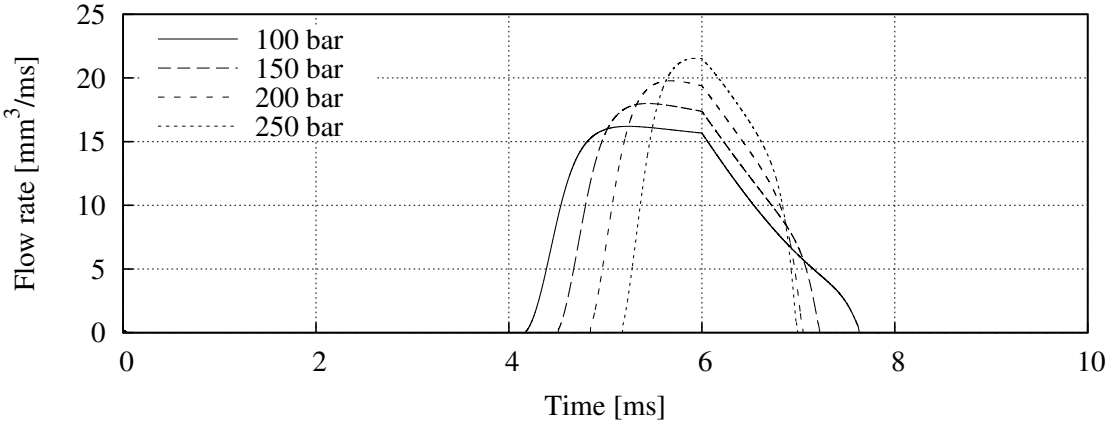


Figure 5.10: Comparison of the flow rate versus time for the three orifice injector at low engine load for different opening pressures.

Figures 5.10 to 5.13 show how the flow rate compares for different opening pressures. Like the pressure results, the important difference in the flow rate is the peak flow rates attained and the injection durations. The reason these features are similar to those of the pressure results is that the flow rate and the pressure are directly proportional.

In these figures it can be seen that the pressure drops off towards the end of injection. This drop off from its peak to zero is fastest for higher opening pressures because the pressure in the sac is largest, resulting in a large pressure difference driving the fuel. In an engine, this is desirable because the fuel cut off is more abrupt, preventing poor quality sprays from forming at the end of injection. The low load and low opening

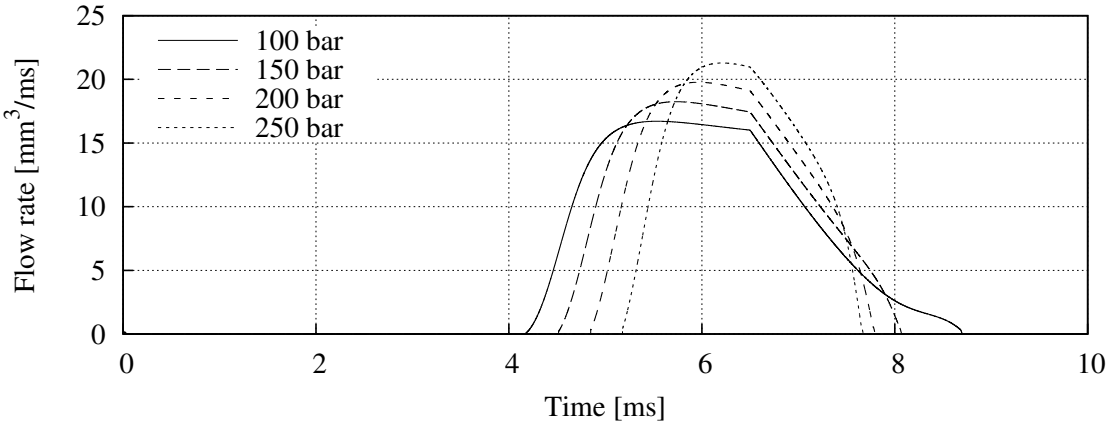


Figure 5.11: Comparison of the flow rate versus time for the three orifice injector at medium engine load for different opening pressures.

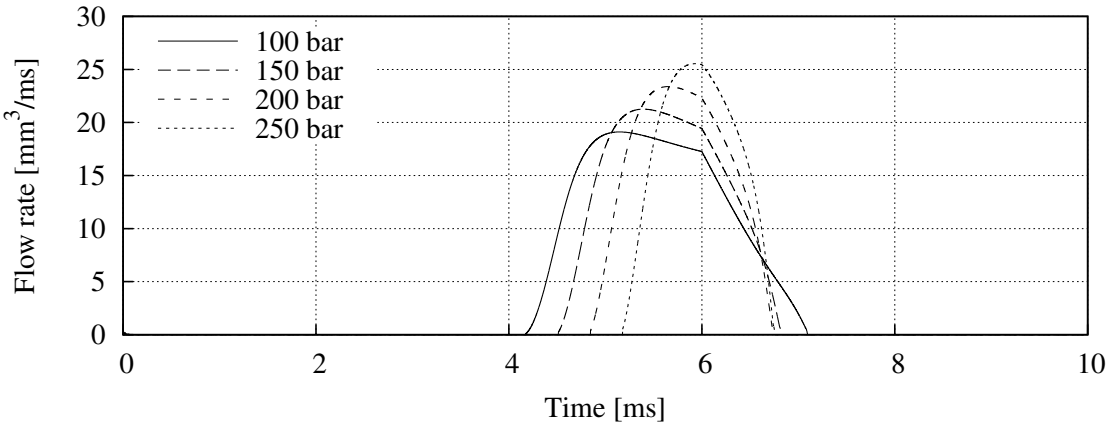


Figure 5.12: Comparison of the flow rate versus time for the four orifice injector at low engine load for different opening pressures.

pressure conditions however, show the flow rate decreasing gradually towards the end of injection (see Figure 5.10 for example). For high opening pressures and medium engine loads, the injected fuel should atomise well over the entire injection event.

5.3.2 Flow rate through a single orifice

In Chapter 3, it was mentioned that the spray from a four orifice injector penetrated more slowly into the chamber than if injected by a three orifice injector. This is also discussed by Rice [33] in more detail. This suggests that the exit velocity, and therefore injection flow rate, is lower for a four orifice injector. Comparing the flow rate of the three and the four orifice injectors in Figures 5.10 to 5.13 however, it can be seen that the average flow rate for the four orifice injector is higher, which seems counter-intuitive.

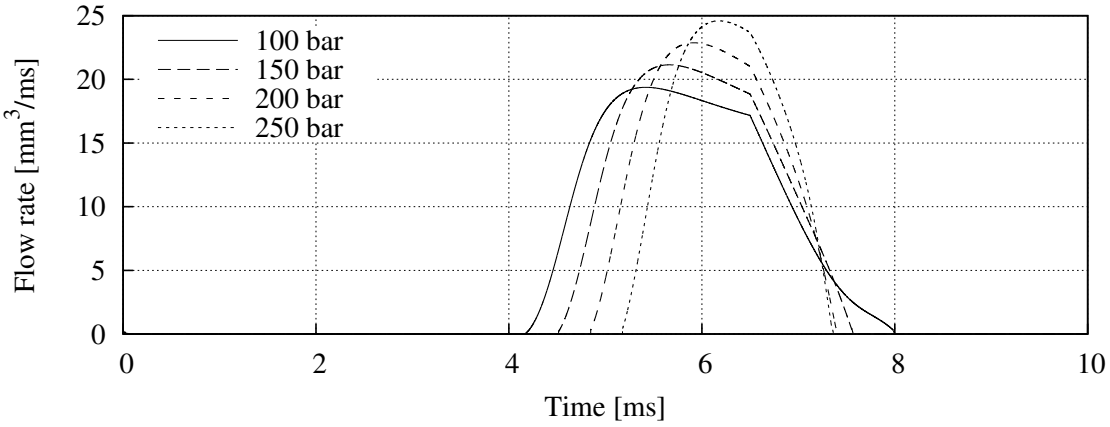


Figure 5.13: Comparison of the flow rate versus time for the four orifice injector at medium engine load for different opening pressures.

In an attempt to explain this occurrence it is necessary to present the flow rate through a single orifice of the injector. This is done by dividing the total flow rate by the number of discharge orifices. The results of this are shown in Figures 5.14 and 5.15 which show the flow rate through a single orifice for an opening pressure of 10 MPa and 25 MPa at low and medium load conditions.

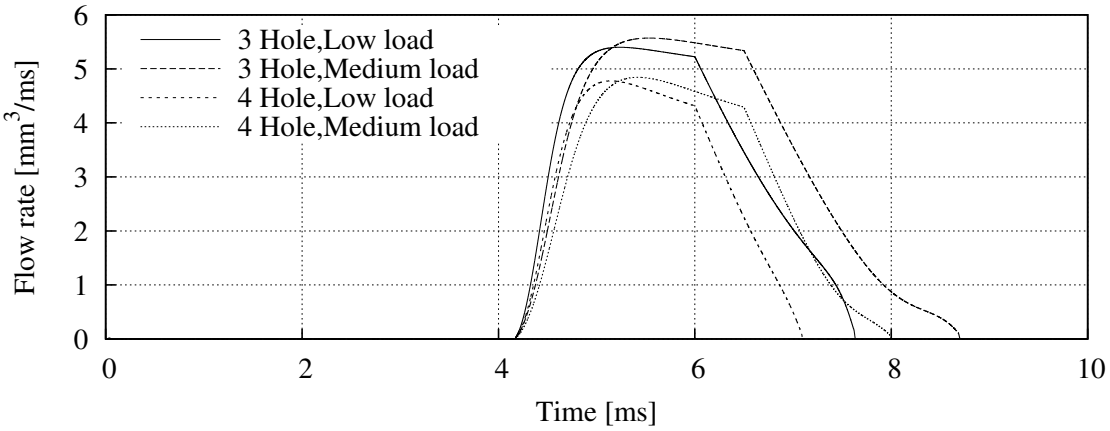


Figure 5.14: Comparison of the flow rate through a single orifice of a three and four orifice injector at low and medium engine loading conditions for an injector opening pressure of 10 MPa.

Now it can be seen that the flow rate through the three orifice injector is larger for all load and opening pressure conditions in comparison to the flow rate through the four orifice injector. The three orifice injector offers greater constriction to the flow, allowing more time for the pressure to build up to drive the fuel resulting in the higher flow rates. The three orifice injector would therefore have a better atomised, dispersed and more penetrating spray. The figures show that increasing the number of orifices

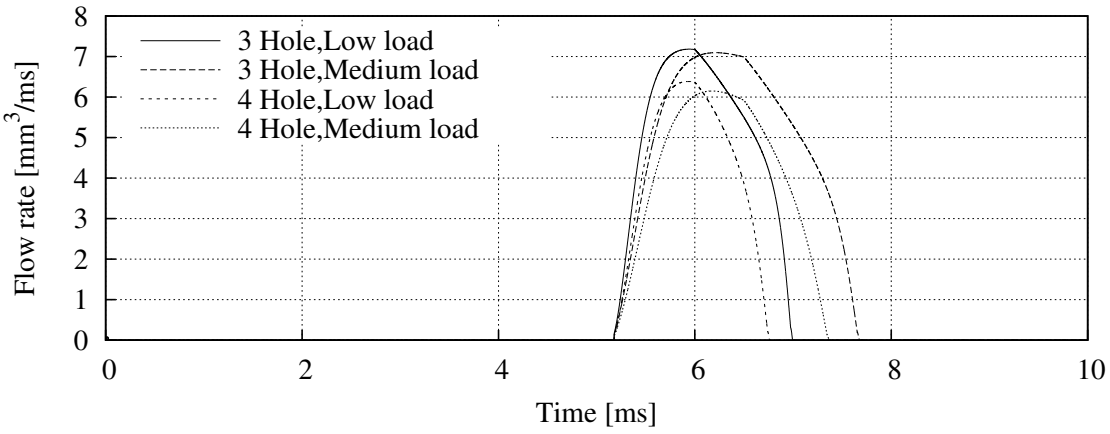


Figure 5.15: Comparison of the flow rate through a single orifice of a three and four orifice injector at low and medium engine loading conditions for an injector opening pressure of 25 MPa.

in the injector is a compromise between having a high flow rate where there are fewer orifices, and injecting a larger volume in a shorter time with more orifices.

5.3.3 Injected and supplied flow rate comparison

By comparing the supplied fuel flow rate in Figure 4.9 to the injected flow rates of Figure 5.10 to 5.13, the amplification of the supplied flow rate by the injector system can be observed. The flow rate supplied by the pump is 15 mm^3/ms while the injected rate ranges from 16 mm^3/ms for a three orifice, low load simulation to 25 mm^3/ms for a four orifice, medium load simulation. Consequently, the most benefit is gained from the pump system at high engine loads and opening pressures.

In Figures 5.10 to 5.13 the injected flow rate decreases gradually after reaching its peak, and then there is a sudden change, where the flow rate decreases more rapidly with time. This time coincides with the end of the supply phase of the pump.

5.4 Needle lift

The needle displacement provides the most accurate information about when injection starts and ends. Thus, it is important to discuss these injection characteristics in relation to the needle lift. The needle lift also has an influence on the pressures in the system

that also needs to be discussed.

Injection characteristics

Throughout injection, the pressures and flow rates are always affected by the needle lift, but the magnitude of its influence is difficult to quantify while the pump is supplying fuel. Once the pump stops delivering fuel, the pressure profiles and consequently the injected flow rates are a function of the needle lift and remaining pressure differences only. Figures 5.16 to 5.19 show the line and sac pressure with the needle lift. The sac pressure and the flow rate are very similar and thus the flow rate is not presented.

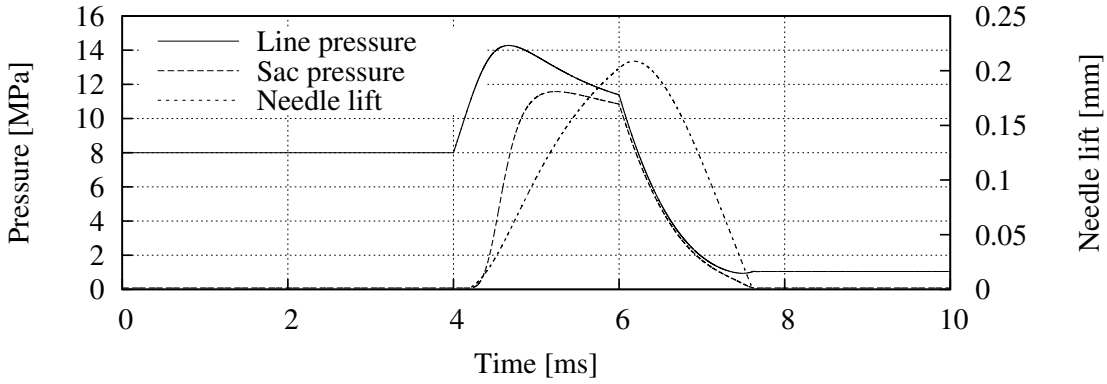


Figure 5.16: Line and sac pressure with the needle lift versus time for a three orifice injector, low engine load and 10 MPa opening pressure.

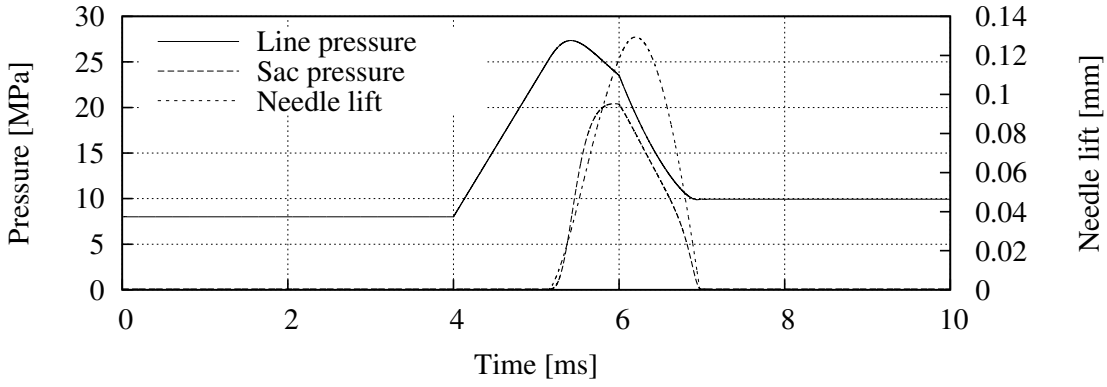


Figure 5.17: Line and sac pressure with the needle lift versus time for a three orifice injector, low engine load and 25 MPa opening pressure.

Two observations can be made from these figures that give confidence in the model. They are that the needle lift starts only once the line pressure has exceeded the opening pressure, and the sac pressure increases only once the needle lifts. The behaviour of the injector has therefore been captured in the model.

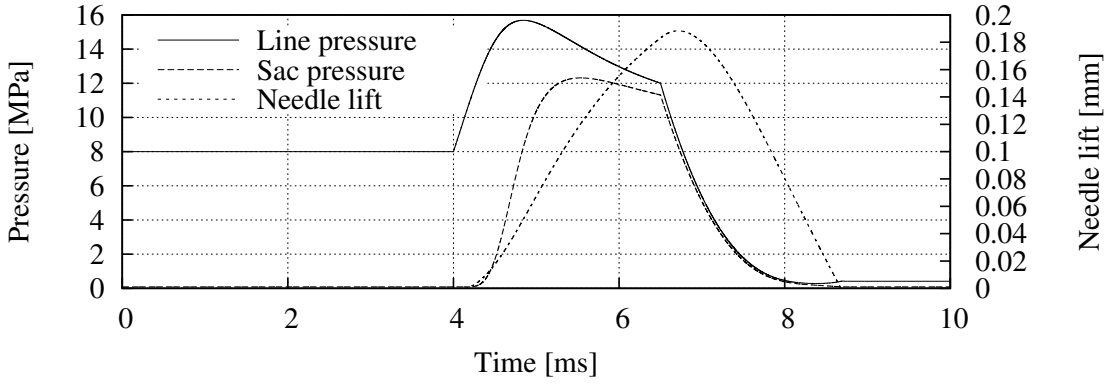


Figure 5.18: Line and sac pressure with the needle lift versus time for three orifice, medium engine load and 10 MPa opening pressure.

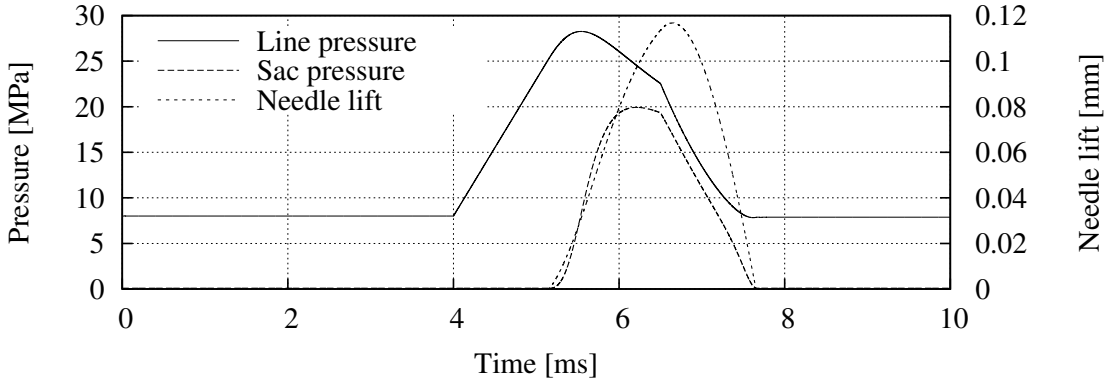


Figure 5.19: Line and sac pressure with the needle lift versus time for a three orifice injector, medium engine load and 25 MPa opening pressure.

Comparing the two pressures and the needle displacement, it can be seen that the pressure is very low, long before the injector actually closes. Because the sac pressure is close to the chamber pressure before the needle has closed, the injection event has finished prematurely due to lack of fuel. The sac and line pressures have dropped so low, that towards the end of injection, the injected flow rate has also dropped substantially. This explains what was stated above, that the flow rate drop off at the end of injection is too gradual.

The 25 MPa opening condition shows a different trend where the flow rate drops off more rapidly at the end of injection. This is because the line and sac pressures have remained high enough that a large pressure difference over the nozzle exists. This means that obtaining a steady residual line pressure before and after injection is important to the model.

Dependence of the pressure on the needle lift

Figure 5.20 shows the derivative of the line and sac pressure with time and the needle displacement. The figure is for a three orifice injector under medium engine loading conditions. This variation of load and number of orifices is shown because the features are most clearly visible. Figure 5.20 is useful to aid in explaining how the needle interacts with the line pressure.

It must be noted that the pump supply will also have an influence on the line pressure in addition to the needle motion. By considering the change in the line pressure before injection where only the pump acts and during injection where only the needle influences the pressure, their combined effect can be better understood.

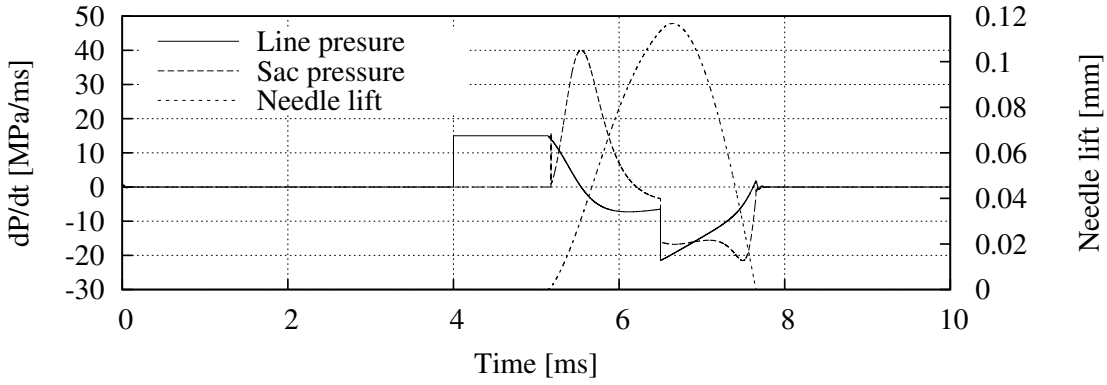


Figure 5.20: Time derivative of line and sac pressure versus time for a three orifice injector under medium engine load conditions for a 25 MPa opening pressure.

For high opening pressures, it can be seen that there is some interaction between the needle motion and the pressures at the end of injection. Figure 5.20 illustrates these better by showing the rate of change of these pressures with time and the needle lift.

From 4 ms to about 5 ms in Figure 4.9, the rate of change of pressure with time is constant when the pump is supplying fuel. During this time, the needle has not lifted and the line pressure is not sufficient to overcome the closing spring force. Consequently, the rate of change of the sac pressure is zero.

From about 5 ms, the rate of change of the line pressure decrease rapidly as the needle starts to lift thereby expanding the volume and the fuel flows into the sac volume. The pump is still supplying fuel at a constant rate, but the fuel leaving the line dominates the pressure that results. The sac pressure increases rapidly despite the needle motion

because there is a large pressure difference between the line and sac volume driving the fuel.

Just before 6.5 ms, the rate of change of the line pressure starts to increase. At this time, the pressure difference between the sac and line volumes is small (see Figures 5.1 to 5.4) and so the flow rate in and out of the line are similar.

At 6.5 ms, the pump stops supplying fuel, both the sac and line pressure rates drop discontinuously. This discontinuity is due the pump supply being modelled as a square wave. A more accurate pump supply curve would remove the discontinuity. After the minimum, the pressure rate increases up to zero as the needle starts contracting the line and sac volumes. Once the needle has reached its original closed position, injection has ceased and there can be no more change in both the sac and line pressures.

The above discussion shows that there is interaction between then needle motion and the pressures within the injector. This interaction is particularly important toward the end of injection, where the needle motion helps maintain the injection pressure, despite the pump no longer supplying fuel.

Chapter 6

The common rail model

Like in mechanical injectors, common rail injection pressures are difficult to measure or predict. Thus, using the penetration equations is again difficult since the driving pressure is unknown. This chapter details the development of a model that will be used to simulate a common rail injection system and predict the injection pressure.

Because there are similarities between the common rail and mechanical injector, the common rail model was built on the existing mechanical injector model. Initially the common rail injector was simulated in Scicos, but with growing model complexity, Scicos became slow and nonresponsive. As a solution to this, the model was reconstructed in C++ so that better results could be obtained.

6.1 Injector behaviour

To begin modelling the injector, its behaviour needs to be understood in detail. Only then can assumptions be made and equations developed that accurately describe the behaviour of the injection system.

6.1.1 Common rail system

The common rail injector derives its name from the fuel accumulator (common rail) that acts as a pressure reservoir to multiple injectors and is supplied by a single pump.

The fuel in the rail maintains an approximately constant pressure while being supplied with fuel by the pump, even during injection [37]. Since the rail pressure is constant, and so too the pressure throughout the system, the injector can no longer be actuated by a pressure signal as in a mechanical injector. Therefore electronic control of the injector is used, which can operate independently of the pressure in the system, engine speed and engine load. By introducing electronic control into the control system, many of the disadvantages that occur in mechanical injectors are also overcome. The control of injection is provided by the Electronic Control Unit (ECU) [37].

In Figure 6.1 an electronically controlled injector is shown. The diagram is only illustrative of the system, showing only the components that are important for modelling the injector.

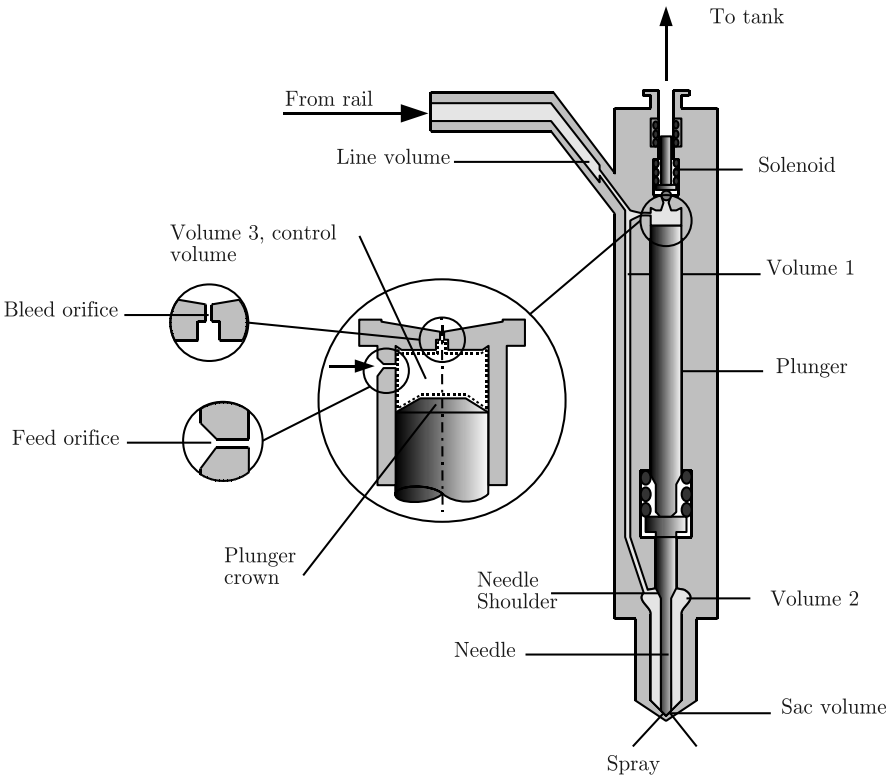


Figure 6.1: Electronically actuated common rail injector showing the different components and internal volumes that are needed for the model.

The importance of each of the components to the operation of the injector is discussed in the following sections.

Pressure balance

Like the mechanical injector, the common rail injector needle lifts when the forces acting on it are unbalanced. In mechanical injectors, the closing force is provided by the spring, but this is not the case in common rail injectors. Between injections, the pressure in each volume is equal. There is therefore equal pressure acting on the needle faces in volume 2 and on the plunger crown in the control volume. The area on which the pressure in the control volume acts is larger than the area of the needle faces at volume 2. Thus there is a large closing force maintaining the injector in a closed state.

Opening the injector

To open the injector, the forces acting on the needle can no longer be balanced and must be such that the needle will lift. Thus, the force resulting from the pressure in the control volume, F_{cv}, which acts down on the needle must be less than the force due to the fuel pressure in volume 2, F_2, which acts upwards. The only way F_{cv} can be varied is by changing the pressure in the respective volume. Thus, to open the injector, the control volume pressure must be released sufficiently that the needle will lift.

This drop in the control volume pressure is achieved by energising the solenoid above the control volume which lifts a ball that opens the bleed orifice. When the bleed orifice is open, fuel in the control volume escapes back to the tank and the pressure in the volume drops. The control of the system is therefore an electronic/fluid amplification system [37]. Injection will continue provided this bleed orifice remains open.

The solenoid does not control the needle directly because the response would be too slow or a very large solenoid would be required, which would have very high power requirements. Modern third generation injectors still use electronic control, but the needle motion is controlled directly through a piezoelectric stack. The use of the piezoelectric stack gives faster response of the needle [38].

Closing the injector

The injector is closed by de-energising the solenoid, thereby closing the bleed orifice. With the bleed orifice closed, pressure can once again build in the control volume. Once the pressure has built up sufficiently, the needle will close and injection will stop.

The electronic control unit (ECU)

The ECU allows the time when injection starts, the number of injections and the duration of injection to be controlled. Thus the injection event can be made up of multiple shorter duration injections. These are classified as the pilot injection, the main injection and secondary injection events. The inclusion of the pilot injection allows for more gradual combustion and a reduction of emissions [37].

The mechanical injector suffers from being limited to one injection per stroke as only very complex cam profiles would make multiple injections possible. The precision and cost required in making these complex cams make this option uneconomical. It is also not possible to change the injection duration independently of the engine load and speed to optimise the amount of fuel delivered.

Another advantage of the common rail injector is that through the control of the ECU and feedback from the engine speed, the amount of fuel delivered to each cylinder can be varied to produce a smoother torque output profile. This reduces vibration in the engine.

Pumping system

The pump continuously acts to maintain the rail at a constant pressure. The pumping system requires its own control so that the rail pressure does not get too high and fails. The rail therefore has a pressure sensor that opens a drain valve that releases the excess pressure by allowing some fuel to return back to the tank.

An advantage of the common rail over the mechanical injection is that the pumping system is decoupled from the injection event. As a result, the duration of the injection and the amount of fuel injected is unaffected by the pump. This is one of the reasons

that electronic control of the injector is possible.

Injection

Besides the actuation method, the injector operates in a similar way to the mechanical injector. Needle lift opens the passageways that allow the fuel to travel to the nozzle tip and to be injected. The flow behaviour is similar to the mechanical injector.

Due to the injector being fed by a constant and high pressure accumulator, the flow rate through the injector is approximately constant and high. The resulting high velocity results in spray that is well atomised and has good penetration.

6.1.2 Assumptions

Now, with a better idea of how the system works, some assumptions can be developed. Several assumptions were only used in the Scicos model, but were discarded as more complexity could be introduced with the C++ model.

The assumptions that are used here are similar to those in Section 4.1.3 and so are not explained again. Some assumptions have been abandoned as the model developed in order to improve the accuracy of the solution. These differences will be discussed as they are included into the model.

1. The solenoid is not modelled. Rather its affect on the control of the system, which is to open the bleed orifice, is modelled by setting the bleed orifice as either open or closed.
2. The time that the solenoid is energised for and the time that the bleed orifice is open are the same.
3. The common rail acts as a perfect accumulator, and thus any fluctuations in the pressure are negligible, even during injection [37].
4. Volumes containing fuel do not change size due to changes in pressure.
5. The needle is rigid. This is reasonable as the effect that a non-rigid needle has on the injection event is small [27].

6. Gravitational forces are negligible in comparison to the forces present in the injector.

7. Cavitation is ignored.

8. The discharge coefficient of the flow through orifices is set at 0.6, which is typical for flows through an orifice [23].

9. There is no leakage of fuel out of the injection system.

10. Variation in bulk modulus and density with pressure are not taken into account in the Scilab model because this model is an extension of the mechanical injector and it keeps the system simple. This assumption will be abandoned in the C++ model, where adding the extra complexity is a simple process.

11. Temperature remains constant.

12. Flow within the nozzle is one dimensional along the axis of the passage.

In assumption 1, the electrical behaviour of the solenoid is excluded from the model. The solenoid's purpose, which is to open the bleed orifice, must be included or the injector model would be inaccurate. It is chosen to simply model the bleed orifice as open during injection and closed at all other times. Inclusion of the solenoid would be a recommended refinement to the model, allowing for prediction of the delay between the firing pulse and the actual time where the injector would be open. The minimum opening times of the injector could then also be predicted.

Assuming that the system is rigid means no expansion or contraction of any internal volumes of the injector is possible when there is a change of pressure of the fuel. This is a reasonable assumption because the pressure changes in the system are relatively small, resulting in only small changes in the volumes.

6.2 Injector geometry

The common rail injector model requires information about the size of the internal volumes, flow cross-sectional area between volumes and the dimensions of the needle.

These dimensions were obtained by disassembling an identical injector and, where necessary, cutting it and measuring the required features. Cutting the injector introduces heat that may distort the injector and result in inaccurate measurements. To account for this, a sensitivity analysis will be done to understand how this will affect the model. Figures 6.2 to 6.5 show photographs of the different components that were measured to obtain the required inputs for the model.

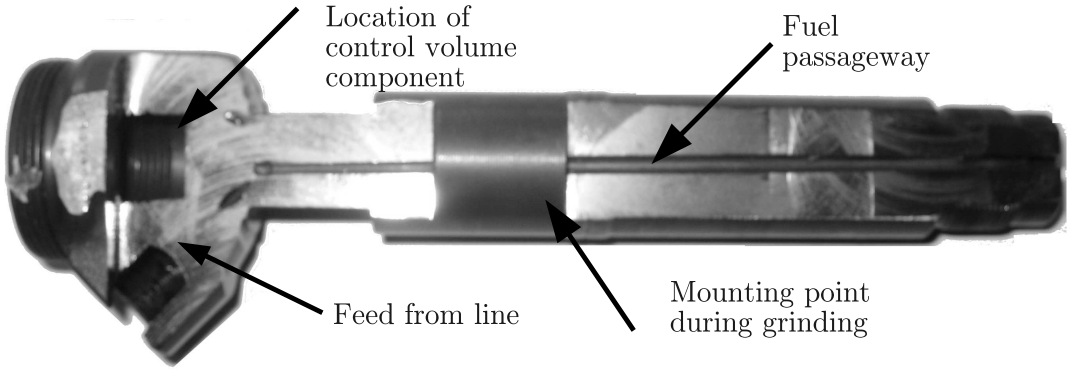


Figure 6.2: Photograph of the sectioned body of the injector showing the passageway of the fuel to the nozzle.

Figure 6.2 shows the body of an injector that has been ground down to show the passageway that the fuel flows through and from this, the diameters of these passageways were measured. Because the injector was not ground down in the same plane as this passageway, it is not visible throughout its length and thus, the passageway for the fuel from the line is not apparent in the figure. It is however assumed that the diameter of this passageway is uniform throughout the injector. The location of the control volume component shown in Figure 6.3 is indicated in Figure 6.2.

In Figure 6.3, it can be seen that different degrees of wear on the surface of the bore has occurred. At the very top of the bore, there is an area that is worn significantly differently from the rest of the bore. This area shows the limit of the plunger's motion, but also gives an indication of the size of the control volume of the injector, which is also useful in the model. In this figure, the location of the bleed and feed orifices is also shown, however the actual orifices are not visible because the component has been ground down too far. The diameters of these orifices were measured on another similar injector in The School of Mechanical Engineering Metrology laboratory.

Figure 6.4 shows the nozzle for the common rail injector. A passageway where the fuel

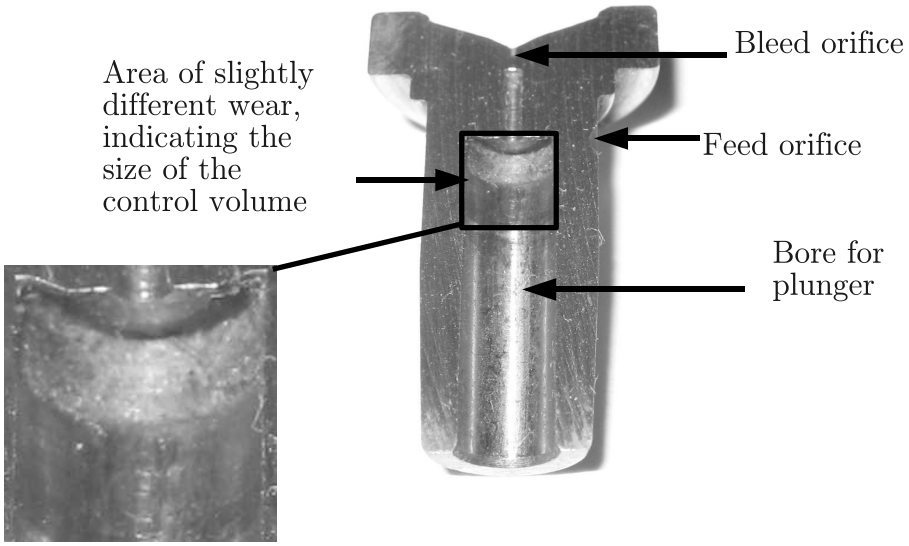


Figure 6.3: Photograph of the control volume component showing the control volume, the bore for the plunger, and the feed and bleed orifices

flows through is shown on the right of the photograph. This passageway lines up with that of the passageway in the body of the injector in Figure 6.2. An internal volume is indicated in this photograph.

Figure 6.5 shows the injector needle and the shoulders where its diameter changes along its length. The fuel pushes against these shoulders to open the injector during injection.

6.3 Scicos model

Once again, Scicos is used to model the injector. Many of the equations used in the common rail injector are similar to those used in the mechanical model. Thus, the mechanical model was used as a base that was adapted to model the common rail injector.

6.3.1 Scicos equations

The equations governing the common rail system are developed in the same way those for mechanical injectors in Chapter 4. Differences arise due to the different geometry of the common rail injector and its pumping and control systems.

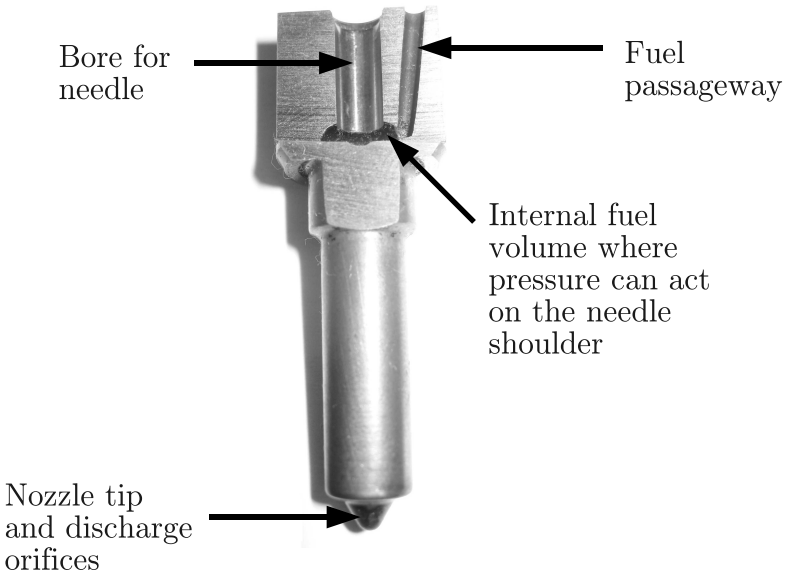


Figure 6.4: Photograph of the nozzle of the injector showing the fuel passageway and an internal fuel volume.

Fluid equations

The common rail can be modelled in a similar way to the mechanical injector, thus the equations have a similar form. The primary difference is that the control volume needs to be included. The following equations were used to describe the fluid flow of the injector in the Scicos model:

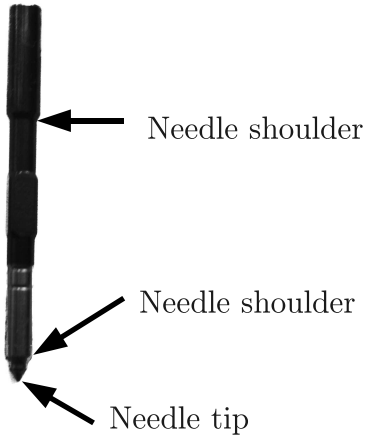


Figure 6.5: Photograph of the injector needle showing the shoulders and the needle tip.

$$\begin{aligned}
\frac{dP_1}{dt} &= \frac{\beta}{v_1 - xA_{1,2}} \left[Q_{in}(t) + A_{1,2}\dot{x} - Q_{1,2}(t) - Q_{1,3}(t)\right] \\
\frac{dP_2}{dt} &= \frac{\beta}{v_2 - xA_2} \left[Q_{1,2}(t) + A_2\dot{x} - Q_{2,a}(t)\right] \\
\frac{dP_3}{dt} &= \frac{\beta}{v_3 + xA_1} \left[Q_{1,3}(t) - A_1\dot{x} - Q_{3,b}(t)\right]
\end{aligned} \tag{6.1}$$

where dP_1/dt is the change in pressure in volume v_1 which extends from the rail to the line, into the injector and to the needle tip. Volume v_2 is the sac volume plus the volume created by the needle displacement. Volume v_3 is the control volume above the plunger. Modelling this volume is the only addition to the common rail model over the mechanical model.

Equation (6.1) represents the time derivative of pressure within a volume of the injector. The accuracy of the solution obtained can be improved by increasing the number of volumes modelled and decreasing the size of each division. A limit as to how many volume divisions can be made is that for each division, an additional ordinary differential equation (ODE) must be solved. Computation time therefore increases rapidly when greater complexity is included.

In Equation (6.1) it is noticed that P_1 and P_2 are affected positively by the area and velocity term whereas P_3 is affected negatively. This is because a positive plunger velocity represents a flow rate into the volume in v_1 and v_2, but a flow rate out in v_3.

In Equation (6.1) it is seen that there is a sac volume. However the injector that is used for testing is a valve covered orifice (VCO) injector that has no sac. In order to model the pressure in the volume immediately before the orifice, it was necessary to create an artificial volume and thus the inclusion of this sac volume. This volume is small, and therefore should not dominate the solution.

The flow rates from v_1 to v_2 are as in Equation (4.5). Equation (6.2) shows the flow rates into and out of v_3.

$$Q_{13}(t) = a_{1,3}c_{d,f}\sqrt{\frac{2(P_1 - P_3)}{\rho}}$$
$$Q_{3b}(t) = a_{3,b}c_{d,b}\sqrt{\frac{2(P_3 - P_b)}{\rho}} \tag{6.2}$$

The areas a_{13} and a_{3b} have their usual meaning in that their subscripts show the constriction area of the orifice joining two volumes. Unlike the discharge coefficients c_d in Equation (4.5) which have been assumed to be constant, unique discharge coefficients for the feed and bleed orifice have been introduced in Equation (6.2) representing the discharge coefficients for the feed and bleed orifice respectively. The discharge coefficients $c_{d,f}$ and $c_{d,b}$ are treated as constants in the Scicos model, but can be varied in the C++ model. The importance of being able to vary the value of these discharge coefficients will be shown in Section 6.4.6. P_b is the pressure that the control volume vents to when the bleed orifice is opened.

Needle dynamics

The needle dynamics for the common rail system is similar to the mechanical injector except that the balancing of the forces is different due to the pressure acting on the crown of the plunger. This is similar to Equation (4.7).

$$\ddot{x} = \frac{1}{m}\left(P_1 A_{(1,3)} - P_3 A_0 + F - c_1\dot{x} + k_1 x\right) \tag{6.3}$$

So, all that has changed from the mechanical injector to the common rail injector is that the pressure P_3 acts on area A_0 instead of the atmospheric pressure.

The maximum lift of the needle is limited by the injector. This is a boundary condition that needs to be imposed on the model. This limit is also introduced into the model by [28]

6.4 Conversion to C++

While modelling the injector in Scicos, some differences between the simulation results and the experimental results were observed. It was hoped that by dividing the injector into smaller volumes and removing some simplifying assumptions, better results would be attained.

Improving the model with additional equations proved to be difficult because Scicos become slow and non responsive. Scicos also includes many libraries that may not be needed for a solution, which increases the solving time of the simulation. Thus, it was decided to convert the Scicos model into a C++ program.

In the transition to C++, it became necessary to use numerical methods for the required integration. These methods are explained first. The basic outline of the program is presented to clarify its operation. Following that, the equations that are used in this program are presented. Fundamentally these equations are not different to those used in Section 6.3.1. The only differences arise due to the increased number of volumes taken into account and the inclusion of the variation of density and bulk modulus with pressure.

6.4.1 Numerical integration method

The solution requires that numerous ODEs must be solved. An analytical approach would be difficult because there are many variables and they are all dependent on each other. Thus, a numerical integration is required.

The C++ program used trapezoidal integration as a first approximation. In the interest of speeding up solving time and accuracy, a fourth order Runge-Kutta method was later implemented. Runge-Kutta methods are commonly used for solving ordinary differential equations [39].

Trapezoidal integration

From the Riemann sum, integration is the process of calculating the area created by two points on a curve and the x-axis as a rectangle, where the difference between the points tends to zero. In numerical integration, the difference between these points does not tend to zero because this would increase the time required to solve the solution. Consequently, errors are introduced into the solution.

A better approximation to calculating the area under the curve by using rectangles is to use trapeziums. This gives a closer approximation to the actual solution than using rectangles, but again requires very small time steps for sufficient accuracy. Trapezoidal integration does provide simplicity because it can be used to integrate any function provided the current and previous points are known.

Runge-Kutta (RK)

Runge-Kutta methods provide better solutions to integration than the trapezoidal method by reducing the truncation error [39]. Runge-Kutta methods are used to solve equations of the following form [39]:

$$\frac{dy}{dx} = f(x, y), \tag{6.4}$$

which is in the same form as the equations that need to be solved in the model.

There is a significant difference between Runge-Kutta and trapezoidal integration. The Runge-Kutta method requires the equation that is being integrated. Trapezoidal integration only requires the x and y values.

An explanation of the numerical methods used here must begin with Euler's method which is the simplest form of the Runge-Kutta method which was ultimately used in the model. The one step Euler method assumes that the slope at the beginning of the interval is the same as the slope over the entire interval [39]. With this assumption linear extrapolation over the interval is carried out to calculate the value at the end of the interval. Thus:

$$y_{i+1} = y_i + f(x_i, y_i)h. \tag{6.5}$$

For sufficiently small time steps between intervals h, this method can approximate the actual solution well, but this is at the expense of computation time. If the time step size is large, then a significant error is introduced into the solution. This can be seen in Figure 6.6.

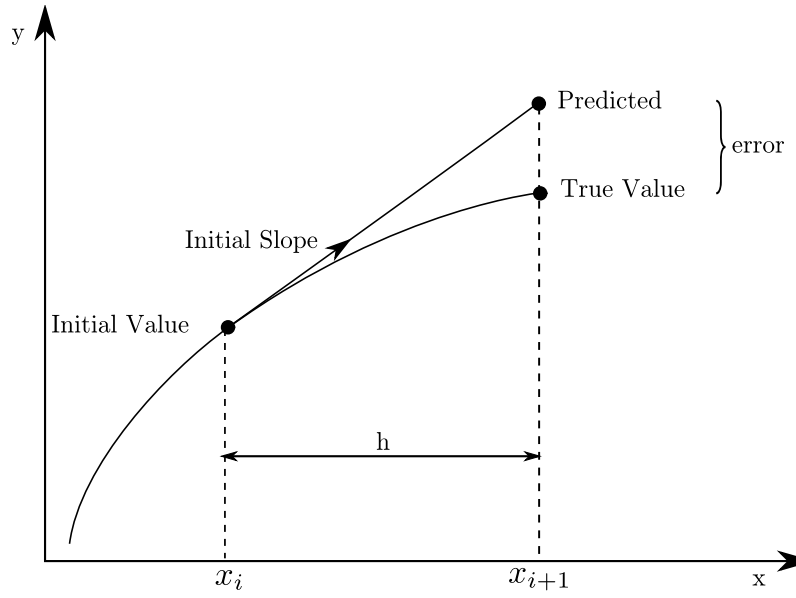


Figure 6.6: Euler's approximation of numerical integration.

The error for each time step is cumulative. Thus the error can become large very quickly. Improvement to the Euler's method is achieved by getting better approximations of the slope over the interval.

Heun's method (also known as a second order Runge-Kutta) calculates the derivative at the beginning and end of the interval. The derivative at the second point is based on the value calculated from the Euler's method. See Figure 6.7(a).

These derivatives are then averaged to calculate the next point. Thus there is a correction that is occurring to the Euler's method [39]. The effect of this can be seen in Figure 6.7(b). Correction to Euler's method occurs in other integration methods as well.

Heun's method is therefore given by:

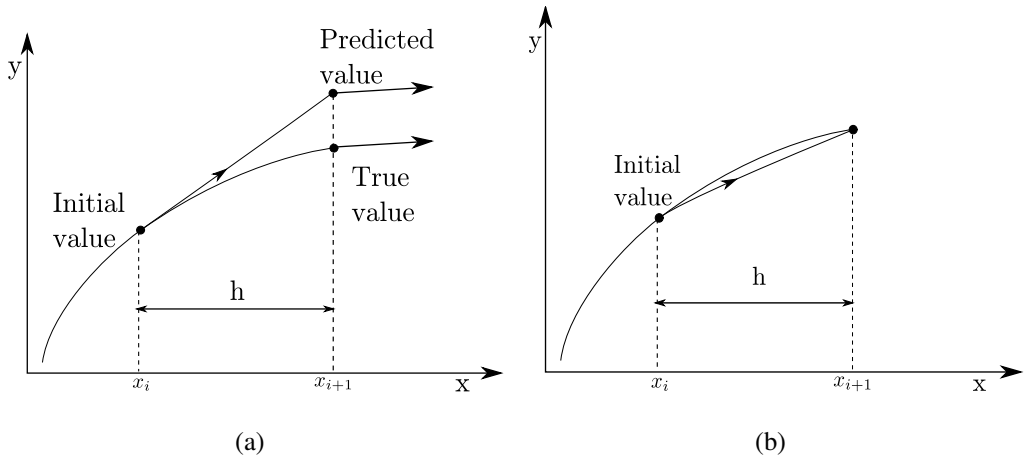


Figure 6.7: The slope at the beginning and end of Heun's approximation.

$$y_{i+1} = y_i + \frac{f(x_i, y_i) + f(x_{i+1}, y^0_{i+1})}{2} h \tag{6.6}$$

where y^0_i is the intermediate approximation of the gradient [39].

The Heun's approximation is actually a special case of the second order Runge-Kutta approximation. It is presented because it shows how the average slope over the interval can be approximated.

The fourth order Runge-Kutta has many versions, but the most common is where four approximations of the derivative are taken. The Heun's method, or second order Runge-Kutta, requires only two approximations of the gradient to be calculated.

For a time dependent problem the equation to be used is:

$$\frac{dx}{dt} = f(t, x). \tag{6.7}$$

From this, constants which represent the slopes at different points of the solution interval are constructed in the following form:

$$\begin{aligned} k_1 &= f(t, x_n) \\ k_2 &= f(t + \frac{1}{2}h, x_n + \frac{1}{2}k_1 h) \\ k_3 &= f(t + \frac{1}{2}h, x_n + \frac{1}{2}k_2 h) \\ k_4 &= f(t + h, x_n + k_3 h) \end{aligned} \tag{6.8}$$

Note that the preceding constant is used in calculating the following constant. For example, k_1 is used in the calculation of k_2. Therefore, this method of numerical integration is very efficient when solved on a computer [39].

The slopes calculated are then averaged to obtain the solution at the end of the interval. The classical Runge-Kutta approximation uses the following weighting system to obtain an average.

$$x_{n+1} = x_n + \frac{1}{6}(k_1 + 2k_2 + 2k_3 + k_4) \tag{6.9}$$

This weighting of the slopes to calculate the solution places more emphasis on the slopes in the middle of the solution interval. The classical Runge-Kutta method is used because it offers an efficient solution for computational solving.

Application of RK method to the common rail model

The common rail equations are far more complicated than Equation 6.7, requiring numerous results from multiple ODEs. Thus, the form of the equation changes to include multiple time dependant variables and their constants. For two ODEs, Equation 6.7 becomes:

$$\frac{dx}{dt} = f(t, x, y)$$

$$\frac{dy}{dt} = g(t, x, y). \tag{6.10}$$

The slopes across the interval need to be calculated for x and y. The constants for $f(x)$ and $g(x)$ are k and i respectively.

$$\begin{aligned}
k_1 &= f(t, x_n, y_n) & i_1 &= g(t, x_n, y_n) \\
k_2 &= f(t + \frac{1}{2}h, x_n + \frac{1}{2}k_1 h, y_n + \frac{1}{2}i_1 h) & i_2 &= g(t + \frac{1}{2}h, x_n + \frac{1}{2}k_1 h, y_n + \frac{1}{2}i_1 h) \\
k_3 &= f(t + \frac{1}{2}h, x_n + \frac{1}{2}k_2 h, y_n + \frac{1}{2}i_2 h) & i_3 &= g(t + \frac{1}{2}h, x_n + \frac{1}{2}k_2 h, y_n + \frac{1}{2}i_1 h) \\
k_4 &= f(t + h, x_n + k_3 h, y_n + i_3 h) & i_4 &= g(t + h, x_n + k_3 h, y_n + i_3 h).
\end{aligned}$$

Notice here the constants of k are used in the calculations for the constants of i and vice versa which also makes the number of calculations that actually need to be done much less.

Now the equations need to be combined to obtain the solution. They have the same form as the Equation (6.9). Thus the solutions $F(x)$ and $G(x)$ are approximated by:

$$x_{n+1} = x_n + \frac{1}{6}(k_1 + 2k_2 + 2k_3 + k_4)$$

$$y_{n+1} = y_n + \frac{1}{6}(i_1 + 2i_2 + 2i_3 + i_4)$$

The C++ common rail model requires eight ODEs to be solved, thus there are eight unique sets of constants that must be solved for.

6.4.2 Program flow

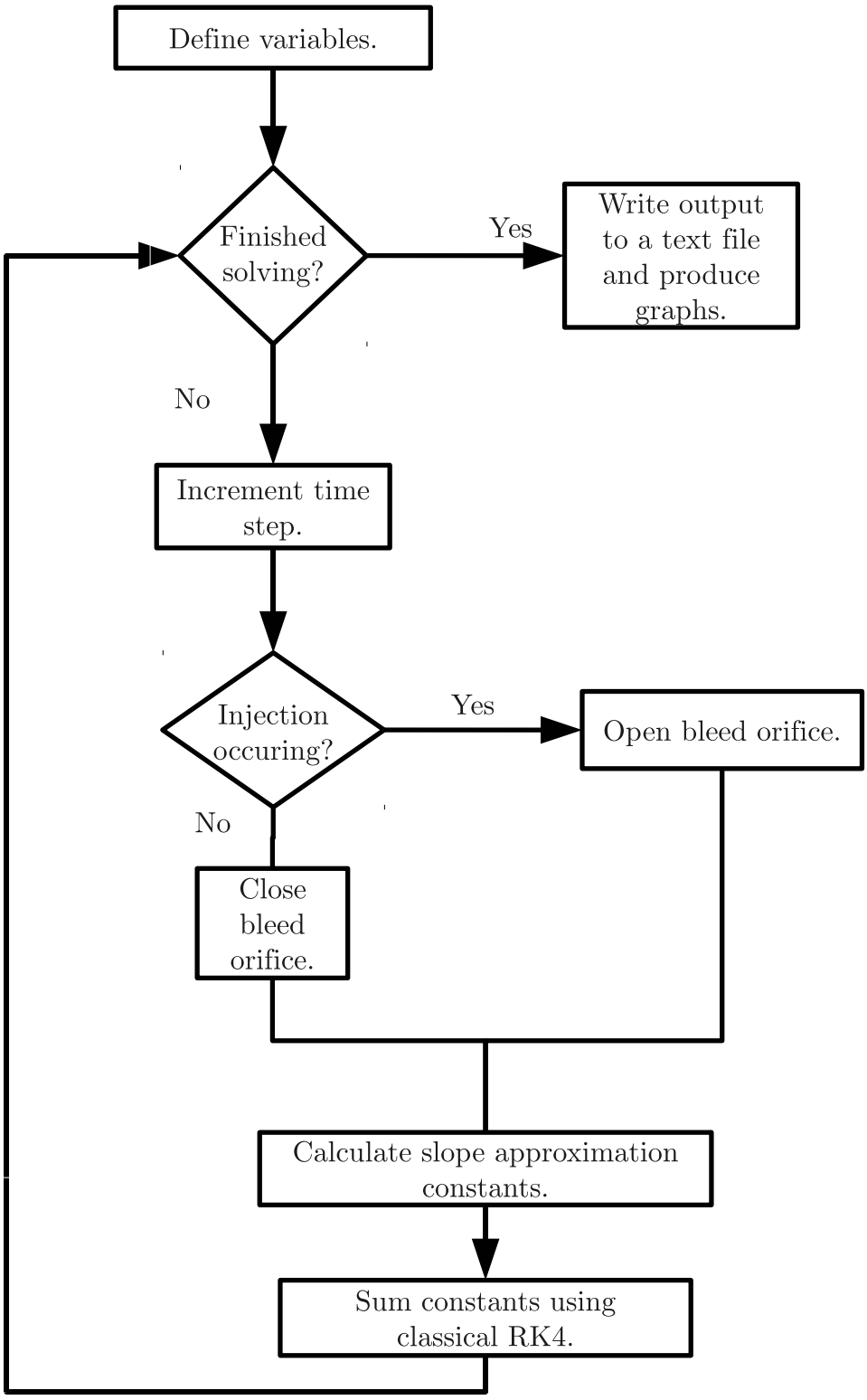


Figure 6.8: The flow of the program for the C++ solution.

The structure of the C++ program can be seen in Figure 6.8. The full listing of the program is presented in Appendix C.3. The first decision block controls how long the

program runs based on the desired start and end time inputs. Typically the start time is set at zero. The program runs from the start time to the end time in increments that are defined by the user. This increment is the time step size of the model or h in the RK approximation.

The current time that the program is solving for is the summation of all the increments that have been run so far. The current time of the solution is then compared to the end time. If the current time equals or exceeds the end time, then the solution is complete and the results can be saved. If not then the decision is taken to continue solving. The main part of the program occurs within the loop defined by this control function.

The second decision block within the main loop controls when injection occurs. Injection must occur at some point within the solution time. The injection is defined by its own start and end time, the difference of which gives the injection duration.

In Section 6.1.2, the assumption was made that the electrical component of the solenoid would not be included in the model. The bleed orifice would be opened to indicate the start of injection. Thus, the second decision block opens the bleed orifice during the injection time already defined. If injection is not occurring, then the bleed orifice is set as being closed. All calculations are then carried out in the final two blocks within the main loop. This section represents the greatest portion of the solution in terms of computation time as this is where all the equations are solved. Once the solution is complete, all the output values required are written to a text file on which post-processing can be carried out.

6.4.3 C++ common rail injector equations

The equations defining the injector behaviour can now be developed. Like the mechanical injector, the common rail equations need to be separated into the fluid and needle parts.

Fluid equations

To describe the fluid component, the internal volumes of the injector have been divided into five volumes. This division occurs where there are significant constrictions to the flow.

In the Scicos model, volume v_1 encompassed the line and many of the internal volumes of the injector. In order to improve the solution, this volume has been divided into three smaller sub-volumes. The line feeding the injector became a unique volume v_l, and the internal volume of the injector is split further into two. The first volume, v_1, is from the line through to the chamber where the fuel acts on the shoulder of the needle. This volume has two outlets, one to the control volume v_{cv}, and the other to the next volume v_2. Volume v_2 is from the chamber to the needle tip, but does not include the sac volume.

Equation (6.11) describes the fluid component injector accounting for the additional volumes:

$$\begin{aligned}
\frac{dP_l}{dt} &= \frac{\beta(P_l)}{v_l}\left[Q_{r,l}(t) - Q_{l,1}(t)\right] \\
\frac{dP_1}{dt} &= \frac{\beta(P_1)}{v_1}\left[Q_{l,1}(t) - Q_{1,2}(t) - Q_{1,3}(t)\right] \\
\frac{dP_2}{dt} &= \frac{\beta(P_2)}{v_2 - xA_{2,3}}\left[Q_{1,2}(t) + A_{2,3}\dot{x} - Q_{2,3}(t)\right] \\
\frac{dP_3}{dt} &= \frac{\beta(P_3)}{v_3 - xA_3}\left[Q_{2,3}(t) + A_3\dot{x} - Q_{3,A}(t)\right] \\
\frac{dP_{cv}}{dt} &= \frac{\beta(P_{cv})}{v_3 + xA_{cv}}\left[Q_{1,cv}(t) - A_{cv}\dot{x} - Q_{cv,b}(t)\right]
\end{aligned} \tag{6.11}$$

where Q_r is the flow rate out of the rail. Notice that volumes v_1 and v_l have no velocity and area components because the volumes do not change during injection. P_1 has two outlet flows, one into volume v_2 and one into the control volume. In equations (6.11), the bulk modulus β is shown to be a function of the pressure in the respective volume,

this is a refinement of the C++ model. The flow rates Q have the same form as in Section 6.3.1 and the mechanical model in Section 4.1.4

Needle dynamics

The equation for the needle dynamics can be written as a Macaulay functions for the C++ program. The Macaulay function is convenient because it can be treated as an 'if' statement, dependent on the needle lift.

$$m\ddot{x} = P_1(A_1 - A_3) + P_2(A_3) - P_3(A_{cv}) - k_s x - c\dot{x} - k_{sac}\langle 0 - x\rangle - k_{limit}\langle x - x_{limit}\rangle \tag{6.12}$$

When the needle moves too far it impacts with the body of the injector and cannot move any further. In terms of forces, it means a very large force decelerates the needle once it travels too far. This force behaves like a very stiff spring and is analogous to deformation occurring. Thus, a spring constant that limits the needle motion, k_{limit} is introduced. Similarly, k_{sac} is introduced to account for the forces that arise when the needle starts interacting with the seat of the injector, and the constant c, acts to dampen out energy in the system. The spring constants k_{limit} and k_{sac} have values significantly larger than any other springs in the system by several orders of magnitude because they are due to deformation of the injector. The damping constant is selected to be as small as possible so that it does not dominate the system's behaviour.

6.4.4 Akribis

The Akribis is a device capable of measuring the injected fuel's flow rate for every injection. The Akribis introduces an extra component into the system which may affect the solution and needs to be included in the model. The operation of the Akribis is explained before the equations that define it are developed.

Akribis operation

Figure 6.9 shows a schematic of the Akribis. The injector injects into a filled fuel volume that is separated from a nitrogen filled volume by a piston. The nitrogen volume is maintained at a pressure of 2.8 MPa, and thus, the pressure in the fuel and nitrogen volumes are equal. Because the two volumes are sealed from each other, there is friction when the piston moves that must also be accounted for in addition to the mass of the piston which will have its own inertia. At the start of injection the piston is stationary, and as fuel is injected, there is a pressure rise in the fuel chamber. This causes an unbalancing of forces resulting in displacement of the piston which when measured, provides a means of determining the volume of fuel delivered.

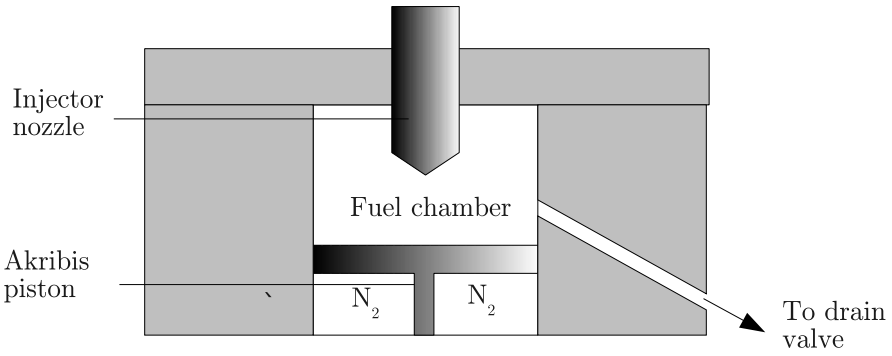


Figure 6.9: Akribis schematic showing the piston, chamber and nitrogen volume.

The Akribis therefore has a fluid and piston component that needs to be modelled. These equations are derived in a similar way to those used for the common rail injector.

Akribis fluid component

The equation for the Akribis is similar to the fluid equations used for the injector presented above. The pressure in the Akribis fuel chamber is expressed in terms of bulk modulus, fuel volume, piston displacement, piston area and the injected flow rate. The drain valve does not need to be included because the Akribis is only drained after the injection event. Equation 6.13 defines the dP_A/dt for the Akribis fuel chamber, as follows:

$$\frac{dP_A}{dt} = \frac{\beta(P_3)}{v_A + A_p x_p} \left[Q_{2,3}(t) - A_p \dot{x}_p - Q_{3,A}(t) \right] \tag{6.13}$$

where A_p is the area of the piston, v_A is the volume of the Akribis fuel chamber, x_p and $\dot{x_p}$ are the displacement and velocity of the piston respectively.

Akribis piston component

Fuel and nitrogen pressure act above and below the piston respectively. When the pressures are equal, the piston undergoes no acceleration. When the fuel chamber pressure varies as a result of injection, the pressures are no longer balanced and the piston is displaced. The acceleration of the piston is given in Equation (6.14) as

$$\ddot{x_p} = \frac{1}{m_p} \left(P_{N_2} A_p - P_A A_p \right). \tag{6.14}$$

The acceleration $\ddot{x_p}$ is dependent on the mass of the piston m_p, the area of the piston and the pressure above and below the piston.

6.4.5 Bulk modulus and density

The model is constructed using the fuel properties of ISO 4113 calibration fluid so that the results can be compared to the experimental results. This calibration fluid has properties that are similar to those of diesel as seen in Figure 2.3. The fundamental difference is that the calibration fluid has a lower flash point which makes it safe for testing purposes, but this does not change the results. For modelling, the important properties are the bulk modulus and density, and their variation with pressure. Equation (2.13) is the best fit equation for bulk modulus versus pressure that was used in the model, and is presented again below:

$$\beta(P) = 11.667P + 1.4 \times 10^9.$$

The variation of the fuel density with pressure is also included into the model. This is accounted for using Equation (2.14) presented again here:

$$\rho(P) = (7.61905 \times 10^{-19} P^2 - 6.78571 \times 10^{-10} P + 1.22167)^{-1}.$$

6.4.6 Discharge coefficients

A first approximation taken during the construction of the model was to use a single discharge coefficient for every orifice and area change throughout the injector. Through testing of the model, it was found that the solution was sensitive to the bleed and feed orifice discharge coefficients. These orifices control the response of the injector and thus require individual values. These discharge coefficients vary with time due to the transient nature of the flow which makes their evaluation a complex topic, whose investigation is beyond the scope and objectives of this project. Discharge coefficient information that is available is typically only for steady state flows which obviously do not apply to this system.

A solution however that compensates for variable discharge coefficients still needs to be found. This will be achieved by using experimental results and selecting values for these discharge coefficients that give the correct injected flow rate profile. The experimental tests that will be used to compare to the simulation will therefore be discussed next.

Chapter 7

The common rail equipment

In this chapter, the capabilities of the experimental equipment, and the procedure and precautions that need to be taken to obtain satisfactory results, will be discussed.

7.1 The injection Test Stand

An injector test stand was custom built by Innov8, which is capable of measuring the injected flow rate and capturing images of the spray structure during the injection event. This equipment was used to measure the injected flow rate of a common rail injector in this research. This section divided into the injection system, which details the injector and its system, the Akribis which measures the injected flow rate through the injector, and the image capturing system, which makes spray visualisation possible which are different components of the Test Stand.

7.1.1 Injection system

The standard components of an injection system are present in the test stand and can be seen in Figure 7.1. There are fuel lines, a common rail and two injectors. A high pressure pump (not visible in Figure 7.1) is attached to an electric motor. The system can only test one injector at a time as a safety precaution, because each injector is part of its own system. One injector is used for the flow measurement unit and the other

injector for capturing images of the injection event, which will be discussed later.



Figure 7.1: Photograph showing the injector, rail, Akribis and fuel lines for the test stand.

The system uses a Siemens common rail and two Bosch 0411 100 181 injectors which are six orifice injectors with an orifice diameter of 0.173 mm. The orifice diameters were measured in The School of Mechanical Engineering Metrology Laboratory. This is a first generation injector typically used on light motor vehicles. This type of injector, due to being actuated by a solenoid, is only capable of two injections per power stroke, a pilot and main injection.

The rail pressure is maintained by a common rail fuel pump that is driven by a five kilowatt electric motor. The motor speed can vary from 100 to 1000 revolutions per minute. The fuel pump is fitted with pressure release valves on the low and high pressure sides of the pump. As a result, the pump does not supply fuel to the rail if it is not required, as it is wasteful of energy, and does not over-pressurise the rail which could be dangerous.

The entire system allows for the injection event to be controlled in great detail by computer systems that run the test stand. The system is capable of five consecutive injections per revolution of the motor. The injection duration and the delay between injections can also be specified, thus making it possible to simulate pilot injections and the main injection event. The rail pressure can be set in the range from 30 MPa to 2000 MPa, however, caution should be taken as the injector cannot withstand a pressure of 2000 MPa, as it is designed to operate safely at a maximum of 1400 bar. Finally, the pump speed can also vary, making it possible to see how quickly the pump is capable

of re-pressurising the rail and how this affects subsequent injections.

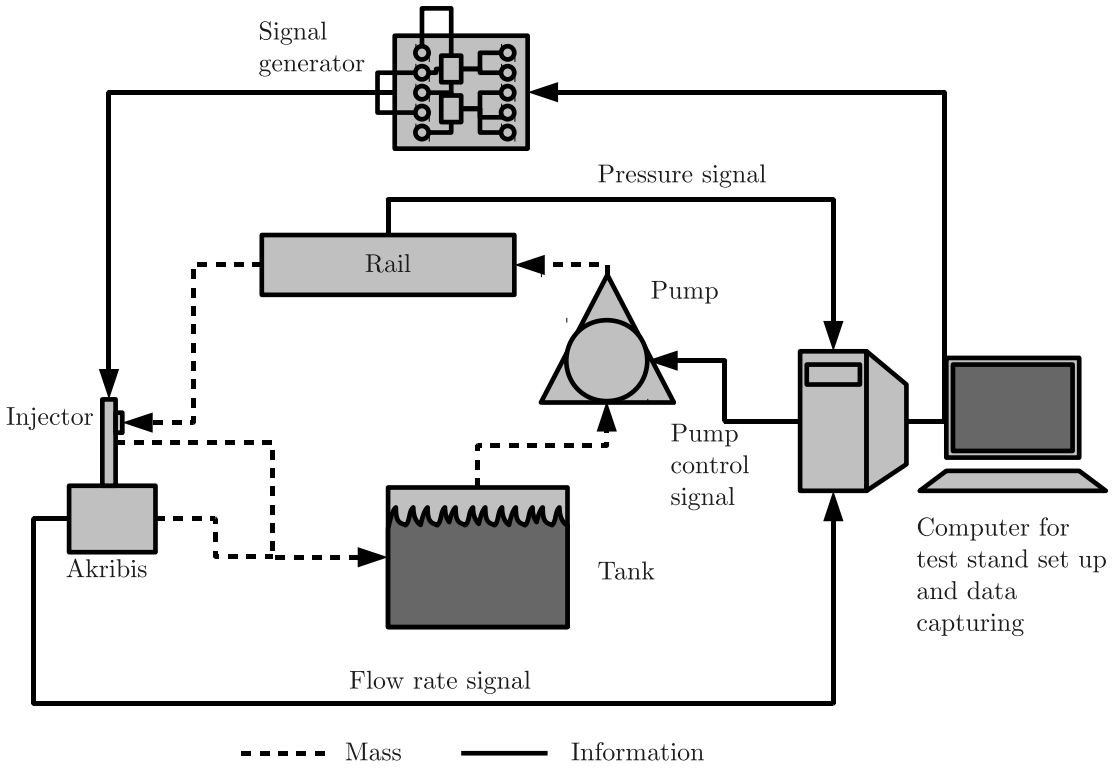


Figure 7.2: The common rail test stand system circuit.

Figure 7.2 is the system diagram, showing how the mass and information is passed within the system. The mass and information transfer consists of the fuel and the signal firing pulse, the pressure and the delivery data respectively. In Figure 7.2, only a single computer is shown that sends the desired signals and captures the data. The test stand however, consists of three computers that drive the system and capture data. Figure 7.2 combines all of these computers into a single black box for simplicity.

The information transfer in the system has to do with actuating the injector and receiving the measured data. In the stand, the signal that actuates the injector is provided by the signal generator which creates the correct signal dependent on the required test conditions set by the user at the computer. The information received at the computer is the data measured by the Akribis for the flow delivered and the pressure measured in the rail.

The transfer of mass is the fuel that is supplied to the injector by the pump. All the injected fuel returns to the tank so that it can be re-injected. In the common rail injector, some fuel that is delivered by the pump is not injected, but rather is used in the control

of the injector. This fuel leaves out the top of the injector, but also is returned to the tank through its own fuel return line.

7.1.2 Test fuel

Testing will be done with ISO 4113 as a test fluid, which has properties comparable to diesel, without the high flash point, thus eliminating the possibility of combustion. ISO 4113 is an accepted industrial injector testing fluid [29]. The properties of ISO 4113 are discussed in Chapter 2.

7.1.3 Pressure measurement

The pressure in the common rail is measured by a Kistler pressure transducer. The common rail is generally fitted with a pressure transducer that is used in the control system to regulate the rail pressure. This transducer does not measure to the accuracy of the Kistler.

7.1.4 Fuel delivery measurement

Flow measurement of the injected fuel is carried out by the Akribis unit, which measures the volume of fuel delivered with time by measuring the displacement of a piston by the injected fuel. From this, differentiation of the measured delivery with time gives the injected flow rate. This section will explain how the Akribis system works and how the measurements are taken.

Akribis volumes

The injector injects into the Akribis volume which is filled with fuel. The volume contains a piston which can move to equalise the pressure on the fuel side and the other side which contains nitrogen that is pressurised to 2.8 MPa. The fuel filled volume in the Akribis is therefore also at a pressure 2.8 MPa, which represents the chamber pressure in the engine.

During injection, the pressure rise in the Akribis volume unbalances the forces acting on the piston which causes piston motion. This motion is detected by a linear variable differential transformer (LVDT), which converts the motion into a digital signal representing the volume of the fuel injected. The flow rate versus time is calculated by differentiating the delivery versus time results provided by the LDVT.

The injector volume is drained after every injection event at a time well after injection is completed so as not to interfere with the results. If the fuel volume were not drained, the pressure would eventually build up and cause failure of the Akribis. The piston can then return to a zero position to await the next injection event.

Akribis response to fuel and nitrogen compressibility

The Akribis readings can only be interpreted as completely representative of the injected flow rate if the pressures in the Akribis are the same before and after injection (before draining). If the pressures are different, then the fuel has been compressed in its volume and therefore has not displaced the Akribis piston sufficiently. Because the nitrogen volume is large, it is reasonable to assume that it maintains constant pressure, even when the piston is moving. Thus, the pressure after the injection will be the same as that before injection and very little error is introduced.

Akribis response to the size of the fuel volume

The piston motion in the Akribis is driven by the pressure rise in the fuel volume. Thus the pressure rise needs to be such that the piston responds quickly to an injection. According to Innov8 Technologies Ltd [40], the fuel volume is minimised in order to maintain the accuracy of the measurement and reduce errors.

Akribis response to piston mass

The effect of the needle mass on the results is difficult to quantify. On the one hand, the piston introduces a mass into the system with its own inertia. This inertia will delay the response of the system to the injection event and introduce oscillations in the measured delivery once the injection has ended. On the other hand, the pressure differences that

cause motion in the piston are large and the mass is small, so inertia effects may be small. When interpreting the results, it is necessary to take the piston mass into account as the inertia that it introduces into the system may affect the results. In the common rail simulations in Chapter 6 the motion of the piston is taken into account so that its effect can be evaluated.

7.2 Uncertainty analysis

The test rig was newly commissioned just prior to testing by the manufacturer and therefore it is assumed to be correctly calibrated and that the measurements are accurate. The uncertainties associated with the Akribis unit and the Kistler pressure transducer are shown in Table 7.1. The values have been extracted from Innov8 Technologies Ltd [40].

Table 7.1: Measured delivery and pressure uncertainty.

Parameter	Units	Accuracy
Delivery	mm^3	$\pm$ 1 %
Akribis timing	ms	$\pm$ 0.02
Pressure	MPa	1 %

7.3 Methodology

The precautions can be divided into three categories. These are safety, which is the most important, precautions that ensure that the test stand is not damaged during testing and precautions that aid in obtaining good test results.

7.3.1 Precautions

1. Ascertain the location of the emergency stop buttons and use them when necessary.

2. Ensure that none of the emergency stops are depressed before trying to start the machine.

3. Before starting the test stand, check for flammable fuels that may ignite when any switches are activated.

4. Do not tamper with any high pressure lines, especially when there is any pressure in the system.

5. Handle the high pressure air, nitrogen and fuel lines carefully.

6. The following needs to be ensured to start and run the test stand otherwise the safety interlocks will prevent the test stand from starting:

   - There is sufficient nitrogen pressure (2.8 MPa).
   - There is sufficient air pressure (0.6 MPa).
   - All the glass doors on the spray testing side of the stand are closed.
   - The Akribis and the pump cooling oils temperatures fall between 19°C and 21°C.

7. Ensure that the drain valve controller in the power cabinet is switched on. It may be switched off if spray visualisation tests have been carried out recently.

8. Do not switch off the power with the circuit breaker before the computers have been shut down fully. Doing so may result in loss of data if they have not been saved properly.

9. Wait until the test stand is completely purged of air before starting tests. Purging the circuit box in the test stand protects the circuit from fuel residue and purging the Akribis unit with nitrogen ensures that the injector injects into an inert environment, thus protecting the stand.

10. When switching the stand on, if any lights on the power cabinet door do not illuminate, the 'LAMP TEST' button can be pressed. This will switch on all the lights to see if any are not operational and need to be replaced or if there really is an error in the stand.

11. When setting the electric motor speeds, it is advisable to first set a low speed and if everything is operating properly, the speed may be increased

12. When requiring high rail pressures, run the electric motor at 1000 rpm so that it is not overstrained. If the motor is overstrained, it will cut out and a full restart will have to be carried out.

13. Do not exceed the maximum operating pressure of the injector or the rail.

14. Do not energise the injector for too long because the solenoid will burn out.

15. The Akribis can drain a maximum fuel volume of 150 mm^3 per injection. Therefore the pressure and duration parameters should be chosen so that this is not exceeded as the Akribis may drain during injection which would interfere with the results.

16. Check that the drain rate level is about 12.5 mm^3/ms. This is the specified drain rate that gives optimal performance.

17. While testing, check the control panel on the back of the control cabinet to ensure that the drain valve is not continuously draining. This will burn out the drain valve solenoid.

7.3.2 Procedure

1. Switch on the water chiller.

2. Open the nitrogen cylinder to provide nitrogen to the stand.

3. Switch on the air compressor and wait for it to pressurise the accumulators to 0.6 MPa.

4. Open the air supply valve.

5. Switch on the extraction fan.

6. Switch the purge switches to the ‘ON’ position.

7. In the control cabinet, make sure the connector for the Akribis is inserted.

8. Make sure the switch for Akribis testing on the door of the power cabinet is on the ‘AK’ position.

9. Close the circuit breaker on the power cabinet by rotating the switch clockwise, the Akribis and control computers should start automatically.

10. Switch on the test stand by pressing the 'TEST STAND' button on the power cabinet door.

11. Start the Akribis oil pump by pressing the 'AK COOL OIL PUMP ON' button.

12. Start the test fuel pump by pressing the 'TEST PUMP ON' button.

13. Check the pressure valves on the test stand. Adjust the air purge, nitrogen purge and nitrogen valve to obtain the correct pressure required by the test stand.

14. Allow time for the Akribis and main circuit board chamber to be purged.

15. Start the common rail drive motor by depressing the 'CR DRIVE ON' button. There is a safety delay of approximately ten seconds before the light will show that the motor is ready.

16. Start 'CADAC', the computer program that controls the test stand, located on the control computer's desktop.

17. Press 'F10' on the keyboard to bring up the diagnostic screen. Green dots indicate that a requirement for the safe operation of the test stand is in order, whereas red indicates a system fault. All these requirements need to be green before proceeding.

18. Set the motor speed on the motor settings window on the control computer to 100 rpm, and increase it gradually until the motor is running at 1000 rpm.

19. Set the injection parameters on the 'Injector firing and control' screen by pressing 'F8' on the keyboard. Here the pressure, injection durations and number of injections can be set. For Akribis testing, the injections must also be synchronized to the pump. Being synchronized to the pump ensures that the results are repeatable by forcing the injector to inject at the same point in the pumping cycle of the supply pump.

20. Click 'APPLY' to begin injecting.

7.3.3 Capturing data

The data capturing procedure is listed separately as it takes place on the Akribis computer. The data capturing has two modes:

1. Free run. Free run captures the data and displays it on the screen but does not save the data. Multiple injections can be recorded, but only the first is displayed.
2. Save the data. This is where the data is saved to the computer.

Both capturing methods have importance. Item one, free run, has two uses, firstly, tests can be quickly analysed to decide their relevance before they are saved and processed. Secondly, the drain rate profile needs to be looked at to set the drain level of the Akribis. The 'save data' mode allows the data to be recorded for later analysis.

Capturing and saving data

Capturing and saving data for Akribis testing is carried out on the Akribis computer.

1. The file path of the test can be specified in the 'Results' window.
2. Once injection has started, capturing of the data can be started.
3. Data processing is carried out in a separate program called Test Scope. Here the waveforms are exported to text files, and plots can be exported directly from Test Scope, but further processing can only be done from a separate program.
4. Test Scope exports into a text file that, although is efficient in terms of storage, is not useful for post processing. Thus a separate program was written to turn the Test Scope data into a comma separated variable file that Scilab, Matlab or Excel can interpret.

7.3.4 Proposed tests

The injector will be tested at its maximum rated pressure of 140 MPa for different injection durations. The injection duration should vary from short durations (475

μs) which represent pilot injections to very long injections (1500 μs) where transient dynamics of the fluid and injector are no longer present. Intermediate durations represent typical opening durations (600 μs - 700 μs) of the injector. For each test carried out, the rail pressure and injected flow rate will be measured.

Chapter 8

Common rail experimental results

Data for flow rate, fuel delivered and pressure were recorded for injection durations from 475 μs to 2000 μs at a rail pressure of 140 MPa. The data collected has been processed and presented as a series of plots below.

8.1 Data averaging

For every injection duration tested, data for thirty injections were recorded and averaged. Figure 8.1 shows the delivery of the average and a single injection. This illustrates how much variation there is between injections which is important when evaluating the repeatability of each injection. Repeatability of the injections, besides being important to research, is also important to engine performance where identical injections produce smoother power curves during engine operation [10, 37, 41]. Too much injected fuel results in high exhaust emissions and too little would affect performance adversely.

Figure 8.1 shows the seventh injection and the average of all thirty injections superimposed. The seventh injection is chosen arbitrarily; any of the other injections would give similar results. This result is presented to show the repeatability of the experiment. The final volume of fuel delivered for the seventh injection is approximately 3% higher than the average volume delivered. This difference could arise from slight variation in the length of injection which alters the amount of fuel delivered or could be attributed to the measuring system. The transient features which appear at 2.1 ms and 2.8 ms are a

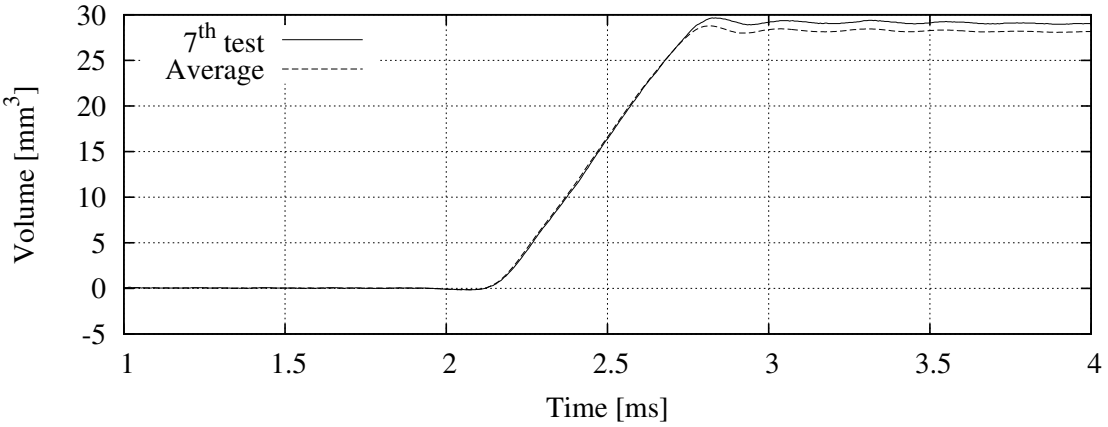


Figure 8.1: Comparison between the average and individual values for volume versus time for the injection events.

result of the measurement equipment rather than additional, smaller injections. Because the variation is small, the ability of the control system to meter almost exactly the same amount of fuel for multiple injections without a feedback system, is verified. To this research, Figure 8.1 illustrates that the results are repeatable and that no significant external factors interfered with the measurements taken.

8.2 Delivery

The total volume of fuel delivered for each injection duration from 475 μs to 2000 μs is shown in Figure 8.2. This figure shows how the volume of fuel delivered is dependent on increasing the injection duration.

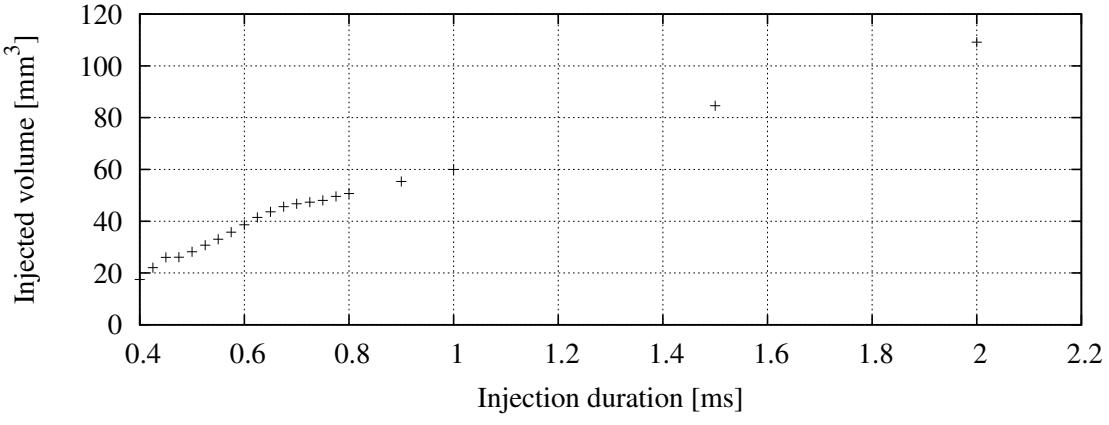


Figure 8.2: Injected volume versus injection duration.

More data points are shown for injection durations less than one millisecond as this is the typical operating condition of engine. The figure shows that the amount of fuel delivered increases with injection duration. Since the flow rate remains constant during injection due to a constant rail pressure, this result is expected. The data would not pass through the origin because there is a minimum energising time that the solenoid requires before the injector will open. In addition the control volume requires time to depressurise sufficiently before allowing the injector to open.

There is deviation from the linear trend in Figure 8.2 at 0.65 ms where there is a 'bump' in the curve. This feature can be understood by considering Figure 8.5, where between the 0.6 ms and 0.7 ms, there is an oscillation in the flow rate that has an effect on the overall delivery. Similar reasoning can be applied to the smaller bump that occurs at 0.45 ms. Smaller intervals in duration were tested, between in 0.6 ms and 0.7 ms, and all the results support that a 'bump' would occur. This bump occurs because the injector closes on the peak of one of the oscillations in the flow rate.

The reason for this (or any other) oscillation during injection is not obvious. Possible causes are water hammer effects, changes in the state of the flow, needle motion or a response to the drop in pressure from the pump. After about 0.7 ms injection durations, the flow rate begins to follow a better linear trend as the oscillations have less effect on the average delivery due to the length of the injection duration.

In terms of future testing, it can be seen that the two millisecond injection injected about 120 mm^3, which is approaching the 150 mm^3 limit of the Akribis and significantly longer injections should be avoided. It is expected that the limit would be reached at about 2.8 ms by extrapolating beyond the measured points, assuming that the pressure would remain at 140 MPa.

8.3 Rail pressure

Figure 8.3 shows the rail pressure versus time for the 500 μs to 900 μs injection durations when the setpoint pressure in the rail was 140 MPa. Figure 8.3 shows the rail pressure versus time for the 500 μs injection only, making the pressure features clearer.

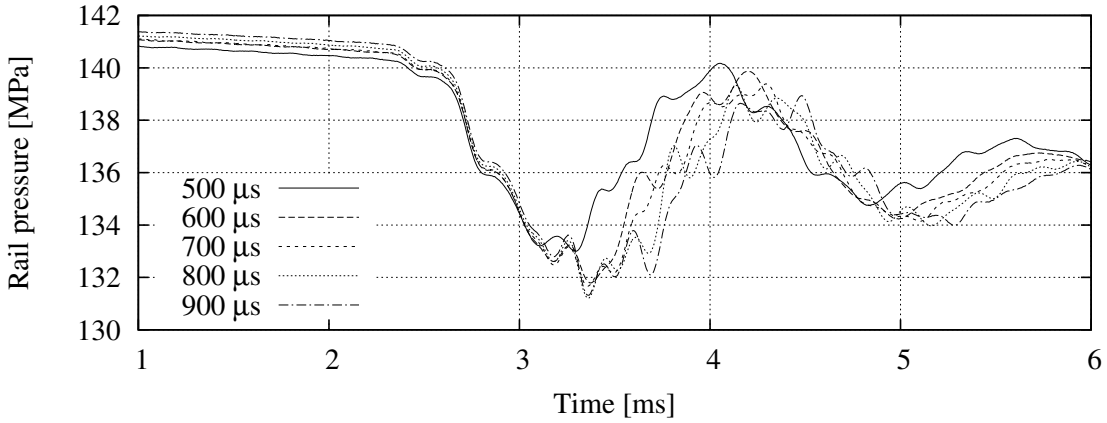


Figure 8.3: Rail pressure versus time for various injection durations.

Pressure variation

In Figure 8.3, the rail pressure versus time for injection durations from 500 μs to 900 μs, it can be seen that at the start of measurement, the initial pressures are not identical. The 500 μs injection has an initial pressure of 140.75 MPa while the 900 μs injection has an initial pressure of 141.25 MPa. This deviation is small, being less than 1% of the set point pressure of 140 MPa. Some deviation in the pressure is expected due to the unique pressure responses by the pump that is affected by the different injection conditions such as different injection durations. The control system constantly supplies and releases pressure to try and maintain a constant set-point pressure of 140 MPa. Thus, the reference point where injection is set to start is at a point where the pressure is slightly higher than the set-point pressure. The system however, also injects at the same point in the pumping cycle, so that the reference pressure is as similar as possible during for each injection test. The deviation between the different measured pressures could also be due to the uncertainty of the measurement equipment, as the deviation falls within the uncertainty range. This initial deviation is therefore accounted for.

Pressure features

The pressure profile shows many interesting features of the injection event. Figure 8.4 is a schematic of the rail pressure versus time, indicating these features and making their identification in Figure 8.3 easier. The first interesting feature is that the pressure decreases slightly as the measurements begin. This occurs because the pressure is

released gradually by the control system to prevent the rail pressures from exceeding the set value.

The next feature shows the moment when the solenoid has opened the bleed orifice. When the bleed orifice opens, the pressure in the control volume is released and causes a slight, abrupt pressure drop in the system labelled 'bleed orifice opens'. The pressure drop can be seen in the Figure 8.3.

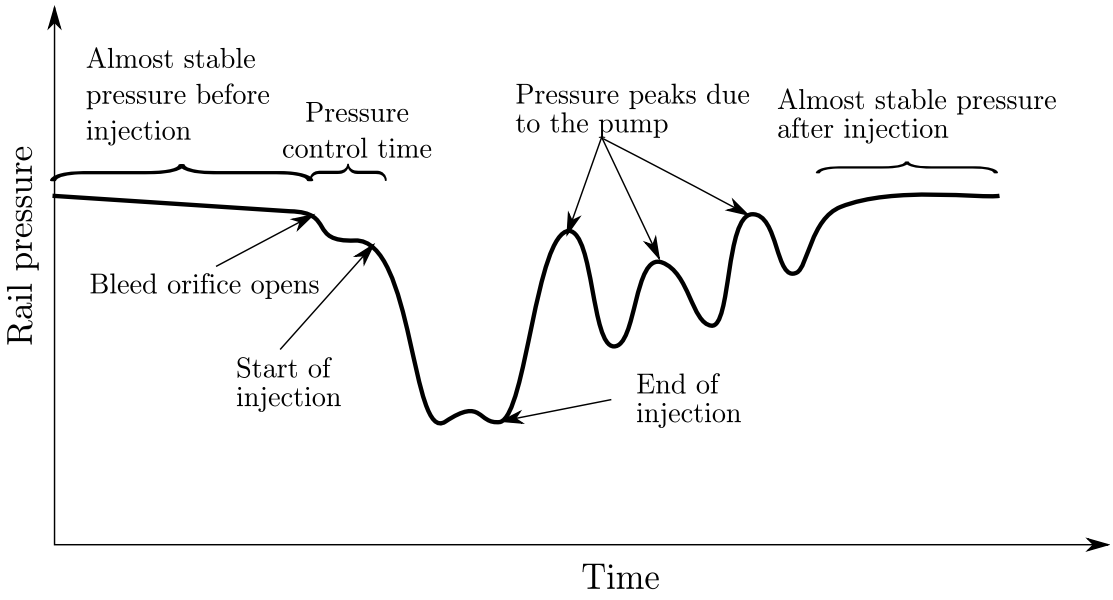


Figure 8.4: A schematic of rail pressure versus time illustrating the pressure features that are visible in the pressure profiles.

Once the pressure in the control chamber has dropped enough, the injector opens, and the pressure again drops sharply as the fuel is injected. The beginning of this feature is labelled as the 'start of injection' in Figure 8.4.

There is a delay between the time when the bleed orifice opens and when the injector opens which will be called the 'pressure control time'. This is the time that it takes for the control volume pressure to drop. It can be seen in Figure 8.3 that this time is small in comparison to the injection duration. A short delay between when injection is initialised by the solenoid and when it actually starts is desirable, because the system responds quickly when the bleed orifice is opened and makes control of the system easier.

In Figure 8.3, it noted that the pressure control time is the same for all injection durations shown. This time is only dependent on the geometry of the injector and the

rail pressure and is independent of the injection duration. In the control of the injector, these relationships are desirable because the behaviour of the injector is repeatable and predictable.

It can be seen in Figure 8.3 that the main pressure drop representing the pressure drop for the main injection event, is largest for the 900 μs injection. This is because the injector is given more time to inject fuel thereby allowing more fuel to leave the system.

Note that the 'Pressure control time' is smaller than the main injection event. This is desirable because only a small amount of fuel pressure is lost to the control of the system. The injector is therefore efficient in its use of the pressure provided by the pump by not wasting energy in its control.

The end of the injection event is marked by an increase in the pressure (see Figure 8.4). Following the 'end of the injection', the pressure in the rail returns to the set rail pressure. It can be seen in Figure 8.3 that the pressure increase is sinusoidal. This is because each lobe of the pump is 120° out of phase and, each peak corresponds to one lobe of the pump restoring the pressure.

8.4 Flow rate

In this section the injected flow rate results are presented. The injection flow rate and velocity are compared to those of the mechanical injector and effect of the injection duration on the flow rate is considered.

Total flow rate

Figure 8.5 shows the flow rate versus time for injection durations of 500 μs to 900 μs. The injector is injecting for all non-zero values of the flow rate.

It is observed in the figure that once injection has ceased, there are small fluctuations in the flow rate. These fluctuations are purely due to the measurement equipment. From this plot, the dependence of the flow rate on injection duration can be seen, and a comparison between the actual injection duration and the set duration can be made.

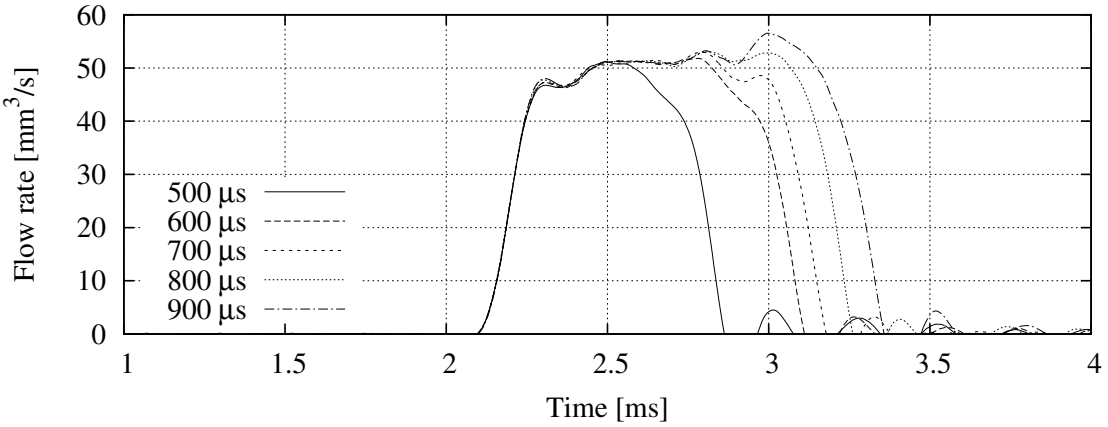


Figure 8.5: Flow rate versus time for 500 μs to 900 μs injection durations.

For each injection duration, the average flow rate does not vary significantly and remains approximately 52 mm^3/ms. This is unlike the flow rates shown for the mechanical injector in Chapter 4 which were significantly lower and varied more with time due to the varying supply pressure. This implies that the pressure before the orifice remains approximately constant. The longer injections, with injection durations greater than $\sim$ 700 μs, show fluctuations in the flow rate, but it is uncertain what is the cause.

The flow rate per orifice

Because the common rail injector has six orifices, the actual flow rate per orifice needs to be considered to compare the benefits over the mechanical injector. Figure 8.6 shows the total flow rate divided by the number of injector orifices (n=6) for the common rail system.

Figures 8.6 and Figure 5.15 allow the injected flow rates through a single orifice to be compared for the common rail and mechanical injector respectively. Figure 8.6 shows that the flow rate through a single orifice is between 8 mm^3/s and 9.5 mm^3/s in the common rail tests while in Figure 5.15 the flow rate for the mechanical injector is seen to be about 7 mm^3. This difference is unlike what is expected considering the large differences in pressures present in each system, and therefore, what is the advantage of using the more complicated common rail system?

Besides the additional control that the common rail system offers, the common rail also has better atomisation characteristics [13, 14, 17]. This can be shown by considering

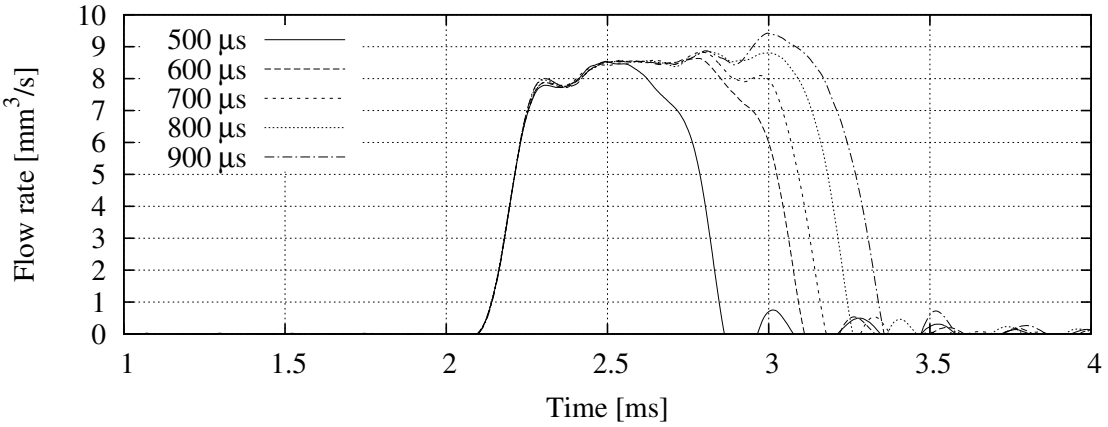


Figure 8.6: Flow rate versus time for 500 μs to 900 μs injection durations through one of the six injector orifices.

the exit velocity of the fuel for the common rail and mechanical injection systems. The exit velocity is simply the injected flow rate divided by the flow area:

$$V = Q/A.$$

For the mechanical injector the flow area A, can be calculated from the orifice diameter of 0.24 mm to be 0.045 mm^2. The flow area for the common rail injector is calculated from the discharge orifice diameter of 0.173 mm and is 0.024 mm^2. The exit velocity is therefore 157 m/s and 340 m/s for the mechanical and common rail injector respectively. This high exit velocity for the common rail injector means that there is much more energy imparted to the system and the spray will atomise and penetrate better. The extra velocity also introduces turbulence into the injected jet, which will help disperse the spray. As a consequence, the air/fuel mixture is better when the common rail system is used, which aids in reducing exhaust emissions.

The actual injection duration

From Figure 8.5, it can be seen that the actual injection time deviates slightly from the specified energising time of the solenoid by considering the duration where each curve is non zero. For example: a 500 μs injection duration actually lasted 800 μs. The same delay can be seen for all the injections

The delay arises because the control volume requires time to pressurise fully before

the injector will shut and the needle must then move into a closed position from its fully open position. Inertia of the needle and the fluid will also contribute to this phenomenon, but their effects will be small due to the large forces in the system.

It can be seen in Figure 8.5, that at 2.5 ms (which is 500 μs after injection was set to start), the flow rate decreases indicating that the bleed orifice has closed and that the state of the system has changed. Thus, even though the measured injection duration is longer that what was specified, this is only due to the dynamics of the system.

Effect of the injection duration

In comparing the flow rates for different injection durations in Figure 8.5, it is seen that the flow rate profiles are similar while injecting, but diverge as the injector closes. During injection the pressure remains approximately constant (see Figure 8.3) and so the flow rate profile can be expected to remain the same while injecting. Consequently, determining if transient and cavitation effects occur cannot be done by only varying the injection duration because they would occur identically in each test.

Apparent secondary injections

In Figure 8.5 it can be seen that after the injection, secondary smaller peaks exist, suggesting that secondary injections occur. This is not the case; these apparent secondary injections are only oscillations within the measurement system due to the Akribis piston inertia that dominates after the sudden shut-off of the injector.

8.5 Pressure and flow rate

By combining the pressure and flow rate data, features become apparent that could not be discerned by analysing each individually. This will show the delay between when injection actually starts and when it is detected at the rail and the effect of water hammer on the injection event.

Detecting injection at the rail

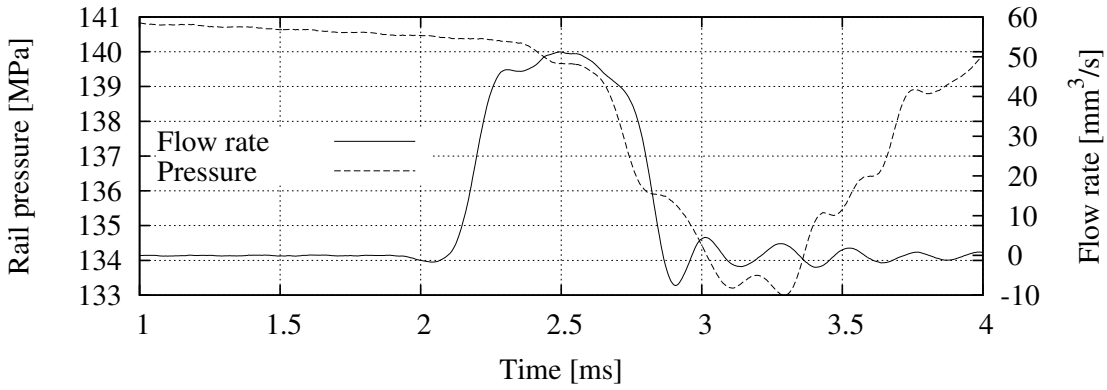


Figure 8.7: Rail pressure and flow rate versus time for the 500 μs injection.

Figure 8.7 shows the rail pressure and the flow rate superimposed upon each other, showing the interaction between them. Surprisingly, the Akribis has measured 600 μs of injection before a pressure drop is experience at the rail, whereas it would be expected that these events would occur simultaneously. This delay occurs because it takes time for the pressure signal to travel from the injector to the rail. This pressure signal travels at the speed of sound c, through the fuel, which is dependent on the bulk modulus and density of the fuel as shown in the following equation presented by Munson et al. [23]:

$$c = \sqrt{\frac{\beta}{\rho}}.$$

The distance from the injector to the rail is approximately 80 mm. If a constant bulk modulus of 1.8 GPa and density 850 kg/m^3 between the injector needle tip and the pressure sensor are assumed (based on Figure 2.3 and 2.4), then the time taken for the pressure signal to travel from the injector tip to the rail can be calculated. Doing this yields a delay of 550 μs, which is approximately what is observed in the results. If a pressure transducer were placed close to the sac, the pressure would be more in phase with the flow rate. Although the signal is delayed by 600 μs, it still yields information about the pressure at the discharge orifice, albeit out of phase with the measured injected flow rate.

Figure 8.7 shows that the rail pressure does not affect the injected flow rate for a 500

μs injection because the pressure only drops in the rail close to the end of the injection. This is because the duration is shorter than the time taken for the signal to reach the rail. For very long injections this is not true and the rail pressure does have an effect on the injection. This shows that knowledge or predictions of pressure closer to the injector would be useful to understand more fully what is happening within the injector.

Water hammer

In Figure 8.8, the flow rate for a 2000 μs injection is presented. Although this injection is significantly longer than what is typically used, it shows interesting features due to its long duration. The injection duration is long enough that pressure signals begin to affect the flow rate delivered later in the injection event.

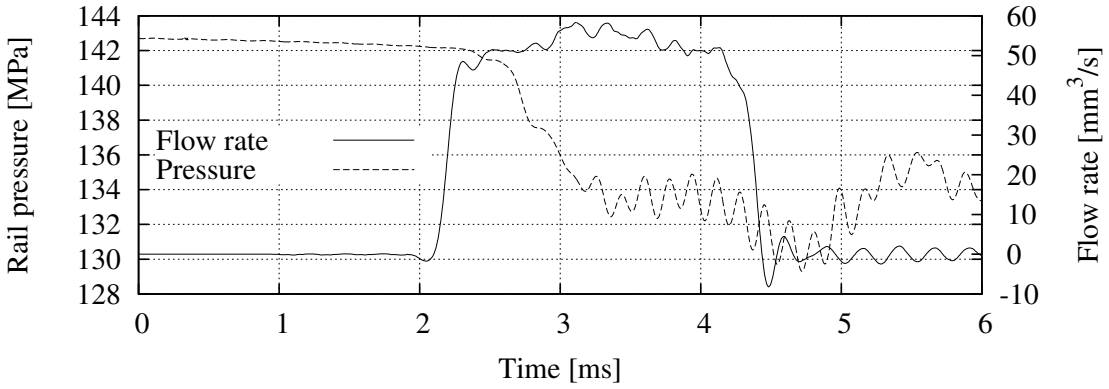


Figure 8.8: Rail pressure and flow rate versus time for a 2000 μs injection.

For the first millisecond of injection (from just after 1 ms to 3 ms) there is little oscillation in the flow rate while the pressure signals are travelling through the volumes of the injector to the rail and back again to the injector. However, from 3.2 ms (or 1.2 ms after the start of injection) there are more oscillations. Also at 3.2 ms, oscillations are visible in the rail pressure, which are the pressure signals that are travelling within the volumes of the injector.

It is reasonable to assume that these oscillations are due to the pressure signal created by opening the injector when considering the time taken for the signal to be detected in the rail. It was mentioned above that the injection event is only detected at the rail approximately 550 μs after it has occurred. A return trip of the same signal would take almost the same time, bringing the total travel time up to about 1100 μs. It is

expected that the time taken for the return signal would be longer than the initial signal to the rail because the pressure (and therefore bulk modulus and density) has dropped, thereby lowering the speed of sound of the fuel. Water hammer effects also do not cause significant changes to the flow rate for very long injections and therefore delivery is unaffected by water hammer. This can be seen in Figure 8.8 where the average flow rate is within an approximately 8% range throughout the majority of the injection. This is completely unlike the flow rate predicted by the mechanical model where the flow rate would decrease rapidly as injection proceeds.

8.6 Orifice pressure calculation

Knowledge of the flow rate measured by the Akribis makes it possible to calculate the pressure before the orifice using Equation (8.1) which describes the flow rate through an orifice [23].

$$P_{inj} = 2\rho_f \left(\frac{Q}{n a_o c_d} \right)^2 + P_a. \tag{8.1}$$

The sac pressure P_{inj} can be calculated with the injected flow rate Q, the Akribis chamber pressure P_a, the fuel density ρ_f, the discharge coefficient c_d and the orifice area a_o. Note that the injector has six orifices which must be taken into account to calculate the area. In using Equation (8.1) some simplifications are made. A constant discharge coefficient of 0.6 is assumed based on the calculation presented in Appendix F. Although this is simplistic, especially in terms of transients and cavitation, it gives a good indication of the pressure before the orifice during injection.

Equation (8.1) is used to calculate the pressure before the orifice for a 500 μs injection and this pressure is shown in Figure 8.9. It can be seen that the pressure is at the chamber pressure for all other times other than during injection. When the injector is not injecting, the needle rests against the bottom of the injector and covers the orifice. Thus, the orifice is separated from the rail by the needle and the pressure falls to the chamber pressure.

At about 2.1 ms, the pressure increases gradually to about 130 MPa before a second

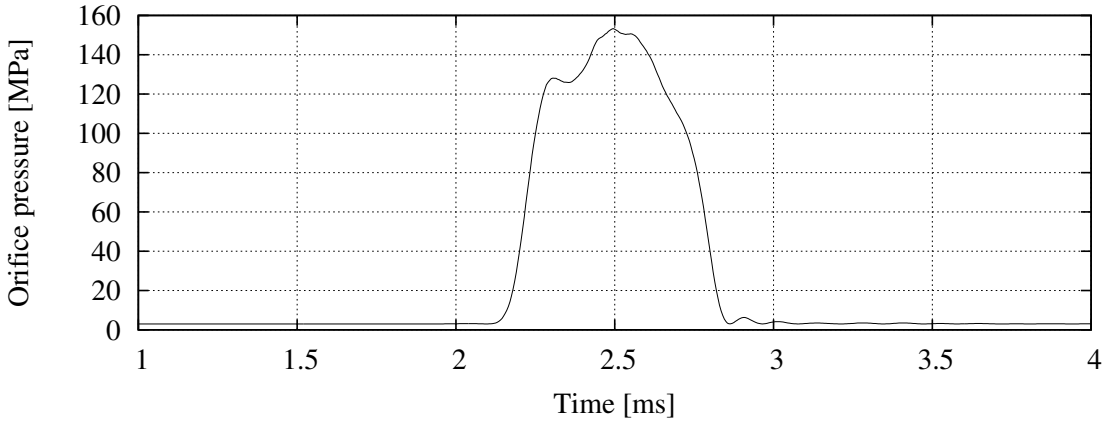


Figure 8.9: Calculated pressure just before the discharge orifice versus time for a 500 μs injection event.

increase which increases the pressure further to just over 150 MPa. Because the injection duration is set at 500 μs, the bleed orifice would shut just after 2.6 ms, thereby ending injection. Thus, at 2.6 ms the calculated pressure drops suddenly until it reaches the chamber pressure again. The first pressure increase occurs while the needle is lifting and therefore this pressure would be strongly affected by this motion. This may explain why the pressure does not quite reach 140 MPa during this time as would be expected. The peak pressure of 150 MPa suggested by the results is unlikely to occur because the maximum pressure should not exceed the set point pressure of 140 MPa. This pressure of 150 MPa can be attributed to the oversimplification of the discharge coefficient since no other parameter in the calculation can vary. There is, however, no way to determine an exact discharge coefficient or its variation during injection without pressure measurements before and after the nozzle of the injector or by measuring the pressure before the orifice and the flow rate through the orifice. Both methods are extremely difficult to carry out due to the small and varying geometry of the injector at the orifice and have not been attempted as this would fall outside the scope of this project.

A comparison of the 500 μs injection flow rate in Figure 8.5 and the pressure in Figure 8.9 shows that their shapes are similar. This is because the flow rate and pressure are proportional to each other. The pressure can be seen to increase rapidly and maintain a high injection pressure, similar to the rail pressure, which maintains a large flow rate during injection. Therefore the injection properties are improved in comparison

to the mechanical injector. This high pressure (and flow rate) results in well atomised and penetrating spray, particularly when compared to the mechanical injector where the injection pressure was much lower. Accordingly, a good air/fuel ratio is achieved within the combustion chamber, thereby reducing emissions.

Chapter 9

Common rail model validation

In is chapter, the results of the common rail simulations are presented. The results obtained here are compared to the experimental results discussed in Chapter 8 to validate the capabilities of the model. Where the experimental results and simulation results agree and that feature is discussed in Chapter 8, only the similarity will be mentioned here, the full details of the feature will not be discussed again. A sample of the output file obtained from the C++ program is presented in Appendix E.

The results are divided into several sections. The discharge coefficient results show the empirical values for $c_{d,f}$ and $c_{d,b}$ that were used. This section arises because of the error in the solution that occurs when constant values for the discharge coefficients are used. The sensitivity analysis shows the results obtained by varying other injection parameters or fuel properties in the model and observing the change in the solution. Lastly, the results from the simulation are interpreted and compared to the experimental results.

As a matter of interest, a comparison between the C++ model and the Scilab model is shown. Besides showing the improvement in using the C++ model, it also shows the effect of using constant discharge coefficients in comparison to varying them empirically according to the injection duration.

The simulations were all solved for five milliseconds, injection was started at one millisecond by opening the bleed orifice.

9.1 Discharge coefficients

The discharge coefficients used in the model are important because they influence the model strongly. This section will motivate the need for a variable discharge coefficient beyond that of what was mentioned in Chapter 6. The values for the discharge coefficients need to be chosen empirically and justification for why these values are reasonable need to be given.

Constant discharge coefficient

In the early stages of the model development, constant discharge coefficients for the feed and bleed orifice were used. Figure 9.1 shows that the resulting flow rate versus time was too square and the flow rate over-estimated the data slightly. The squareness of the flow rate means that the amount of fuel delivered is also much higher. To make the flow rate profile more rounded at the beginning and end of injection, different values for the discharge coefficient was required. Further evaluation of the results revealed that the required discharge coefficient to give agreement with experimental data also varied according to the injection duration. This is because a single discharge coefficient value represents an average of what occurs over the entire injection. For very short injections, the transient fluid behaviour dominates the solution, whereas long injections have, on average, more steady flow. Thus, the discharge coefficients need to vary according to the injection duration.

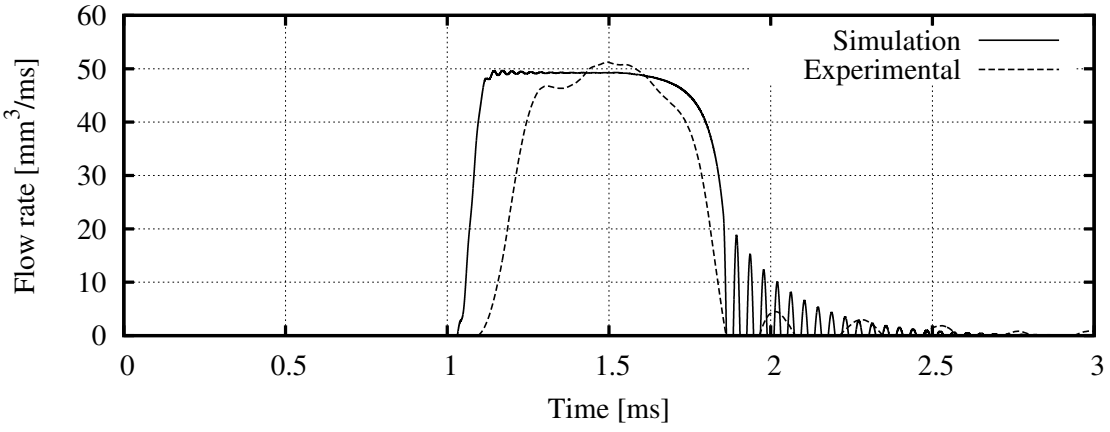


Figure 9.1: Flow rate versus time for experimental and simulated results.

Variable discharge coefficient

The bleed and feed orifices directly control the behaviour of the injector as they form part of the control system and thus, they are the only orifices that require varying discharge coefficients. Later in Section 9.2 where the sensitivity analysis is discussed, this will be shown to be true.

The values for the bleed and feed orifice discharge coefficients were chosen empirically such that the injected flow rate matched the results from Chapter 7. Chung et al. [38] also found that it was necessary to include varying discharge coefficients for the entrance and exit orifices from the control chamber above the plunger. The values for these discharge coefficients are shown in Figure 9.2 and 9.3. The plots show the average discharge coefficients versus the injection duration that give good agreement.

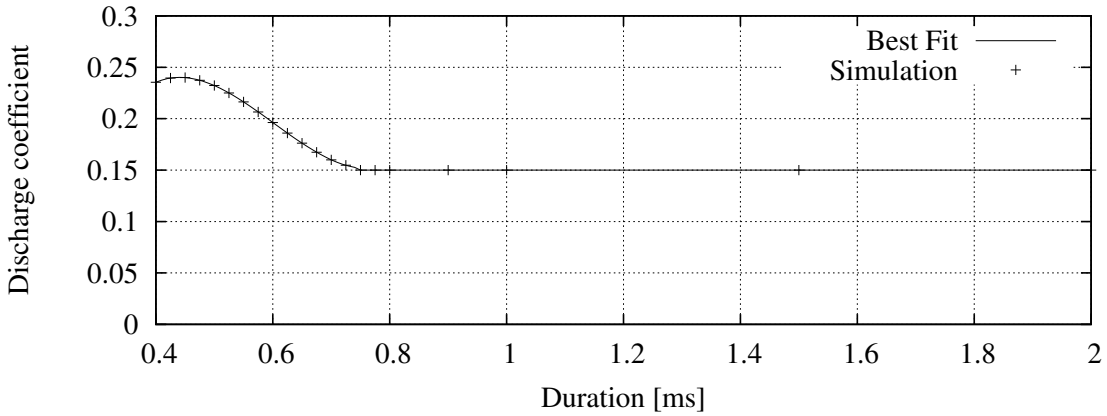


Figure 9.2: Values of the bleed orifice discharge coefficient $c_{d,b}$, versus the injection duration and the best fit equation through the data.

Figure 9.4 shows how the solution is improved by using variable discharge coefficients for a 500 μs injection. It can be seen that the injection duration, average injected flow rate, the rate at which the flow rate reaches its maximum and the way it drops off at the end of injection for the simulation matches the experimental results better. It is expected, due to the very short injection durations, that the flow within the injector would be transient and therefore the discharge coefficients would be dependent on time, thereby justifying the need for different values of discharge coefficient for each injection duration. Very little work has been done on transient discharge coefficients and so steady state theory has to be used to attempt to explain the values that were used for the bleed and feed discharge coefficients and the difference between them. This

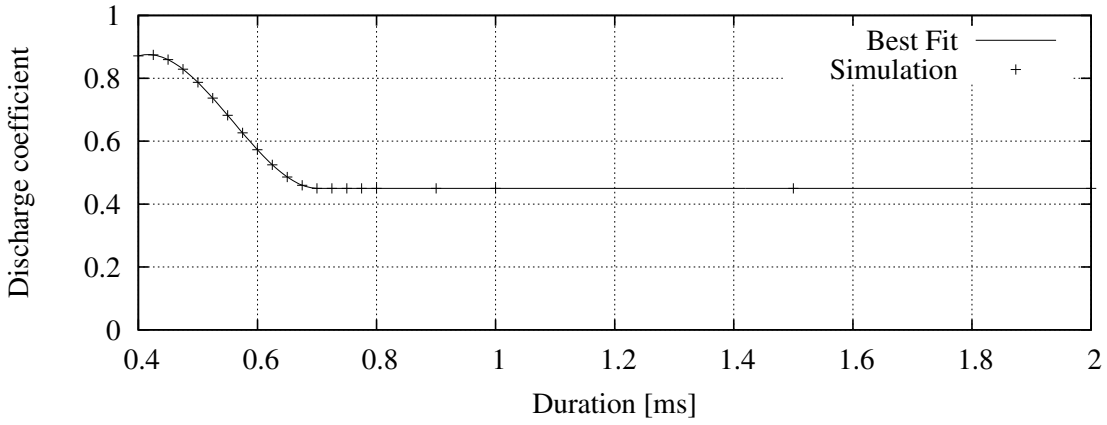


Figure 9.3: Values of the feed orifice discharge coefficient $c_{d,f}$, versus the injection duration and the best fit equation through the data.

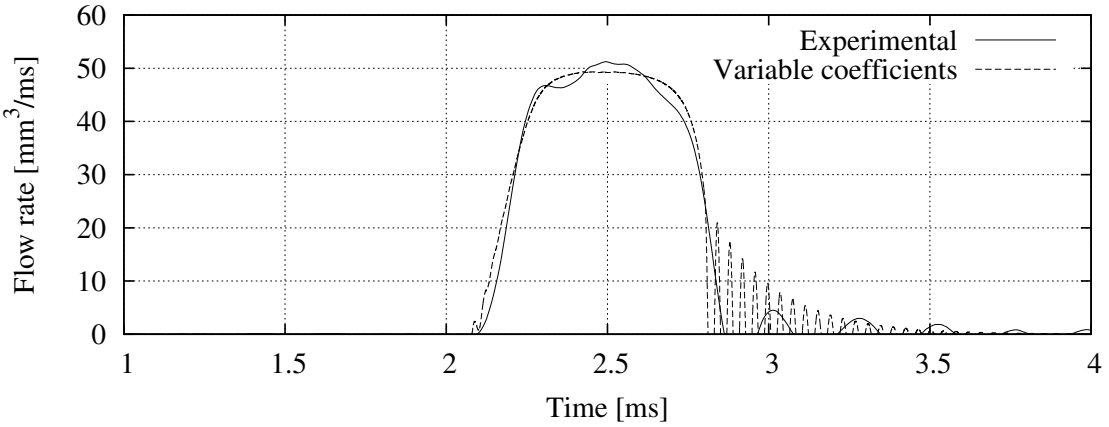


Figure 9.4: Simulated and experimental flow rate versus time for a 500 μs injection with varying discharge coefficients.

steady state theory however, cannot be used to obtain precise values for the discharge coefficients.

Consequences of variable discharge coefficients

Choosing a single discharge coefficient for each injection duration allows the model to fit the data, but the approach is simplistic. It gives the impression that the discharge coefficient values are constant during the injection and vary only with the injection duration. This is untrue; the discharge coefficient will vary with time as is seen in Section 8.6 where the injection pressure exceeded the rail pressure due to a constant discharge coefficient assumption. The values for the discharge coefficients presented

are merely values that fit the data. The empirical approach does not show if the flow through the injector is turbulent, laminar or cavitating.

It should be recognised that other values of $c_{d,b}$ and $c_{d,f}$ would also allow the simulated flow rate to match the measured flow rate, and the values of the discharge coefficients are coupled. A change in one discharge coefficient will result in a change in the other. Thus, there could be many combinations of values that would allow the flow rates to match. It was attempted to select realistic values for the discharge coefficients based on what typically occurs on the geometry specific to that orifice. The geometry of the orifices can be seen in Figure 6.1.

The empirical constants are based on the results for a 1400 bar rail pressure. It is uncertain whether the discharge coefficients shown in Figure 9.2 and 9.3 would be relevant at other injection pressures. A simulation carried out at another pressure would not be wrong in terms of the injector behaviour, but the accuracy of the simulation may be compromised.

Justification for the chosen discharge coefficients

Figures 9.2 and 9.3 show that the bleed orifice has a smaller discharge coefficient than the feed orifice. A lower value for the bleed orifice discharge coefficient is expected as a result of its geometry in comparison to that of the feed orifice. The feed orifice has a gradual transition from the large pipe diameter to the feed orifice that will reduce the restriction to the flow of fuel offered by this orifice. This is a typical result from steady state analysis of flow through orifices. Conversely, the bleed orifice has an abrupt change of area, with an orifice in the centre of another orifice. Both these geometrical features are shown in Figure 6.1.

If the distance between the feed and bleed orifices is not sufficient for the flow to become laminar, then coupling between them will occur. Consequently, the overall constriction is not just due to the smallest constriction, but due to the combined effect of both orifices. This is because the flow is still disturbed by the time it reaches the second orifice. The nature of how these two closely located orifices will jointly restrict the flow is not well understood.

A further complication exists where needle motion introduces a flow rate into or out of the control volume by either entering or leaving the volume, resulting in two flow streams merging perpendicularly. This results in turbulent flow that will cause additional restrictions to the passage of the fuel through this volume [42]. This turbulence is dependent on the difference in velocities of the flows.

The losses associated with the merging of flow have been plotted against the ratios of the different flow rates by Idelchick [42]. The inclusion of this data into the model is however difficult because the flow rate and the losses are dependent on each other. Idelchick also discusses the losses associated with flow in curved passages. The feed orifice and the bleed orifice are perpendicular to each other. Therefore the flow needs to curve, as if moving around a corner, to compensate for this orientation of the orifices in addition to the flow provided by the needle motion. The curving of the flow introduces turbulence and pressure gradients within the control volume that cause losses that are dependent on the radius of curvature [42]. Quantification of these losses is impossible without accurate knowledge of the flow regime and structure within the volume. Therefore the different losses that occur within the control volume from before the feed orifice to after the bleed orifice are:

- the feed orifice discharge coefficient,
- the bleed orifice discharge coefficient.
- the merging of the flow through the feed orifice and the artificial flow due to the needle motion and,
- the curvature of flow that occurs in the control volume due to the orientation of the orifices.

Inclusion of each of these topics to construct accurate discharge coefficients and loss parameters into the model would be very difficult. The easiest way of approaching this problem is to use computational fluid dynamics (CFD). Complications arise because many of these losses are dependent on the flow rates. Thus a CFD model that includes the entire injector would be required. A CFD analysis was not attempted for this project because the detailed geometry required for its implementation was not available and could not be gained from the injector supplier. The losses due to merging and curved

flow would all act cumulatively to cause a very low bleed orifice discharge coefficient. This is why the bleed orifice discharge coefficient shown in Figure 9.2 generally shows lower values than the feed orifice discharge coefficient in Figure 9.3.

Some of the discussions above, for example curved flow in channels or diversion of flow, are features that occur in other places within the injector. These cases have not been analysed because the model has been found to be most sensitive to the losses at the feed and bleed orifices.

In Figure 9.2 and 9.3, it can be seen that the discharge coefficients decrease when the injection duration increases up until about 800 μs when a constant value is reached. In the early stages of injection, vena contracta have not yet formed and the flow is unrestricted. Thus, very high coefficients can be expected. The discharge coefficient decreases rapidly with time as the vena contractas develop. Although Figure 9.2 and 9.3 are very simple approximations of what really occurs, they do show these features well.

It can also be seen that for very long injection durations, the values of $c_{d,b}$ and $c_{d,f}$ become constant for injection durations longer that 0.8 ms. This indicates that the system is at steady state, and the early transient periods do not dominate the behaviour of the injector.

The dependence of the discharge coefficients on the transient flow becomes apparent when attempting to select values of $c_{d,b}$ and $c_{d,f}$ for very short injections. It is very difficult to select values that give the right rate shape at the opening and closing time as well as the right delivery. This is because for very short injection durations transient flows dominate the behaviour of the injector and the flow rate profile, and selecting a single average value is not an adequate approximation. Conversely, for very long durations the discharge coefficients used are likely to be very close to the correct values since the transient flows no longer dominate the solution as is the case with short injection durations.

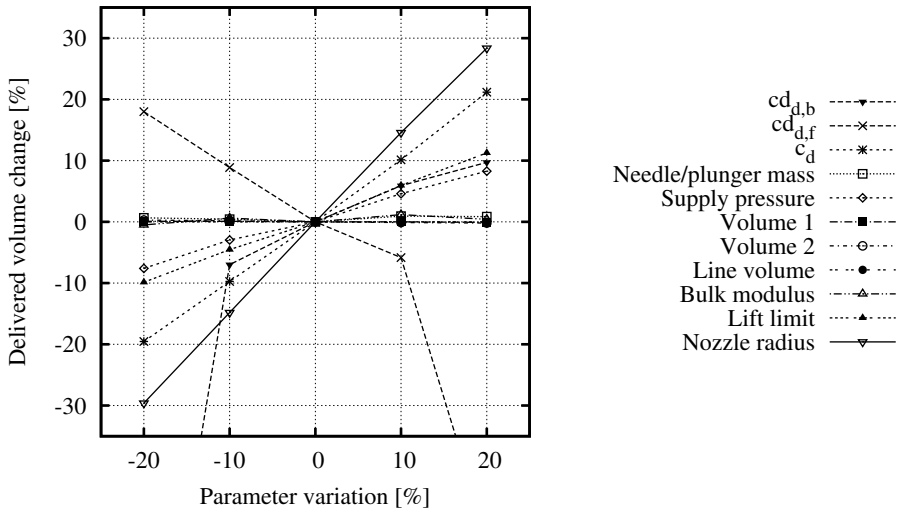


Figure 9.5: Delivered volume change versus parameter variation for the 500 μs injection.

9.2 Sensitivity analysis

A sensitivity analysis shows how the solution is changed by a variable that cannot be precisely defined. Selected variables were changed independently, the solution recalculated and the resulting change can therefore be quantified. Five variations of each variable were used: a reference value and a value ten percent and twenty percent above and below the reference. The sensitivity analysis was carried with the discharge coefficients discussed in Section 9.1.

The sensitivity analysis for a 500 μs injection was carried out on the following parameters: discharge coefficients, the needle mass, the rail pressure, the line volume, the density of the fuel, the internal injector volumes, the needle lift limit and the radius of the discharge orifice. Figure 9.5 shows the percentage change in delivery (as a volume) for the percentage variation of the chosen parameters. Larger variations in the delivery indicate greater sensitivity of the injection to that variable.

In Figure 9.5, the density results have not been shown because density will cause a change in both the mass and the volume of fuel delivered during the injection. The sensitivity analysis for density will therefore be shown separately in Figure 9.12.

It can be seen in Figure 9.5 that some of the parameters varied have a strong influence on the solution. If the flow rate profiles are considered, then the way in which the

parameters alter the injection event can be better understood. A schematic of a typical flow rate versus time plot is shown in Figure 9.6. This schematic will aid in identifying which stages of the injection event are changed by different parameters.

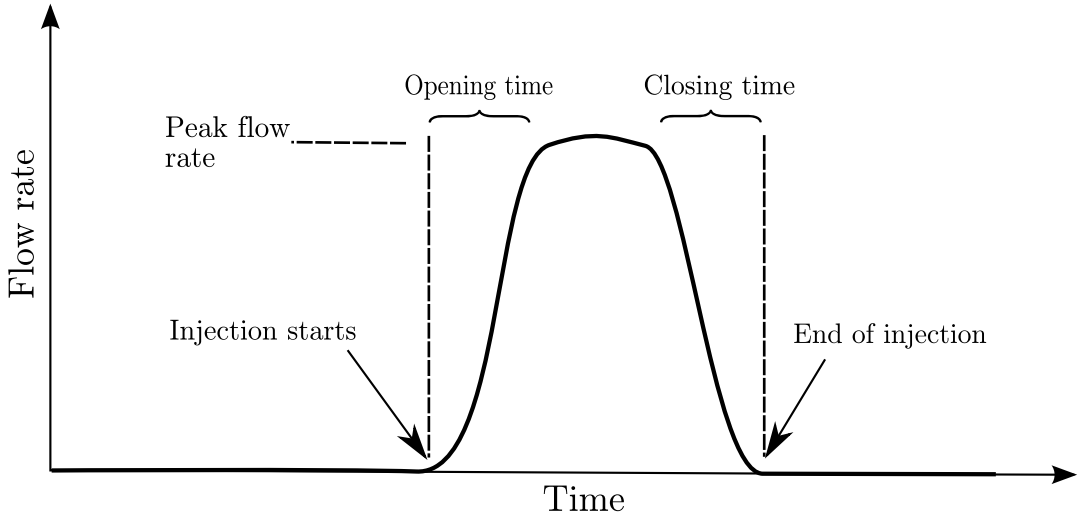


Figure 9.6: The schematic of the flow rate profile versus time from the simulations showing the opening and closing time definitions.

The opening time is how long the flow rate takes to reach its peak once injection has begun. This is the time it takes for the needle to stop lifting, allowing the pressure to build in the sac. The closing time is from when the flow rate decreases from the peak value to zero whereupon injection ends. If the opening time is short, then the response of the injector is fast and the maximum flow rate is reached quickly, thus forming a well atomised spray. A fast closing time means the delay between closing the bleed orifice and the termination of injection is short which is desirable for controlling injection. The opening and closing time of the injector is strongly influenced by the feed and bleed orifice discharge coefficients, as will be shown below.

The bleed orifice

An investigation of the bleed orifice discharge coefficient is carried out because it was found to have such a strong impact on the solution in Section 9.1. Because this value had to be chosen empirically, it is necessary to evaluate how different values would alter the solution.

Figure 9.5 shows that a 20% decrease in the bleed orifice discharge coefficient reduces

the amount of fuel delivered. This difference from the reference values is significant, being larger than that caused by any of the other values of the discharge coefficient. To understand why this variation occurs, Figure 9.7 is presented which shows the flow rate versus time for the injections.

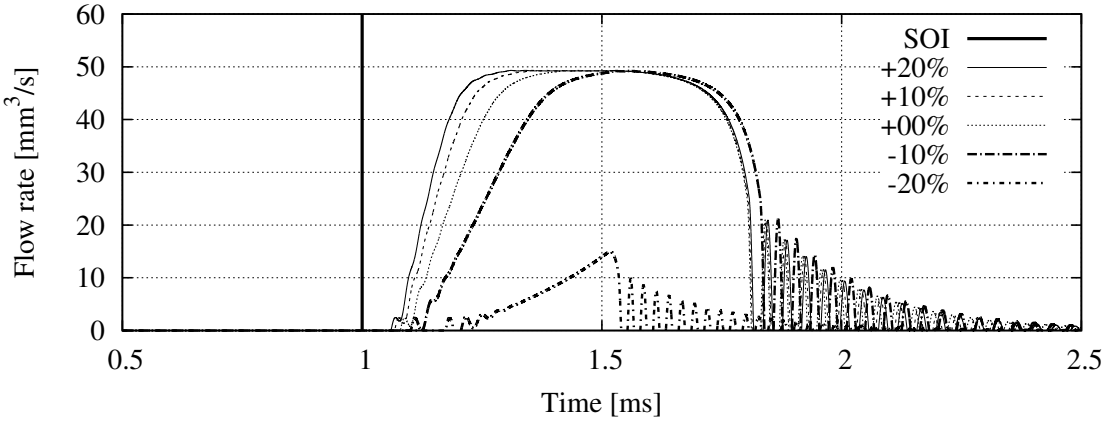


Figure 9.7: Flow rate versus time for the sensitivity analysis performed on $c_{d,b}$ for a 500μs injection.

In Figure 9.7, it can be seen that for a discharge coefficient 20% lower than the reference value, the injector has almost not even opened, and the flow rate is completely stunted. Since the flow at the bleed orifice is restricted more, very little fuel is released when the orifice is opened. Consequently, the pressure exerted on the needle remains high and the injector cannot open fully resulting in the reduced flow rate seen in Figure 9.7. This is detrimental for the engine because not enough fuel is injected into the combustion chamber and the injection velocity is low. Thus, the fuel will most likely not combust completely and efficiently, resulting in more emissions.

The other percentage changes in the discharge coefficients also affect the initial injected flow rate as seen in Figure 9.7. A larger value of $c_{d,b}$ results in a greater initial rate of delivery with a more square-shaped profile, whereas smaller values of $c_{d,b}$ result in more rounded flow rate profiles. Thus, the opening response time of the injector is sensitive to the restriction at the bleed orifice. Because the bleed orifice is shut at the end of injection, it can have no effect on the closing time of the injector. This explains why the flow rate curves are similar from about 1.75 ms to 1.8 ms when injection ends.

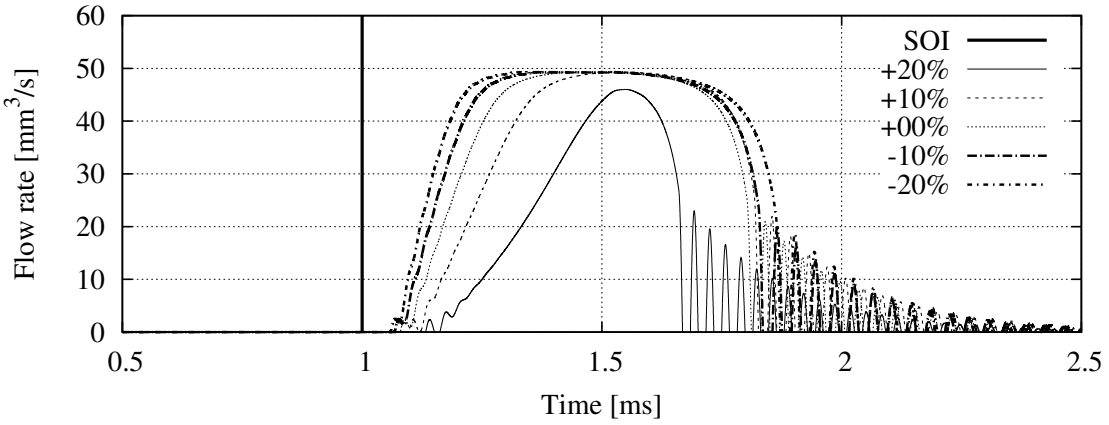


Figure 9.8: Flow rate versus time for the sensitivity analysis performed on $c_{d,f}$ for a 500μs injection.

The feed orifice

In Figure 9.5, showing the sensitivity of the feed orifice discharge coefficient, an anomalous variation occurs when the constriction at this orifice increases. This variation is not as pronounced as in the case of the bleed orifice variation.

Figure 9.8 shows the flow rate results for each variation of the feed orifice discharge coefficient. It can be seen that it is the opening time that changes most severely when this coefficient is varied. The anomalous variation in flow rate arises because the constriction the control volume is filled more rapidly with fuel from volume 1 and the opening time is decreased. Therefore, if the constriction is very small, as in the twenty percent larger coefficient simulation, the pressure in the control volume is maintained and the injector cannot open properly. Thus, a change in feed orifice discharge coefficient affects the solution oppositely to the feed orifice discharge coefficient. Figure 9.8 shows that the closing time of the injector is also altered by the feed coefficient. With less constriction at this orifice the control volume is filled faster, thereby maintaining a higher pressure in the volume for longer. Thus the injector will open slowly and close quickly.

Because the bleed orifice is closed at the end of injection, the discharge coefficient for the feed orifice is most likely correct during this time. This can be said because the closing rates of the injector match well with those of the experimental results seen in Figure 8.5.

The overall discharge coefficient

It was proposed above that the flow will experience little constriction due to vena contractas and cavitation at the start of injection, resulting in a discharge coefficient close to unity. This applies to all constrictions within the injector. As vena contrata and cavitation develop, the discharge coefficient will vary to account for these changes. Thus, the overall discharge coefficient will also vary with time. In the model however, the overall discharge coefficient is constant and therefore a sensitivity analysis on this coefficient is performed. Although the general discharge coefficient is for all the constrictions between the adjacent volumes shown in Figure 6.1 (excluding the feed and bleed orifices), the smallest is at the nozzle. This constriction therefore dominates the dynamics of the entire system. The effect of varying the overall discharge coefficient on the delivery can be seen in Figure 9.5. It shows that decreasing the discharge coefficient c_d (or increasing the constriction) reduces the amount of fuel delivered, as well as the maximum rate at which the injection occurs. This result is expected because flow rate is proportional to the discharge coefficient. In the model, the discharge coefficient was constant throughout the injection. In reality, it would vary with time resulting in more oscillations in the injected flow rate. This could explain the oscillation in the flow rate seen in the experimental results and its absence in the simulations.

In Figure 9.9, the flow rate versus time for the five injections is presented because it shows that the flow rate is affected differently by the overall discharge coefficient in comparison to the bleed and feed orifices.

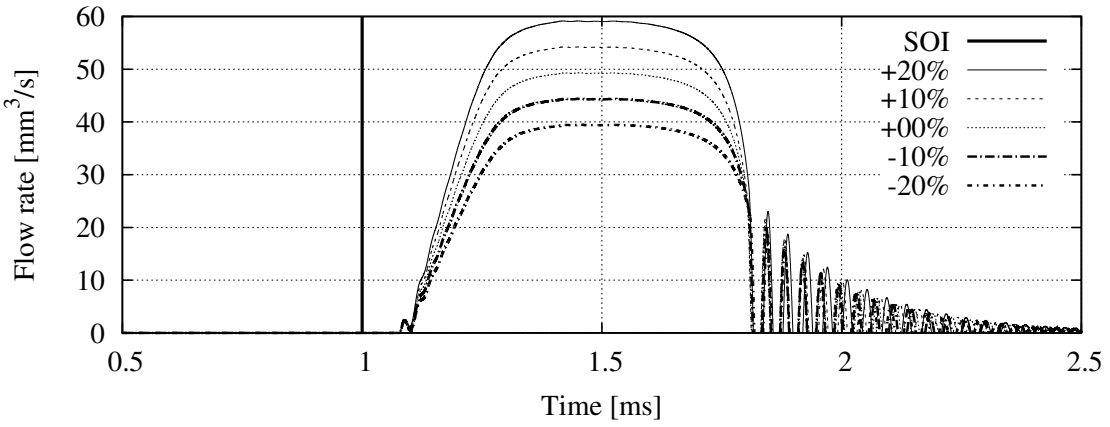


Figure 9.9: Flow rate versus time for the sensitivity analysis performed on the overall discharge coefficient, c_d for a 500μs injection.

Figure 9.9 shows that unlike $c_{d,f}$ and $c_{d,b}$, the opening and closing response times are unaffected by the overall discharge coefficient since this coefficient is not part of the control of the system. The rise times and closing times can be seen to be the same for all the variations of the overall discharge coefficient. The injection duration is therefore the same for all variations of the discharge coefficient. Only the steady state flow rate that occurs in the middle of the injection duration varies.

Needle mass

This sensitivity analysis illustrates the importance in specifying the magnitude of the needle mass, particularly because a rapid response of the needle is required and inertia of the needle will influence this. The measured mass of the needle, plunger and shim was 14.0 grams. The scale used was accurate to one gram, thus any error is less than 10%.

Figure 9.5 shows that the error introduced by the needle mass is very small. This is because the pressures and forces that act on it are large in comparison to its mass and any inertia that it possesses.

Rail pressure

This sensitivity analysis is not performed as an investigation as to how the injection characteristics vary when the injection pressure is lower or higher. Rather, it is carried out to justify the assumption that the rail pressure is constant. Investigating how the spray varies due to the injection pressure is a well explored topic [10, 13, 17] and is not necessary.

The rail pressure is an important parameter to perform a sensitivity analysis on because of its variation with time. There are two reasons for this variation. Firstly, the pressure oscillates due to the pumping and relieving of pressure to maintain the rail at its set point pressure. Secondly, the pressure varies during injection as seen in Figure 8.3 due to the injection event.

The pressure drop due to the injection event in the experimental results can be seen in Figure 8.7. The pressure drops from 142.0 MPa to 131.0 MPa; this is an 8% drop in

pressure over the injection event. The sensitivity analysis was carried out with a 20% variation in the pressure for a comparison. By doing this, the effect of a pressure drop on the simulation is tested by exaggerating its magnitude and duration.

Figure 9.5 shows that the delivery changes by only 20% percent across the pressure variation of 20% above and below the reference pressure of 140 MPa. This is for the entire injection duration, which is unlike the experimental results where the pressure decreased during injection. Thus, the smaller variations that are shown to occur during injection in Figure 8.3 will not have a large effect on the volume of fuel delivered. This shows that the assumption of a constant rail pressure to be reasonable.

System volumes

The line volume is varied because it is difficult to measure accurately and this could introduce errors into the solution. If the volume is large then it begins to behave as an accumulator that would be unaffected by minor oscillations. Conversely, if the volume were small then the solution would be sensitive to this volume. The volumes, v_1 and v_2, within the injector are especially difficult to measure because of their size and location in the injector and therefore a large error could be expected in the values selected for the model. Thus, a sensitivity analysis on these volumes is most certainly required. Volume 1 and 2 would affect the solution in a similar way to the line volume. These volumes are however significantly smaller and thus the solution is expected to be more sensitive to their variation because dP/dt is inversely proportional to volume.

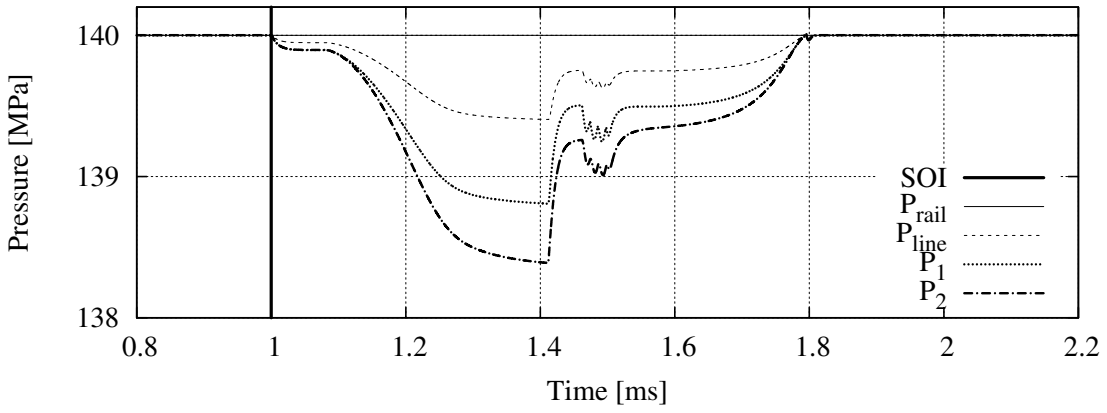


Figure 9.10: The pressure versus time for a 500 μs injection for the rail, line and volume 1 and volume 2.

Figure 9.5 shows that the volume of fuel delivered is independent of any of the injector volumes that were changed for the simulation, within the 20% upper and lower bound of the reference value. By noticing the magnitude of the pressure changes of the fuel that occur within the injector in Figure 8.3, showing the experimental results, and Figure 9.10, showing the simulation results, it is seen that the pressure change with time is small and therefore dP/dt tends to zero. Thus, the flow rate in almost cancels with a flow rate out of a volume and thus dP/dt the respective volume is also close to zero. A variation in any volume would therefore have negligible effect on the solution.

The simulation exaggerates this apparent independence because the rail pressure is assumed to be constant throughout injection and therefore dP/dt in the rail is zero. The rail maintains a more uniform pressure throughout the system, damping any pressure variation in the volumes. In reality more variation in the pressure can be expected, and therefore the results would in fact be more sensitive to changes in the sizes of the volumes.

It was discussed in Chapter 7 that the line volume affects the delay between when the injector is opened at the time when this event is detected at the rail. Despite this, it is expected that the amount of fuel that is delivered would be approximately the same, regardless of the change in volume of the line. The time that the pressure signal takes to travel through the line cannot be predicted by the model due to the instantaneous response of the pressure in a volume to a pressure change in an adjacent volume.

Bulk modulus

A sensitivity analysis is conducted on the bulk modulus because it varies for different fuels like diesel or DME which may at a later stage be tested. In addition, the bulk modulus can also vary if there are contaminants in the fuel and with temperature.

In Figure 9.5, the change in volume delivered for the different bulk moduli is approximately zero. This result is unexpected because in Equation (6.11), dP/dt (and therefore the injected flow rate) is directly proportional to the bulk modulus. As with the internal system volumes, because dP/dt tends to zero throughout the solution, any variation in the bulk modulus will have a negligible effect on the solution. Again, like the system volumes, the constant rail pressure assumption may exaggerate this

apparent independence and in reality the delivery may be more dependent on the bulk modulus than what is shown here. A consequence of this result is that if the test fluid were changed so that the bulk modulus was different, the change in delivery would be minimal. As the injection flow rate would be similar, so would the initial jet exit velocity. Thus, the initial atomisation of the spray would also be similar. This does not imply anything about the spray structure when it has fully evolved, as a different bulk modulus may cause different atomisation, dispersion or penetration characteristics.

Needle lift limit

Because the limit on the needle lift is difficult to measure and it changes due to wear on the shims, a sensitivity analysis is required. In Figure 9.5, the maximum variation in the volume of fuel delivered is 8% for a 20% change in the limit. Therefore, when the shims wear down, more fuel is injected. This occurs because the distance that the needle must travel before closing the injector is different for each limit value. If the distance that the needle must travel is large, then the injector will remain open for longer and more fuel will be injected. The converse is true if the distance that the needle must travel is less.

In Figure 9.11, it can be seen that the time when injection finishes, increases for increasing lift limits. Because the injection duration is 500 μs and the bleed orifice is opened at 1 ms then ideally the injection should end at 1.5 ms A twenty percent decrease in the needle lift limit results in a shorter injection, ending at approximately 1.7 ms, as opposed to about 1.85 ms for a twenty percent larger limit. Therefore when the needle lift limit is small, the injector closing time is better, giving the best response, taking only 200 μs to close. Large lift limits, also have an abrupt drop off in the flow rate, but they occur a long time after the injector should ideally have closed. This delay arises because the needle lift has further to travel from its fully open to a closed position.

Figure 9.11 shows that the average flow rates are all about 49 mm^3/s during the main part of injection. The flow rate therefore is not significantly influenced by the needle lift limit. From this it can be said that the flow area created by the needle as it opens does not alter the injection rate and is not a dominant constriction to the system.

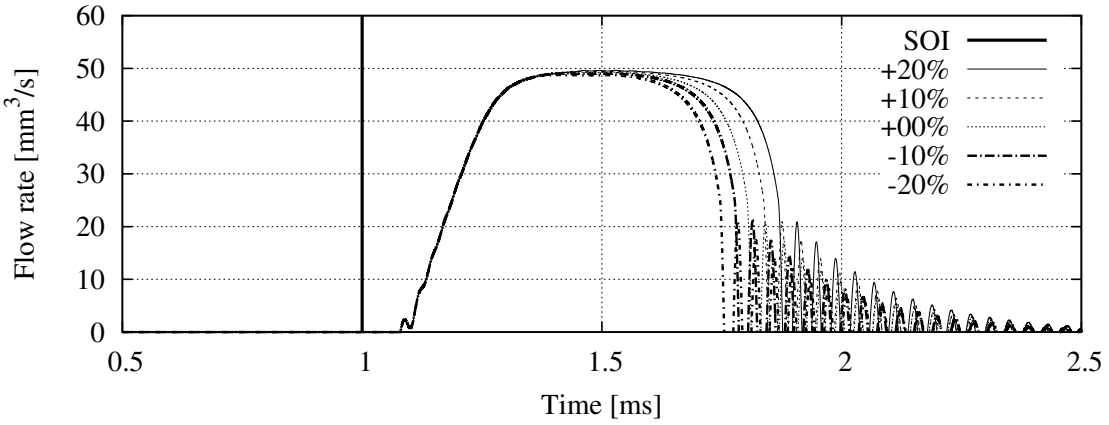


Figure 9.11: Flow rate versus time for the sensitivity analysis on the needle lift limit for a 500μs injection.

Discharge orifice radius

The radius of the discharge orifice is an important parameter as it is the final restriction between the fuel leaving the injector and entering the chamber. The effects of wear are expected to be negligible because tough materials are used to withstand the high temperatures and pressure occurring during combustion. Variations in the orifice radius are most likely to be introduced by measurement errors, which occur due to the small size of the orifices and if the injector is changed. Figure 9.5 shows that besides the bleed and feed orifices, the nozzle orifice radius has the largest effect on the amount of fuel that is delivered by the injector. As the orifice radius increases, so too does the amount of fuel delivered. This is expected as the flow rate is directly proportional to the flow area of the orifice.

Density

During injection, the density can vary due to temperature and cavitation, the effects of which have not been included in the model. Thus the need exists to evaluate the sensitivity of the solution to density. Cavitation causes localised variations in density as unstable vapour bubbles (with a low density) collapse to form pressure concentrations. External factors that may cause density variation are the usage of different fuels (such as DME or biodiesel) or slight differences in the simulated and actual fuels properties. In the model, fuel property data from Catania et al. [32] was used instead of measuring

the actual fuel properties which could be slightly different simply due to different measuring conditions. Of all the ways that variation in density could arise, a change of fuels would have the greatest effect. Temperature would only cause a small variation in density and cavitation would only cause localised variations in density.

Figure 9.5 shows the variation in the volume delivered during a simulated injection event. The mass delivered would show a proportional variation to the volume delivered when the density is constant and therefore has not been included for the sensitivity analysis on any of the other parameters investigated. When the density is no longer constant, both the mass and volume of fuel delivered will change and therefore both have to be shown together to interpret the results correctly. Figure 9.12 is presented which shows the change in volume and mass delivered for a variation in density.

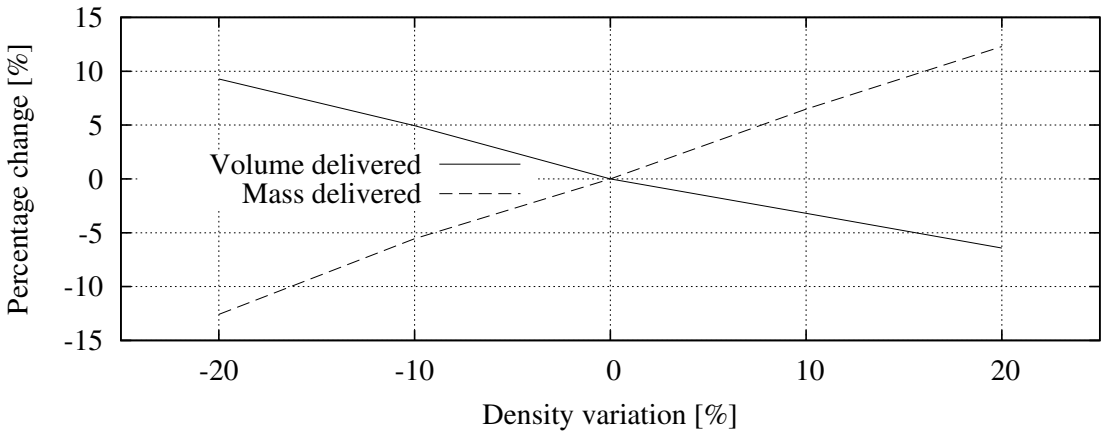


Figure 9.12: Percentage variation in volume and mass delivered for the sensitivity analysis performed on density for a 500μs injection.

Figure 9.12 shows that the volume delivered increased by about 10% for a 20% decrease in density, but the mass delivered decreased by 15%. For a 20% larger density, the mass delivered increases by 12% while the volume delivered decreased by 6%. Thus, on average, more mass is delivered when the density is increased, even though the volume of fuel decreases. The figure also shows the injected volumetric flow rate versus time. The mass flow rate need not be presented because it will provide no more information.

In Figure 9.13, it can be seen that a lower density results in a higher injected flow rate and therefore a higher spray exit velocity from the injector, resulting in better spray properties for combustion. However, the mass delivered decreases, which means that there would be a slight decrease in power as there is less fuel available for combustion.

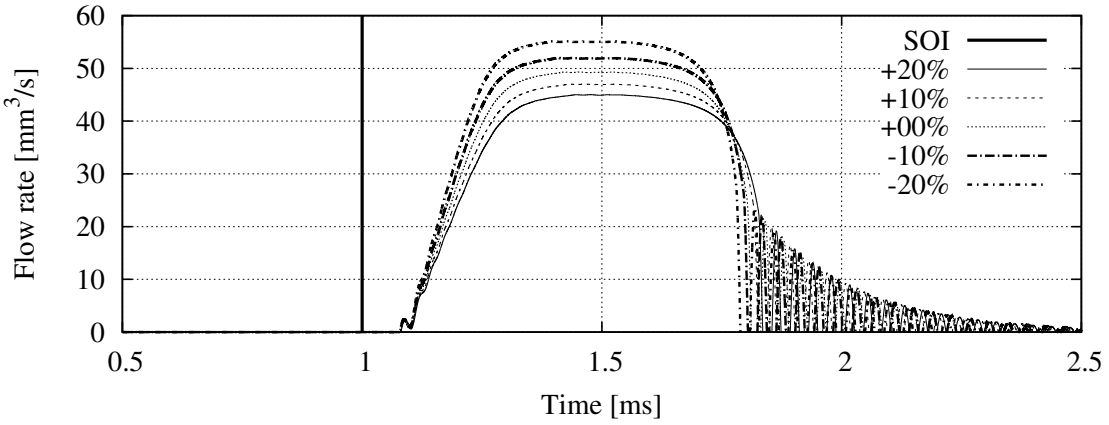


Figure 9.13: Volumetric flow rate versus time for the sensitivity analysis performed on density for a 500μs injection.

In addition, the opening and closing time of the injector varies slightly when the density changes. For low fuel densities, the opening and closing time of the injector is longer than at higher densities. This is because the flow rate into and out of the control volume is influenced by density and therefore it also affects the rate of pressure release in this chamber which controls injection.

Injector diagnosis

The sensitivity analysis, besides showing where problems could have arisen in the selection of values for the model, also provides insight into how wear within the injector changes the delivery and what results can be expected for different test conditions. Square-shaped rate profiles would indicate that the bleed orifice has worn out, whereas rounder profiles indicate the wear has taken place on the feed orifice. Longer injections indicate wear either on the shims or on the feed orifice. Determining which has worn requires consideration of the opening time of the injection as well. If the opening time is unchanged, the shims are worn because this is the only parameter that the shims have been shown to have an influence over. If both the opening time and the duration have increased, then wear on the feed orifice is responsible, as it alters both these parameters simultaneously. A faster flow rate and more delivery in the same amount of time as normal would indicate that the injector nozzles have worn and become larger.

9.3 Scilab vs. C++ model

A comparison between the C++, Scilab and experimental results are shown in Figure 9.14 which shows the injected flow rate against time. This shows the improvement that is gained in the conversion from Scilab to C++.

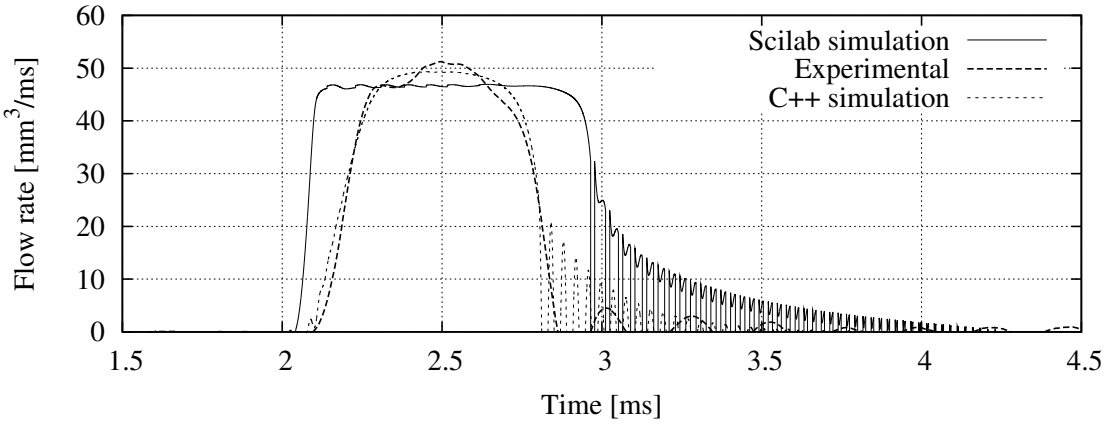


Figure 9.14: Flow rate versus time for Scilab, C++ and the experimental results.

In Figure 9.14, it can be seen that C++ and Scilab both predict the average flow rate well, but only the C++ model matches the profile closely. This difference between C++ and Scilab is significant because it will affect the amount of fuel that is delivered and which Scilab severely over predicts. Table 9.1 shows the important differences between the C++ and Scilab model.

Table 9.1: Comparison of the features of the C++ and Scilab models.

Parameter	Scilab	C++
Time step size	10^{-8} s	10^{-9} s
Number of volumes	Three	Eight
Bulk modulus varied	No	Yes
Density varied	No	Yes
Variable discharge coefficients	No	Yes
Akribis included	No	Yes
Constant Rail pressure	Yes	Yes

The main reason for the improved solution is the inclusion of variable discharge

coefficients. This could be implemented in the Scilab model, but it would be more time consuming than using C++. It was shown in Section 9.2 that the dependence of the solution on the bulk modulus and density was insignificant and therefore it would be unexpected that it would be the cause of the differences between the C++ and Scilab model. Including more volumes into the solution does improve the accuracy of the model, but not as much as by varying the discharge coefficients. The rail pressure was constant in both models, so that is not the cause of the differences between them. The main advantage of using the C++ model is the ease with which additional equations that take into account different components in the injector can be included.

9.4 Injector pressures

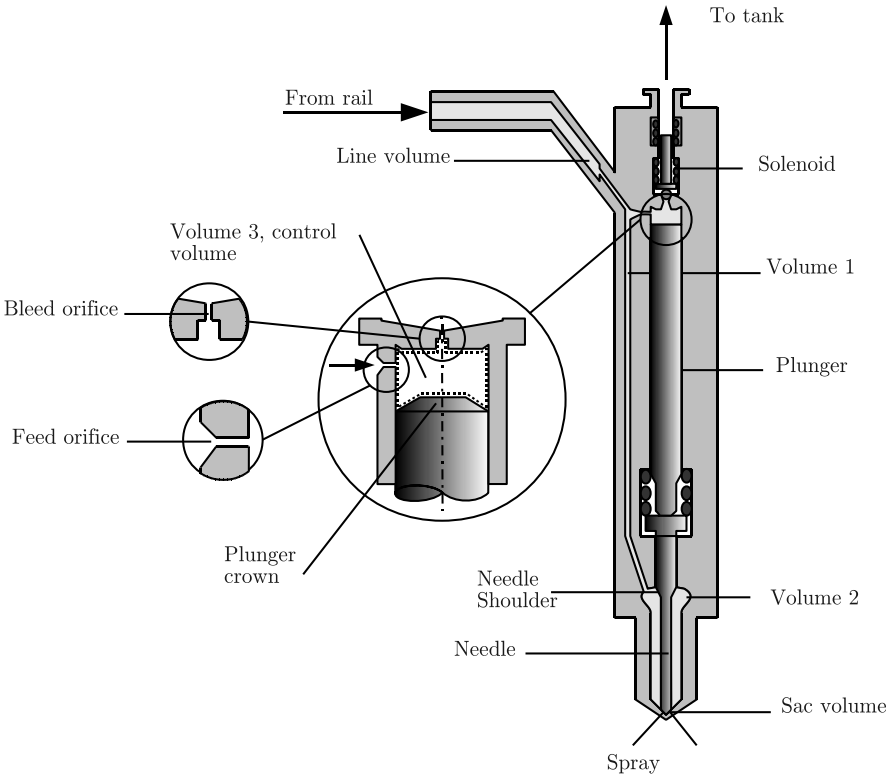


Figure 9.15: Electronically actuated common rail injector showing the different components and internal volumes that are needed for the model.

Figure 6.1 has been repeated here to remind the reader of the different volumes within the injector.

The internal injection pressures for the rail, line, volume 1 and volume 2 were calculated and are presented in Figure 9.16. This figure is identical to Figure 9.10 presented

earlier, but has been reproduced again because of its relevance here. Figure 9.16 shows the pressures in the rail, the line, volume 1 and volume 2 throughout the injection. The sac and control volume pressure have been shown separately in Figure 9.17 because their variation over the injection event is larger.

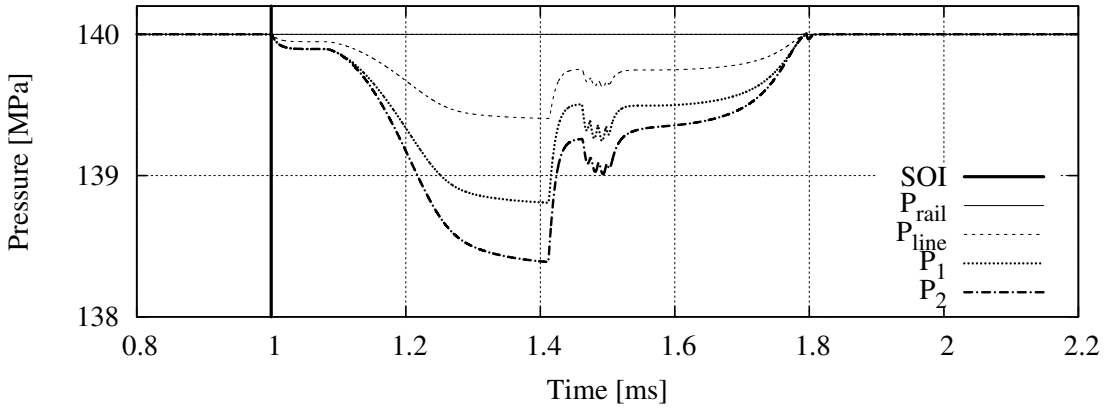


Figure 9.16: Pressure versus time for a 500 μs injection for the rail, line, volume 1 and volume 2.

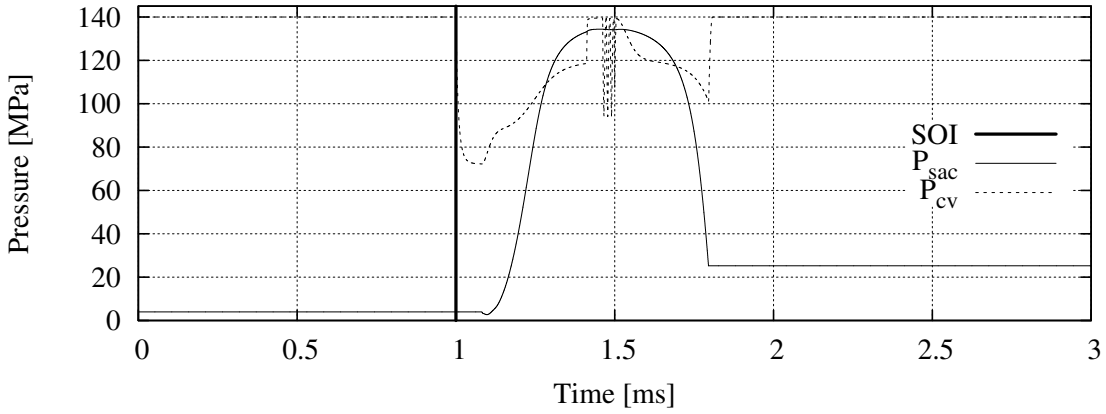


Figure 9.17: The pressure versus time for a 500 μs injection for the sac and control volumes.

The pressures in the control, sac and line volumes are discussed below. The control volume is discussed because it controls the behaviour of the model, the line pressure represents what can be measured on the test stand and the sac pressure represents the injection pressure.

Pressure signal delay

In Section 8.6 it was shown that there are delays between the actual injection event and its detection by the pressure transducer in the rail. This delay means that the rail pressure at the start of injection is unaffected by the injection, because the pressure signal from the nozzle has not yet reached the rail. In the construction of the model, the injector has been modelled as a series of volumes that can respond instantaneously to a pressure disturbance in any adjacent volume. Since all the volumes are adjacent to each other, and they all respond instantly to a disturbance, they are all in fact responding to that disturbance simultaneously. Therefore, any disturbance in pressure anywhere in the injector, is detected immediately in all other volumes in the injector. Thus, as soon as fuel is injected, the pressures will drop which can be seen in both Figure 9.16, where all the internal pressures drop simultaneously when injection is initialised at one millisecond. This illustrates the difference between the simulation and what actually occurs. With knowledge of the difference between the model and the experimental results, the model can be analysed.

Control volume pressure

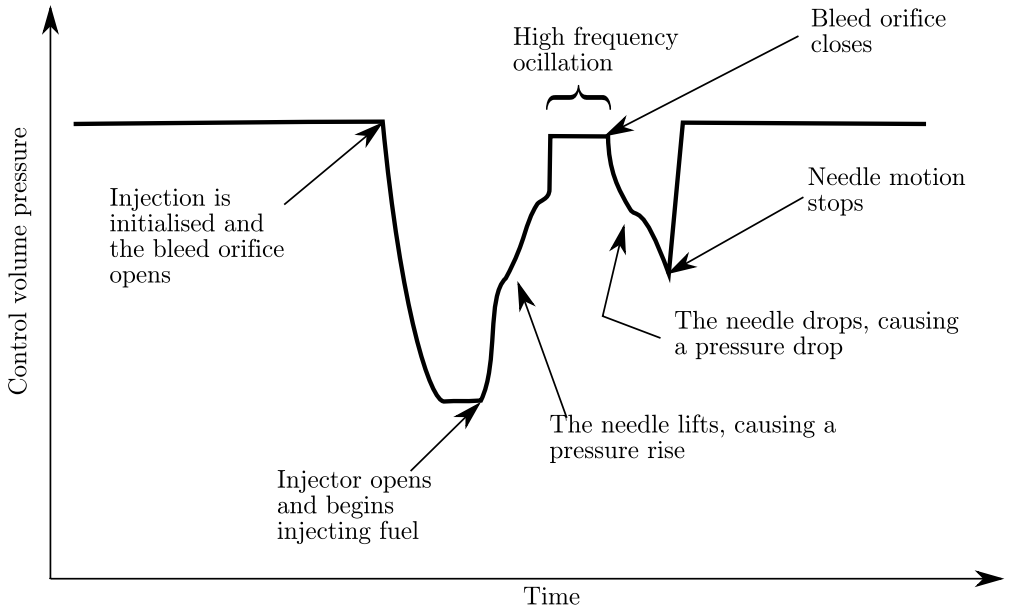


Figure 9.18: A schematic of the control volume pressure versus time.

A schematic of the control volume pressure showing the notable features is presented in

Figure 9.18. In this figure, it can be seen that the time when the bleed orifice is opened and injection starts, is different. This occurs because the pressure in the control volume needs to drop sufficiently so that the net force acting on the needle can lift it off its seat to allow injection to begin. Thus, at the time when the pressure in the control volume reaches its minimum, injection will start. Figure 9.17 shows that this pressure drop is rapid, indicating that the injector responds quickly when the bleed orifice is opened. The magnitude of the pressure drop shows that a large pressure drop is required before the needle will lift. For this simulation, the pressure has dropped approximately 70 MPa from 140 MPa.

The pressure in the control volume starts to rise as seen in Figure 9.17 and 9.18. This pressure rise occurs because the fuel in the control volume is compressed by the needle as it lifts. (See Equation (6.11) to see how the pressure in any volume is dependent on the volume).

The high frequency oscillations have not been shown in Figure 9.18 but can be seen in Figure 9.17. These oscillations arise when the needle travels too far into the control volume. If it travels too far, it interacts with the upper boundary of the control volume and bounces back down. While in contact with the upper boundary of the volume, the needle prevents flow from exiting via the bleed orifice. The remaining volume in the control chamber is small and consequently the pressure here becomes sensitive to the needle motion and any inlet flows from volume 1. The control volume then pressurises and de-pressurises quickly during this time, which is the high frequency oscillations seen in Figure 9.17. This results in rapid, large fluctuations in the pressure. When the injections are short, such as pilot injections, the needle may not travel far enough to reach the roof of the chamber, and the high frequency fluctuation stage of the injection would not occur. It would simply lift slightly, and then close. This feature was also observed by Lee et al.

The end of this high frequency stage marks the closing of the bleed orifice. The oscillations stop because fuel is only flowing into the control volume and not leaving via the bleed orifice anymore. The needle can only close to compensate for the building up of fuel within the control volume. The pressure proceeds to drop because the chamber volume is increasing as the needle moves down. The final abrupt change in the control volume pressure occurs when injection stops, the needle is closed and the pressure can

once again return to the rail pressure.

Pressure features in the internal injector volumes

A fundamental difference between the model and the experimental results is the rail pressure. In the model, the rail pressure was assumed to be constant which obviously is not the case. This difference can be seen by comparing the rail pressure for the model in Figure 9.16 and the experimental rail pressure in Figure 8.7. Nevertheless, certain behaviours of the line pressure in the model mimic the behaviour of the rail pressure from the experiments seen in Figure 8.7 or shown schematically in Figure 8.4. Many of the features have already been discussed in Section 8.3, and therefore need not be repeated here. Similarities will be pointed out since they demonstrate that the model behaves in a comparable way to reality. The line pressure result from the model is compared to the rail pressure from the experiment because the line is the closest volume to the rail.

Both the experimental results and the model show a drop in the rail and line pressure respectively; because the rail pressure remains constant throughout injection, the severity of the pressure drop in the line is damped by essentially having an infinite reservoir to restore it to the set point pressure. If the system was not modelled in this way, then the drop in pressure due to injection would be larger than what is shown in the model. Despite this infinite reservoir, the other internal volumes experience a pressure drop due to an injection event. Two observations about this pressure drop can be made.

Firstly, the magnitude of the drop due to injection is smaller in the model, as observed when comparing Figure 8.7 and 9.16. This is due to the damping provided by the rail mentioned above. The experimental results indicate a pressure drop of about 8 MPa whereas the model shows a drop of only 2 MPa. This difference appears large but actually translates into a difference in injection pressure of less than 5%. Importantly, the response to the opening of the injector is correct, including the pressure relief time discussed in Chapter 8.

Secondly, in Figure 9.16 it can be seen that pressures in volumes 1 and 2 respond immediately to the opening of the bleed orifice and the start of injection. If the time taken for the signal to travel through the injector were included, this would not occur.

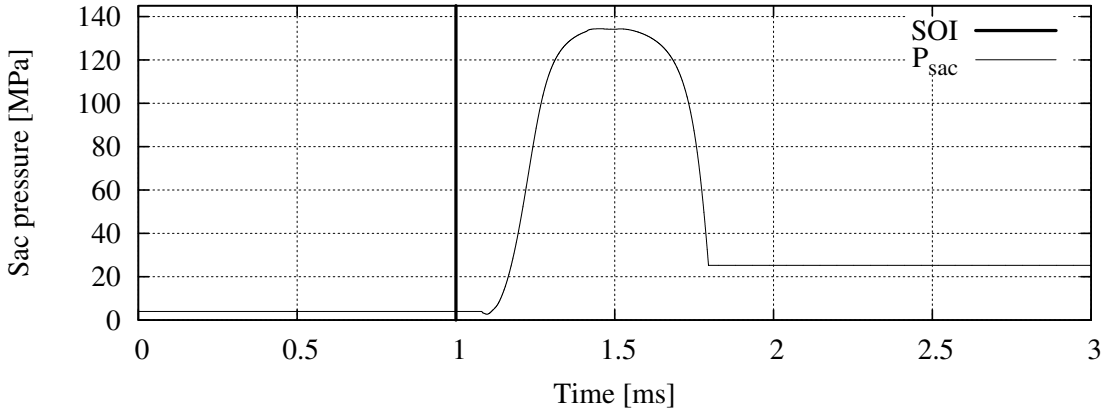


Figure 9.19: Sac pressure versus time for a 500 μs injection.

Instead, the pressure in volume 1 would decrease and then only would the pressure in the line and volume 2 would decrease. This would correspond to the delay that is observed in Figure 8.7.

Following the large pressure drop, there is an increase in the line pressure similar to the experimental results. This pressure coincides with the end of the needle motion after which small pressure oscillations then occur in the volumes. The oscillations are smaller than those that occur in the control volume that were discussed above are due to the flow occurring from the control volume and feeding into the other volumes. The magnitude of the oscillations is smaller because volume 1 is larger than the control volume, thereby dampening the oscillation. Equation (6.11) shows that the change in pressure within a volume is inversely proportional to the volume of the chamber. The end of the oscillation stage once again marks the point where the bleed orifice closes, and the needle then begins to close and the pressures in volumes 1 and 2 become the same as the rail pressure.

Figure 9.16 shows that the internal pressures during injection decrease from the rail to the nozzle tip. This result is encouraging because the pressure should be lowest in the sac during injection and largest at the rail. The pressures in the intermediate volumes should fall between these limits, which they do.

The injection pressure

Figure 9.19 shows that the injection pressure is 130 MPa which is about 7% lower than the rail pressure. Thus when estimating the spray characteristics in a common rail

setup, the injection pressure is similar to the rail pressure. This is unlike the mechanical injector where the line and opening pressures cannot be used as approximations of the injection pressure.

Figure 9.16 shows that the injection pressure in the sac is higher after injection than it was before injection. This is due to the artificial volume that was created so that the injection pressure could be determined in the simulation. Without this volume, the pressure further upstream of the orifice would have to be used, for example, the pressure in volume 2. When the needle closes, this volume becomes separated from the chamber and becomes pressurised by the needle and therefore the higher pressure in the volume after injection than before.

9.5 Test pressure input

The model was adapted to use the measured rail pressure from Chapter 7 as an input. This will show how pressure fluctuations during injection will affect the delivery and allow the results to be compared it those of the constant rail pressure input. This is similar to the sensitivity analysis and will help justify the constant rail pressure assumption that was used in the model.

Pressure result

The pressure results are shown in Figure 9.20 for the rail, line, volume 1 and volume 2 and in Figure 9.21 for the sac and control volume. These figures should be compared to Figures 9.16 and 9.17, where the constant rail pressure assumption was used.

In Section 8.5 it was shown that there is a significant delay in the detection of the injection event at the rail. For this simulation, the point where the injector opened was set to coincide with the first pressure drop in the rail pressure. This decision was made because the speed of sound in the fluid was neglected and the injection event would therefore be in phase with the pressure drop.

Comparing Figures 9.16 and 9.20, it can be seen that when the experimental rail pressure is used in the model, the pressures in the line, volume 1 and volume 2 are

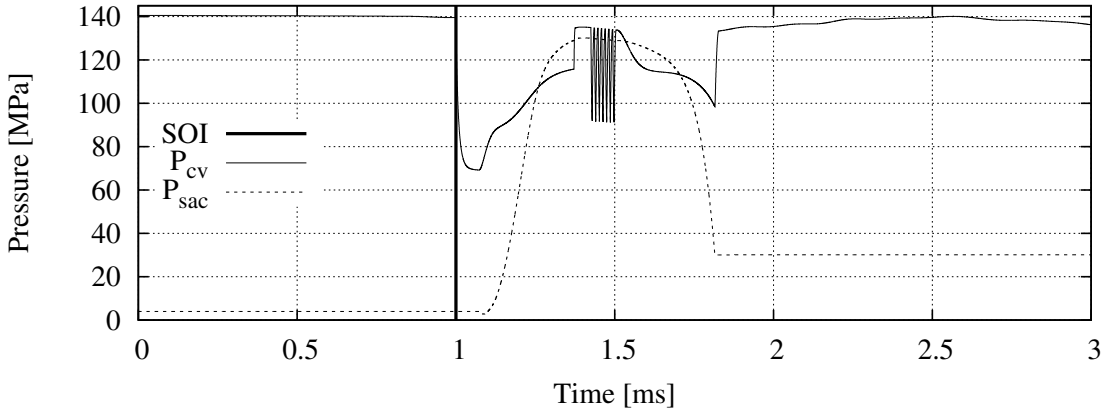


Figure 9.20: Pressure versus time for a 500 μs injection for the sac and control volumes using the experimental rail pressure as the input pressure.

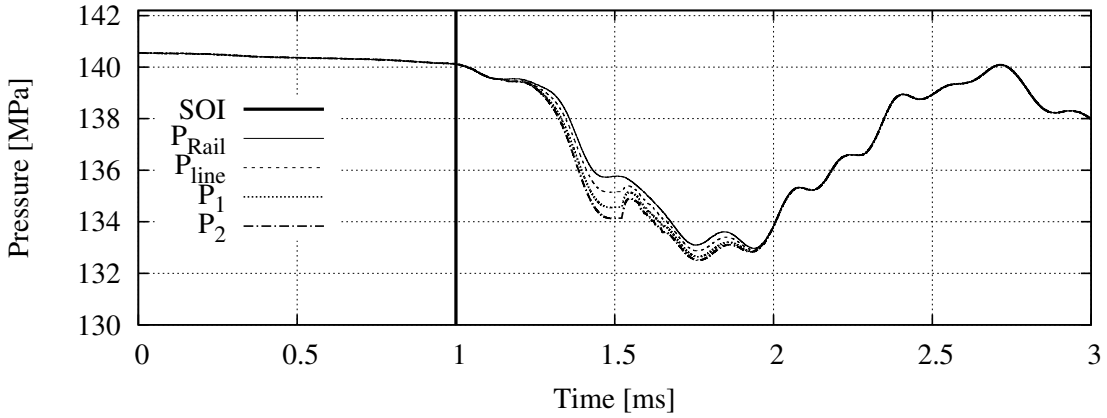


Figure 9.21: Pressure versus time for a 500 μs injection for the rail, line and volume 1 and volume 2 using the experimental rail pressure as the input pressure.

lower than when a constant rail pressure is used. Nevertheless, the pressures in these volumes still follow the rail pressure closely. Although, the differences in pressures between the simulations with constant and experimental rail pressure appear large, in comparison to the set point pressure of 140 MPa, the differences are in fact small. This has already been shown to be true in Section 9.2 where the sensitivity analysis was carried out.

Flow rate comparison

Figure 9.22 shows the rate versus time for the experimental results, constant and external rail pressure simulations. In Figure 9.22 it can be seen that taking the rail

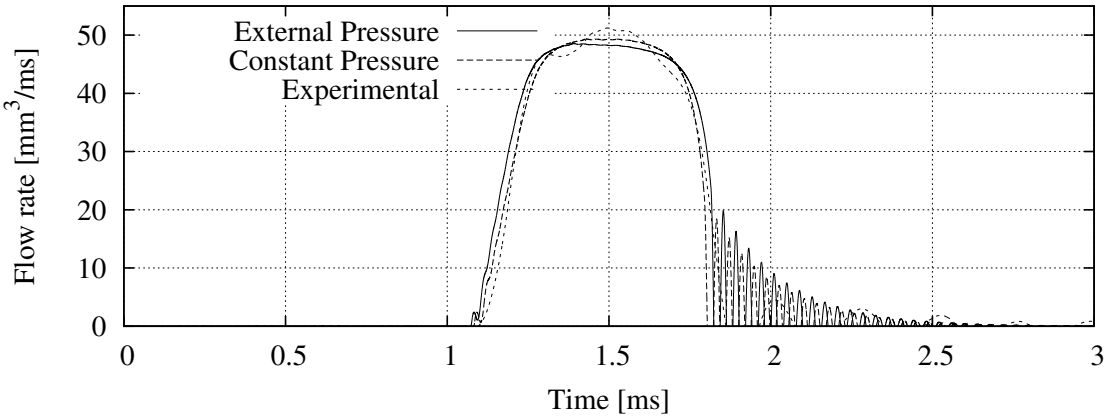


Figure 9.22: Flow rate versus time for a 500 μs injection showing measured results and simulated results for both constant rail pressure and measured rail pressure inputs.

pressure into account does not alter the duration of the injection nor the average injected flow rate. This test once again shows the sensitivity of the system to the rail pressure in a different way to that in Section 9.2 where the rail pressure was varied during injection and that assuming a constant rail pressure does provide suitable accuracy in the model.

9.6 Needle lift

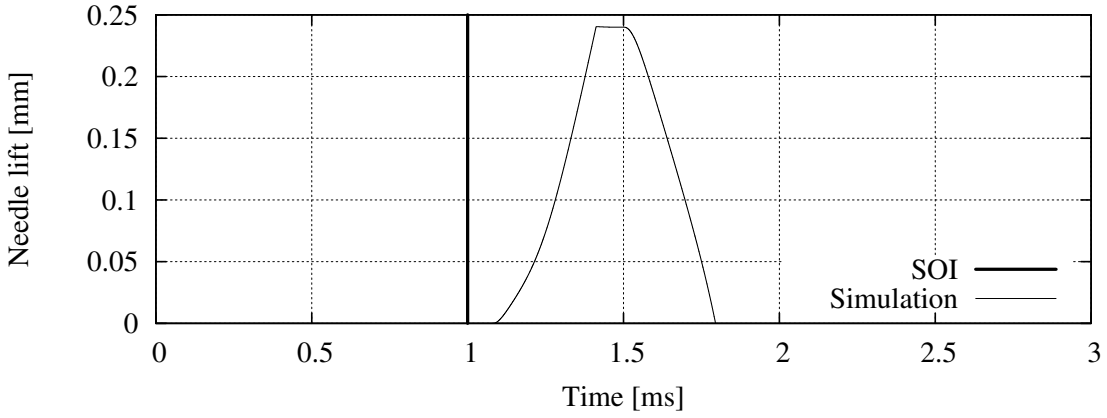


Figure 9.23: Needle lift versus time for the 500 μs injection.

The needle lift for the 500 μs injection is shown in Figure 9.23. Until now it has been stated that the injection does not start exactly when the bleed orifice is opened. But it has not been proved for the model. Figure 9.23 does this by showing that the needle lifts after the bleed orifice is opened at a time later than one millisecond. This delay is

the time that it takes for the chamber pressure to drop enough to allow the needle to lift. It was discussed above that the pressure relief time in the simulation matches well with the time in the experiments.

Chapter 10

Conclusion and Recommendations

This chapter draws the results and discussions of Chapter 4 to Chapter 6 together, explaining how the objectives were met. Interesting features that were found during the investigation are also described. In the recommendations which would allow for better tests and simulations to be attained, are discussed.

10.1 Conclusion

The conclusion presented below represents the important outcomes obtained from the investigations performed. The conclusion is divided by topics, that is, the mechanical injector model, the common rail tests and then the common rail model.

10.1.1 The mechanical model

A mechanical injector was successfully modelled using the definition of the bulk modulus to describe the fluid behaviour within the injector and by modelling the injector needle dynamics by describing it as a mass-spring-damping system.

The model showed that the injection pressure with time was lower than the line pressure. The difference between these pressures was dependent on the opening pressure of the injector and the engine load. Similarly, the opening pressure of the injector was also larger than the actual injection pressure at the nozzle. The average injection

pressure was calculated to be between 30% and 65% of the opening pressure depending on the conditions tested. Thus, it was shown that the line and opening pressures are not adequate descriptors of the injection pressure. If the line or opening pressures of the injector are used in the penetration equations, then the predicted penetration will be overestimated.

It was found that changing the opening pressure of the injector had the largest effect on the average injection pressure. A linear increase in the opening pressure resulted in linear increase in the average injection pressure. The number of orifices in the injector had the next largest influence on the injection pressure. The three orifice injector had larger average injection pressures than the four orifice injector. This can be attributed to the three orifice injector constricting the flow more than the four orifice injector. More orifices in the injector result in lower injected flow rates for each orifice and therefore less atomised and less penetrating spray. The throttling condition had a negligible effect on the average injection pressure. It did however, play a large role in determining the length of injection. The dependence of the injection pressure on the number of discharge orifices, opening pressure and throttling condition makes finding a correlation between them and the injection pressure very complicated.

10.1.2 The common rail experimental tests

Tests were carried out to measure the flow rate for different injection durations ranging from 400 μs to 2000 μs at 140 MPa in a common rail system. The amount of fuel delivered increased with the injection duration while the flow rate remained approximately constant during the injection because the rail pressure was the same for all the tests. These results were compared to the model results.

Using the measured injection flow rate, the injection pressure was calculated by assuming a constant discharge coefficient of 0.6. The results show the injection pressure to be about 90% of the rail pressure. This means that the rail pressure can be used to approximate the injection pressure and used in the penetration equations.

Features in the flow rate profile make it possible to identify when the bleed orifice opens and when the injector opens. By comparing when injection was detected by the Akribis

to when it was detected at the rail, it was observed that the rail lagged the Akribis. This occurs because the pressure signal arising from the injection event travels to the rail at the speed of sound of the fuel. This delay was approximately 550 μs.

The injected flow rate per orifice of the injector was compared to the results from the mechanical injector model. It was found that the flow rates for the mechanical and common rail systems were comparable. However, when the exit velocities of the two systems were compared, it was found that the common rail system had a significantly larger jet exit velocity. This was due to the substantially smaller orifice area of the common rail injector and the higher injection pressure, confirming that the spray characteristics are improved by the common rail system.

10.1.3 The common rail model

A common rail injection system model was constructed and it was found to fit the data well. This model required very little information about the exact details of the internal geometry of the injector, making it a very attractive and relatively simple model to construct.

The model was first constructed in Scilab and then in C++. The C++ model was found to be a better solution because it is simpler to add equations that would improve the model. The C++ model was improved in comparison to the Scilab model by including bulk modulus and density equations that are dependent on pressure, additional divisions of the internal injector volumes and discharge coefficients that varied according to the injection duration.

The varying discharge coefficients provided the greatest improvement to the model, resulting in a model that gave far better agreement to the experimental results than if it was excluded. This varying discharge coefficient represents the variation in the discharge coefficient due to the transient flow that occurs during injection. Because data on transient discharge coefficients is limited, their values had to be chosen empirically.

The model was tested for different injection durations ranging from 400 μs to 2000 μs at 140 MPa. These conditions are the same as the tests used in the experimental set up, allowing comparisons between an actual injector and its model to be conducted.

A sensitivity analysis was carried out on the inputs for the model to determine the effect of any error in specifying these inputs on the solution. Besides the sensitivity to the discharge coefficients, the model was sensitive to changes in the discharge flow area, the limit on the needle motion, the rail pressure and the fuel density. The model was insensitive to changes in the internal injector volumes, the needle mass and the bulk modulus of the fuel.

It was observed in the sensitivity analysis that each of the parameters varied changed the flow behaviour of the injector differently. Using this in conjunction with tests of new and old injectors, it is possible to determine which component of the injector has worn out. This is useful in diagnosing used injectors.

Features in the pressure plots indicate when the bleed orifice opened and when the needle lifted. These features are similar to those observed in the experimental results giving confidence in the description of the injector by the model. These features however cannot be observed in the rail pressure as this was assumed to be constant for the model but they can be viewed in any of the other internal pressures.

The model was tested using the measured rail pressure as an input instead of using the constant rail pressure assumption. By comparing these solutions, it was found that the injected flow rates were very similar. This means that the constant rail pressure assumption is valid.

10.2 Recommendations

The recommendations presented below suggest possible ways of improving the accuracy of the solutions by overcoming problems that were encountered in a better way. These recommendations are divided by topics as covered in this research.

10.2.1 The mechanical model

Recommendations that would improve the mechanical injector model are discussed below.

Convert the model into C++

Converting the model from a Scicos program into a C++ program would make the inclusion of any improvements, such as accounting for variation of bulk modulus and density with pressure of the fuel, easier to implement. Converting the model into C++ could easily be done by adapting the common rail C++ model to be able to model mechanical injectors. In addition, a C++ program would decrease the time taken to solve while at the same time increasing the accuracy.

Pump and throttling system

The mechanical model should include the pump and the throttling system. This would make the flow delivered to the injector more accurate and thereby provide more accurate predictions of the injected flow rates. To do this, accurate knowledge of the pump system is required.

Experimental confirmation

The model needs to be confirmed against experimental results. This could be achieved by measuring the injected flow rate in a similar way to that carried out for the common rail, using the Akribis or a similar flow measurement device.

10.2.2 The common rail experimental tests

Tests should be run at other injection pressures to provide data against which the model could be validated. Another method of confirming the accuracy of the model is to measure the needle lift during injection. The measured needle lift profile could be compared to the simulated needle lift.

Other fuels should be tested and again the results could be compared to those of the model. This would confirm the predictions made in the simulations about how the delivery is affected by a change in fuel bulk modulus and density.

10.2.3 The common rail model

Recommendations that would improve or give greater confidence in the accuracy of the common rail model will be discussed here.

The pump system

The pump system should be included in the model so that the constant rail pressure assumption could be removed. Although this would not change the results substantially as shown in the sensitivity analysis, it would improve the results. This would also help to understand the features observed in the model, especially after an injection event has occurred.

The actuation system

The model was simplified by excluding the solenoid and simulating its result by opening the bleed orifice artificially. It is recommended that the solenoid should be included in the model, as it would allow the minimum opening time of the injector to be determined and compared to the experimental results. This minimum opening time would be dependent on the energising time of the solenoid. Additionally, by modelling the solenoid, the bleed orifice would open gradually which may have an effect on the overall injector behaviour.

Pressure signal delay

Taking into account the speed of sound in the fuel in the model would provide information about the delays that are seen in the experimental results. This would require more detailed knowledge of the internal geometry of the injector, specifically the length between the two orifices. Alternatively, a CFD model could be constructed that would also be able to take this into account. Either way, the infinite speed of sound assumption in the current model would be removed.

Transient discharge coefficients

It was seen in section 9.2 that the model was sensitive to the discharge coefficients at the bleed and feed orifice. It was found that in order to get good agreement with the experimental results, the values had to be chosen empirically. However, this aspect of the model could be improved by having better information about discharge coefficients vary under transient conditions. If accurate discharge coefficients could be obtained, the model would no longer be empirical in nature and would be relevant to a wider range of tests. Again, a CFD model might also be able to predict these coefficients. It may not be necessary to model the entire injector as a model of the control volume only may be sufficient.

Additional tests that should be performed

The model in this research should be tested at other injection pressures to evaluate if the current discharge coefficients used for the 140 MPa simulations are still valid. If they are not, then new values should be found by either testing or by researching what these should be.

The model has only been tested with ISO 4113 and should also be validated with fuels with different properties. Other fuels that could be used are diesel, DME or methanol. Although the properties of diesel are similar to ISO 4113, diesel would provide more accurate information about what occurs during injection. Caution must be taken when testing these fuels because of their flammable nature.

Cavitation

Cavitation should also be included in the model, but again this would require information about the geometry of the injector and may be better suited to a CFD analysis.

References

[1] Office of Transportation and Air Quality U.S. Environmental Protection Agency. Final regulatory analysis: Control of emissions from nonroad diesel engines, May 2004.

[2] United States Environmental Protection Agency. Nonroad diesel emission standards epa420-r-01-052. Staff Technical Paper, October 2001.

[3] Regulation (EC) No 715/2007 of the European Parliament and the Council. Regulation (EC) No 715/2007 of the European Parliament and the Council of 20 June 2007 on type approval of motor vehicles with respect to emissions from light passenger and commercial vehicles Euro 5 and Euro 6) and on access to vehicle repair and maintenance information. Official Journal of the European Union, June 2007.

[4] Standards: Europe: Cars and light trucks. URL `http://www.dieselnet.com/standards/eu/ld.php`.

[5] M.Y. Kim, S.H. Yoon ans B.W. Ryu, and C.S Lee. Combustion and emission characteristics of DME as an alternative. *Fuel*, doi:10.1016/j.fuel.2008.01.032, 2008.

[6] H. Raheman and S.V. Ghadge. Performance of compression ignition engine with mahua (madhuca indica) biodiesel. *Fuel*, 86:25682573, 2007.

[7] K. Wakai, K. Nishda, T. yoshizaki, and H. Hiroyasu. Spray and Ignition Characteristics of Dimethyl Ether Injected by a D.I. diesel injector. *The fourth international Symposium Comodia 98*, 98:537–542, 1998.

[8] S. Theil. The next petroleum. *Newsweek*, August 2005.

[9] K. Bozbas. Biodiesel as an alternative motor fuel: Production and policies in the European Union. *Renewable and Sustainable Energy Reviews*, 12:542552, 2008.

[10] J. B. Heywood. *Internal Combustion Engine Fundamentals*. McGraw Hill International Editions, International edition, 1988.

[11] M. Osenga. Acert takes the lead for Cat Tier 3 diesel. *Diesel Progress*, North American Edition, March 2004.

[12] Volvo construction equipment exhaust emissions reduction - towards "stage iiib/tier 4 interim" non-road diesel exhaust emission standards questions & answers, April 2009.

[13] A. H. Lefebvre. *Atomization of sprays*. Hemisphere publishing corporation, 1^{st} edition, 1989.

[14] E. Giffen and A. Musaszew. *The atomisation of liquid fuels*. Chapman and Hall LTD, 1^{st} edition, 1953.

[15] S. Chandrasekhar. *Hydrodynamic and Hydromagnetic Stability*. Dover Publications, Inc., 1^{st} edition, 1981.

[16] P. H. Martmottant and E. Villermaux. On spray formation. *Journal of fluid mechanics*, 498, 2004.

[17] P. G. Burman. *Fuel injection and control for internal combustion engines*. The technical press Ltd., 1^{st} edition, 1962.

[18] S.S. Sazhin, G. Feng, and M.R. Heikal. A model for fuel spray penetration. *Fuel*, 80, May 2001.

[19] L. C. Lichty. *Internal-Combustion Engines*. McGraw-Hill Book Company, Inc., 6^{th} edition, 1951.

[20] H.K. Suh and C.S. Lee. Experimental and analytical study on the spray characteristics of Dimethyl Ether (DME) and diesel fuels within a common-rail injection system in a diesel engine. *Fuel*, 2007.

[21] J. Yu and C. Bae. Dimethyl ether (DME) spray characteristics in a common-rail fuel injection system. *Proc. Instn Mech Engrs: J. Automobile Engineering*, 217 Part D, 2003.

[22] S.Gupta, R. Poola, and R. Sekar. Effect of injection parameters on diesel spray characteristics. *SAE Techical Paper Series*, 2000.

[23] B.R Munson, D.F Young, and T.H. Okiishi. *Fundementals of fluid mechanics*. John Wiley & Sons, Inc., 4^{th} edition, 2002.

[24] F. Payri, V. Bermudez, R. Payri, and F.J. Salvador. The influence of cavitation on the internal flow and the spray characteristics in diesel injection nozzles. *Fuel*, 83:419–431, 2004.

[25] R. Payri, H. Climent, F.J. Salvador, and A.G. Favenne. Diesel injection system modelling. methodology and application for a first-generation common rail system. *Proc. Instn Mech. Engrs Automobile Engineering*, Vol. 218 Part D: J., 2004.

[26] C.D. Rakopoulos and D.T. Hountalas. A simulation anaylysis of a di diesel engine fuel injection system fitted with a constant pressure valve. *Pergamon*, 1995.

[27] X.L.J. Seykens, L.M.T. Somers, and R.S.G. Baert. Detailed modeling of the common rail fuel injection process. *MECCA, III, 30-39,*, 2005.

[28] H.K. Lee, M.F. Russell, C.S. Bae, and H.D. Shin. Development of cavitation and enhanced injector models for diesel fuel injection system simulation. *Proc Instn Mech Engrs*, 216 Part D: J Automobile Engineering, 2002.

[29] *Code of practice the overhall of diesel fuel injection equipment.* South African Standard, sabs 0166:1984 edition.

[30] A.L. Boehman, D. Morris, and J. Szybist. The impact of the bulk modulus of diesel fuels on fuel injection timing. *Energy & Fuels*, 18:1877–1882, 2004.

[31] L.M. Rodriguez-Anton, C. Aparicio, B. Guignon, and P.D. Sanz b. Volumetric properties at high pressure of waste oil methyl ester compared with diesel oil. *Fuel*, 87:1934–1940, (2008).

[32] A Catania, A. Ferrari, and E. Spessa. Temperature variations in the simulation of high-pressure injection-system transient flows under cavitation. *International Journal of Heat and Mass Transfer*, 51:20902107, 2008.

[33] J. Rice. *Study of fuel injection spray patterns*. School of Mechanical, Industrial and Aeronautical Engineering, University of the Witwatersrand, 2006.

[34] P. Lino, B. Maione, and A. Rizzo. Nonlinear modelling and control of a common rail injection system for diesel engines. *Elsevier, Applied mathematical modeling*, 2007.

[35] P. M. L. Lopes. A comparative study of the combustion characteristics of a compression ignition engine fuelled on diesel and dimethyl ether. Master's thesis, School of Mechanical, Aeronautical and Industrial Engineering, 2006.

[36] J. Kiijarvi. *Diesel fuel injection system simulation*. PhD thesis, Helsinki University of Technology, 2003.

[37] *Electronic engine management for diesel engines. Diesel accumulator fuel-injection system Common Rail*. Bosch, 1999 edition, 1999.

[38] N-H Chung, B.G Oh, and M.H Sunwoo. Modelling and injection rate estimation of common-rail injectors for direct-injection diesel engines. *Proc. IMechE*, Vol. 222 Part D: J. Automobile Engineering, 2008.

[39] S.C.Chapra and R.P.Canale. *Numerical methods for engineers*. McGraw Hill International Edition, International edition, 2006.

[40] Innov8 Technologies Ltd. *Injector Spray Analysis and Flow Measurement Stand. Operating and Maintenance Manual*. Innov8 Technologies Ltd, rev.01 edition, may 2008.

[41] SAE. *Direct Injection Systems for Spark-Ignition and Compression-Ignition Engines*. Society of Automobile Engineers, Inc., 1999.

[42] I.E. Idelchick. *Handbook of Hydraulic Resistance*. CRC press, 3^{rd} edition, 2000.

Appendix A

Image processing code

This program was written to search through the images of Rice [33], and track the spray penetration. The program was written in Scilab 4 using an image processing toolbox. A later version of Scilab has been released, but this code has not been proven to work with this version. Additionally, the program is written assuming a Linux operating system, which means that the way that file paths are constructed are different from a Windows operating system. Apart from this difference, the code should run in Windows.

A.1 Main program

This is the main program that must be executed.

```
//  PROGRAMMED BY THOMAS SPRICH
//  FILE HISTORY
//  v1 - simple image processing of the full image
//  v2 - use the area of interest to define a portion of the image.
    This makes the passing and handling of the image quicker
//     - makes the image smaller by taking out the white space that
    is a there as a result of the
//  v3 - Adjusts the histogram of the image to equalise it.  This
    enhances features, unfortunately it enhance the noise aswell.
    Thus a filter will be need
//  v4 - some noise (such as the knife edge line) is removed by
    subtracting the first image from the current image
```

```
//  v5 - reverse all the images, this should give black sprays on a
    white background. The problem is that the penetration points
    will then not work so be warned. They will probably need to be
    swopped, so instead of being 'less than' it will have to be '
    greater than' when comparing 'grey levels'
//      - The images are now cut, they have no empty space at their
    end
//  v6 - now have to fix up the penetration measuring part of the
    program. This needs to be done so that the image 'change' method
     is used.
//      - The images have not been modified with equalise yet, this
    means that they can all be compared.
//        NOTE: Becareful to extract the line information before the
    Image is rotated for presentation.
//  v7 - Upon attempting to extract penetration information from the
    difference comparison, it was found that it was harder to extract
     the required information. So at this stage, the image
    processing finds the penetration and attempts to remove the noise
     from the images and focusses on the spray area so that the
    images are presentable for papers and so forth

getd('/home/thomas/Documents/Spray_results/John_rice'); //ubuntu

//********************Position of injection in unedited image
RowU=41;
ColU=148;
//********************End Position of injection in unedited image

angle=45;// for the 3 hole nozzle

nozzle=4;
FileName='/home/thomas/Documents/Spray_results/John_rice/d'+string(
    nozzle)+'_'; //u

  Penetration_Tracking=[];
  Jet_Breakup_Tracking=[];
  Plot_names=[];
  Time=[];
for ExpNumInt=100:25:250,      //This is the pressures that were
    tested and forms part of the FOLDER names. This numbers help
```

```
    move in the folders
//// for the 3 hole nozzles
//
  Row =132;    //this refers to the y axis
  Col=302;  //These have been defined so that it is easy to change
      later.

//// begin 4 hole nozzle
// Col =288;
// Row =123.;
////end 4 hole nozzle

  ExpNumStr=string(ExpNumInt);
  Plot_names=[Plot_names , ExpNumStr + " bar"];
  chdir(FileName+ExpNumStr);
  Image0=gray_imread('Frame1.jpeg');
  Image0=Rotated(Image0,angle);

  Col0=1;     //Also makes it easier to incorporate nozzle finding
      later if I was to.
  Spray_Width=80;  //this is the width in pixels of the spray that
      the simplifying images must sorth through
  Breakup_Threshold =0.15;  //This checks if the difference between
      the two pictures is within <Breakup_Threshold> of eachother.
  Spray_Threshold =0.99;  //This checks that the spray image is less
      than <Spray_Threshold> of the Blank Image
 //A tighter threshold value for the spray gives better results.

  px2mm=9/30; //Pixel to mm conversion factor.
  Image0=Spray_area(Image0,Col,Row,Spray_Width);
       Image0=Cut(Image0);
       [x y]=size(Image0);
       x=[];Col=y;y=[];
       Line0=GetLine(Image0,Spray_Width/2+1,Col0,Col);    //This is
           similar to the passing the complete image. This passes the
           smaller image to save memory and processing time.

 images would be much quicker
  PT=[];  //Individual penetration tracking.
  JT=[];  //Individual penetration tracking.
```

```
  for ImageNumInt = 2:1:8,    //this is the images to process
    ImageNumStr =string(ImageNumInt);
    Image_Next=gray_imread('Frame'+ImageNumStr+'.jpeg');
    Image_Next=Rotated(Image_Next,angle);

    //*********this block is for the adaptions to use the smaller
       image
      Image_Next=Spray_area(Image_Next,Col,Row,Spray_Width);
      Line_Next=GetLine(Image_Next,Spray_Width/2+1,Col0,Col);    //
         This is similar to the passing the complete image. This
         passes the smaller image to save memory and processing time
         .
      Image_Next=Image_FixA(Image_Next,Image0);
      Image_Next=Rem_Noise(Image_Next,0.06);
//*********END BLOCK
    Image_Next=Rotated(Image_Next,-90);
    Image_Next=Cut(Image_Next);
    imwrite(Image_Next,'Frame'+ImageNumStr+'.eps');

    Breakup_Point=Find_Breakup(Line0,Line_Next,Breakup_Threshold);
    Spray_Point=Find_Spray_A(Line0,Line_Next,Spray_Threshold,
       Breakup_Point);

    if Breakup_Point<0 then Breakup_Point= 0; end;  //This line is
       here so that jet break up occurs at the nozzle exit
    if Spray_Point<0 then Spray_Point= 0; end;  //This line is here
       so that Spray break up occurs at the nozzle exit
    PT=[PT;Spray_Point];
    JT=[JT;Breakup_Point];
  end;
  Penetration_Tracking=[Penetration_Tracking  , PT];
  Jet_Breakup_Tracking=[Jet_Breakup_Tracking  , JT];
end;
Time=1*(2:1:ImageNumInt)';
xset('window',0);
xbasc(0);

Jet_Breakup_Tracking= Jet_Breakup_Tracking*px2mm;
plot2d(Time,Jet_Breakup_Tracking,[ 1; 2; 3; 4; 5; 6; 7]);
```

```
legends([Plot_names],[ 1; 2; 3; 4; 5; 6; 7],opt='ul');
//**************BLOCK FOR TESTING
xbasc(1);
xset('window',1);
//
Penetration_Tracking=Penetration_Tracking*px2mm;//mm
plot2d(Time,Penetration_Tracking,[ 1; 2; 3; 4; 5; 6; 7]);
legends([Plot_names],[ 1; 2; 3; 4; 5; 6; 7],opt='ul');
xtitle('','Time [ms]','Penetration [mm]');


chdir('/home/thomas/Documents/Masters/Thesis/Scilab_Files/');  //u
mdelete('JohnRice-d'+string(nozzle)+'-full.txt');
write('JohnRice-d'+string(nozzle)+'-full.txt',[Penetration_Tracking])
    ;
//************END BLOCK FOR TESTING
```

A.2 Additional functions

Presented below are the functions that were written and called by the main image processing program. The section name takes the name of the function.

A.2.1 Spray_area

```
//This is a function that will take extract just the spray area from
    the images
//The size of the image is determined from the main file


//funtion result=name[variables transfered]
function New_Image=Spray_area(FImage_Next,FCol,FRow,FSpray_Width),
  New_Image=[];
  i=(FRow-FSpray_Width/2):1:(FRow+FSpray_Width/2);
  FLine=FImage_Next(i,1:1:FCol);

  [x y]=size(FLine);
  FLine1=[];
```

```
  for j=1:1:y,
    if sum(FLine(:,j))>0 then     //This removes excess black area
       from the image that is as a result of the rotating.   The
       extra 1 beause there are FSpray_width+1 lines in the matrix
      FLine1=[FLine1 FLine(:,j)];
    end;
  end;
  FLine=FLine1;
  New_Image=FLine;
endfunction;
```

A.2.2 Rotated

```
//Made By Thomas Sprich 2nd JUNE
//Uses the image Processing toolbox

function rotated=Rotated(Mat,angle)
  temp=string(angle);
   rotated = mogrify(Mat,['-rotate',temp]);
endfunction;
```

A.2.3 GetLine

```
//Made By Thomas Sprich 2nd JUNE
//  Gets the line that I will need for comparison where the spray is
    located.
//Also Flips the Row

function FLine=GetLine(FImage,FRow,FCol0,FCol)  //F suffix is for a
    function.
    FLine=FImage(FRow,FCol:-1:FCol0);  //this is the row and columns
       that are of interest.
                //The line flipping is just a personal preference.
endfunction;
```

A.2.4 Cut

```
function New_Image=Cut(FImage_Next);
```

```
    [x y]=size(FImage_Next);
    FTemp=[];
    for i=1:1:x,
     if sum(FImage_Next(i,:)) < y then
       FTemp = [FTemp ; FImage_Next(i,:)];
     end;
    end;
    New_Image=FTemp;
endfunction;
```

A.2.5 Image_FixA

```
//this function subtracts the new image from the old and fixes
   negative values of the that may occur.

function New_Image=Image_FixA(FImage_Next,FImage0),
      [x y]=size(FImage_Next);
      for i=1:1:x,
        for j=1:1:y,
          FImage_Next(i,j)=((FImage_Next(i,j))/(FImage0(i,j)))^3;
          if ((FImage_Next(i,j)<0)|(FImage_Next(i,j)>1)) then
            FImage_Next(i,j)=1;
          end;
        end;
      end;
  New_Image=FImage_Next;
endfunction;
```

A.2.6 Rem_Noise

```
//funtion that will remove some of the noise
function New_Image=Rem_Noise(FImage_Next,Noise_perc)
  [x y] = size(FImage_Next);
  for i=1:1:x,
    for j=1:1:y,
          if ((FImage_Next(i,j)<(1+Noise_perc)) & (FImage_Next(i,j)
             >1+Noise_perc)) then
             FImage_Next(i,j)=1;
          end;
    end;
```

```
  end;
        New_Image=FImage_Next;
endfunction;
```

A.2.7 Find_Breakup

```
//Made By Thomas Sprich 2nd June
//Decides if jet breakup occurs by stepping through the lines and
    deciding the lines are close enough that nothing happens.  Jet
    Break up point is found.

function [Point]=Find_Breakup(FLine0,FLine_Next,FThreshold)  //
    returns a -1 if there is no spray
     Line_length=length(FLine0);
     counter=2;
     temp=abs(FLine0(counter)-FLine_Next(counter));
     Threshold_Value=FThreshold*FLine0(counter);
     while  ((temp<Threshold_Value) & (counter < Line_length-1)) | ((
         Line_Next(counter) > Line_Next(counter+1))&(Line_Next(counter
         -1) > Line_Next(counter))),
       counter=counter+1;
       temp=abs(FLine0(counter)-FLine_Next(counter));
       Threshold_Value=FThreshold*FLine0(counter);
     end;
     if counter == (Line_length-1) then
       Point=-1;
     else
       Point=counter;
     end;
endfunction;
```

Appendix B

Area change derivation

The area through which the fuel flows caused by the needle lift is assumed to be the shape of a cone from the corner of the seat at an angle perpendicular to the seat towards the needle surface. If this area is larger than the area created by the shortest distance from the seat corner to the centre axis than that area is used.

In figure B.1, the axis is on the central axis, in line with the seat corner. Line y_1 and y_2 are drawn, so as to find the intersection point of the two lines which will define one of the bounds of the cone.

The surface of revolution for any shape can be found from equation (B.1):

$$A_s = 2\pi \int_b^a x(t) \sqrt{\left(\frac{dx}{dt}\right)^2 + \left(\frac{dy}{dt}\right)^2} dt \tag{B.1}$$

For a surface rotated about the y-axis:

$$A_s = 2\pi \int_b^a x \sqrt{1 + \left(\frac{dx}{dy}\right)^2} dy \tag{B.2}$$

The equations for line y_1 and y_2 are:

$$\begin{aligned} y_1 &= -x - r_0 + |h| \\ y_2 &= x + r_0 \end{aligned} \tag{B.3}$$

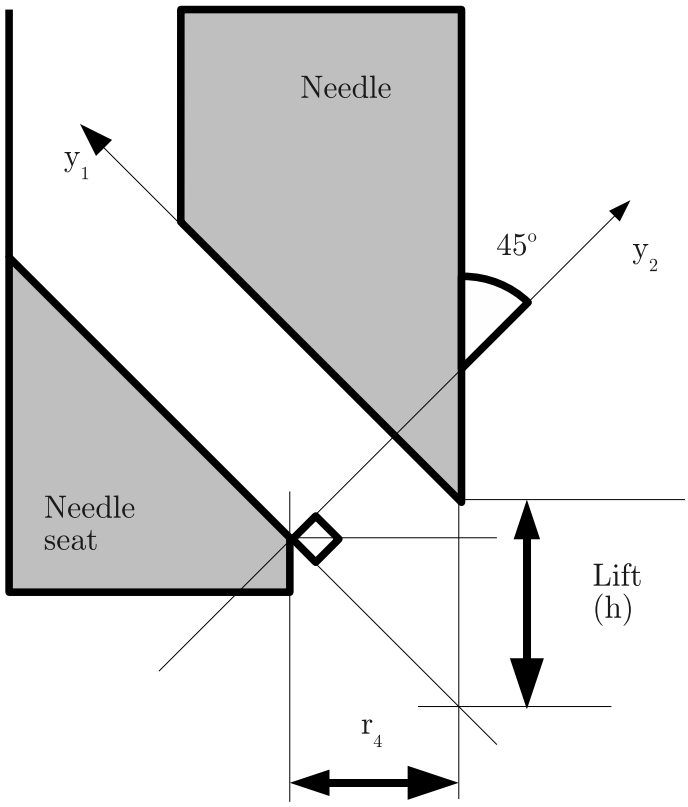


Figure B.1: Schematic used for calculating the change of area caused by the needle lifting of the injector seat

The x intercept and y interxept are:

$$\begin{aligned} x_i &= \frac{-2r_0 + |h|}{2} \\ y_i &= \frac{4r_0 + |h|}{2} \end{aligned} \tag{B.4}$$

The y value becomes the upper bound of the integral of the integral in equation (B.2). The lower bound is zero as it is in line with the origin about which the values are calculated. The x term comes from equation y_1 written in terms of x and solving equation (B.2) in terms of y_1. Thus equation (B.2) becomes:

$$
\begin{aligned}
A_s &= 2\pi \int_b^a (y_1 - r_0)\sqrt{1 + \left(\frac{dy1}{dx}\right)^2}\, dy_1 \\
&= 2\pi \int_0^{y_i} (y_1 - r_0)\sqrt{1 + \left(\frac{d(y_1 - r_0)}{dy_1}\right)^2}\, dy_1 \\
&= 2\sqrt{2}\pi \left[\frac{y_1^2}{2} - r_0 y_1\right]_0^{\frac{4r_0 + |h|}{2}} \\
&= 2\sqrt{2}\pi \left[\frac{\left(\frac{4r_0 + |h|}{2}\right)^2}{2} - r_0 \frac{4r_0 + |h|}{2}\right]
\end{aligned}
\tag{B.5}
$$

Appendix C

Injector models

C.1 Mechanical model

Figure C.1 shows an example of the Scilab program used for solving the mechanical injector model.

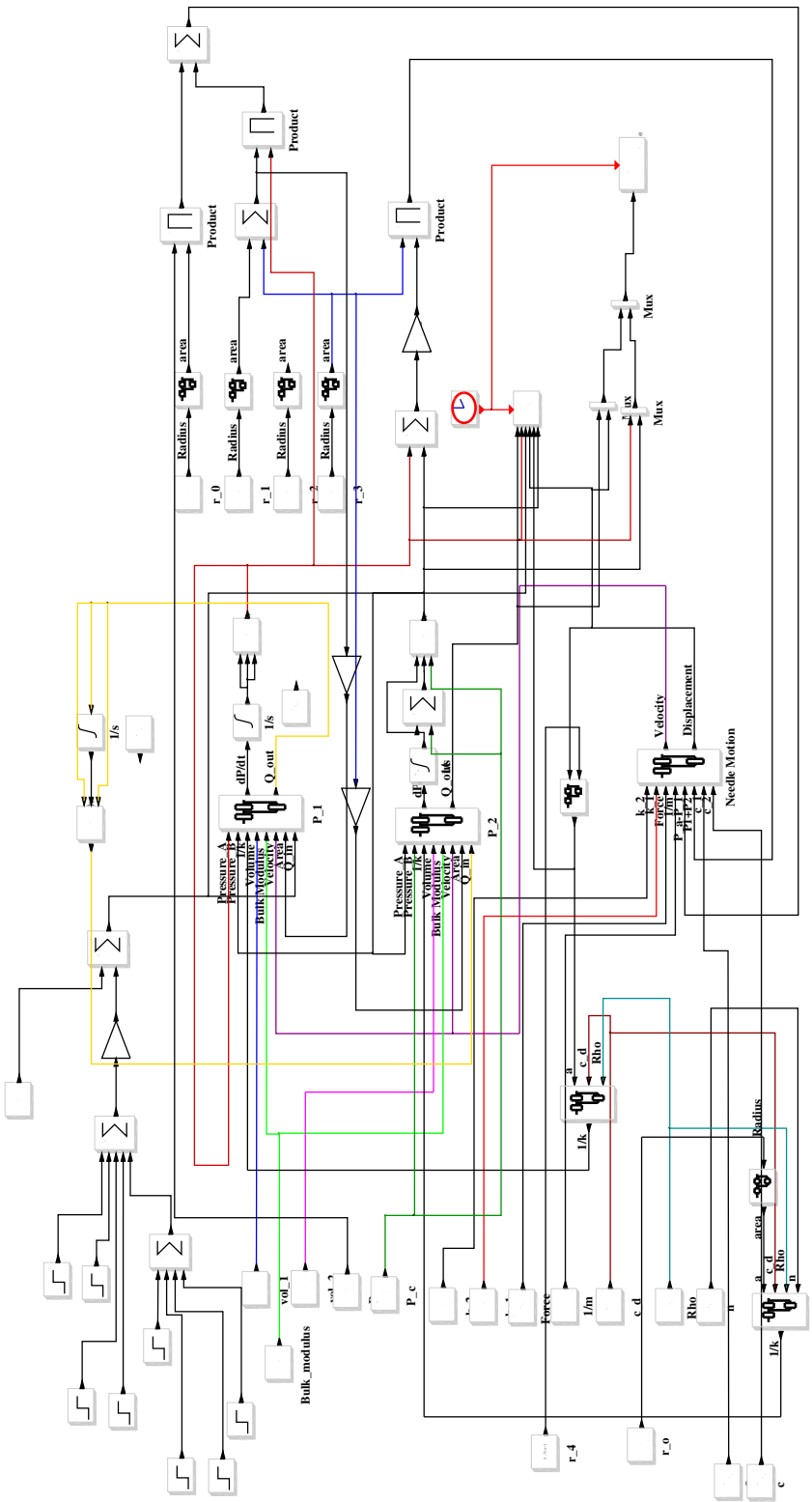


Figure C.1: The Scilab model

C.2 Common rail model

The geometric inputs for the common rail model are shown in Table C.1. Additional inputs that were used in both the Scilab and C++ model are shown in Table C.2. The Akribis geometric information and Nitrogen pressure inputs are shown in Table C.3.

Table C.1: Common rail injector model geometric inputs.

Parameter	Value	Units
r_{r1}	1e-3	m
Line length	0.15	m
r_{cv}	2.13e-3	m
r_{il}	1e-3	m
r_1	2e-3	m
r_s	0.6e-3	m
r_3	1.07e-3	m
r_f	0.15e-3	m
r_b	0.275e-3	m
r_o	0.0850e-3	m
Volume 1	4.4e-7	m^3
Volume 2	4.5e-7	m^3
Volume sac	1.8e-8	m^3
Volume above bleed orifice	3.2e-8	m^3
Volume control	0.7e-8	m^3

Table C.2: Additional common rail injector model inputs for the Scilab model and the C++ program.

Parameter	Value	Units
c_d	0.6	-
k (spring in the needle plunger assembly)	30e3	N/m
k (interaction)	1e9	N/m
Rail pressure	140e6	Pa
Atmospheric pressure	2.85e6	Pa
Plunger assembly mass	0.015	kg
Number of holes	6.0	-
Needle lift limit	0.24e-3	m
Chamber pressure	28e5	Pa

Table C.3: Akribis related inputs used only in the C++ program.

Parameter	Value	Units
Akribis fuel volume	0.208e-7	m^3
Nitrogen volume	.50	m^3
Piston radius	5.5e-3	m
Akribis piston mass	0.01	kg

C.3 Common rail model program source code

The C++ program presented below has been written to work on a Linux operating system, and has not been verified to work on any other operating system.

```
/*
 * Thomas Sprich
 * version History
 *
 * To Follow was completed on the 01/07/09
 *
 * The Graph plotting part was removed and now is handled by
 * "plot find coefficients.cpp"
 *
 * Program can now be varied to do finding coefficients or
    sensitivity
 * by changing the file path that the program outputs to and
    adjusting
 * the control variable of the program.
 *
 * To follow was completed on the 25/06/09
 *
 * The Runge Kutta was not quite right and required some fixing.
    This
 * involved moving the time_step_size or h into the f(x) instead of
 * hf(x)  Showed no difference to the results though.
 *
 * To follow was completed on the 06/06/09
 *
 * The program was changed so that it was broken down into smaller
    parts.
 * It should now be easier to make it more efficient (at least partly
    )
 * if required.  The move was made so that the mass rate out could be
 * extracted easily.
 *
 * The mass rate is now extractable
 *
 * To follow was completed on the 02/06/09
 *
```

```
* The sensitivity analysis has the volume of fuel delivered exported
* to a file
*
* To follow was completed on the 29/05/09
*
* The density variation was fixed so that it is actually taken into
* account.  To do this a new variable was created that had to be
    passed
* to the dp_dt function and from there to the den vs press function.
* This den_fact var is a variable that is multiplied to the output
    var
* from the den function.
*
* Same thing for the bulk modulus as for density
*
* To follow was completed on the 21/05/09
*
* The sensitivity now outputs to its own unique folder called 'error
    '
*
* The program now does 5 different changes to the variables. 20%
    above,
* 10% above, normal, 10% below, 20% below.
*
* The program runs in a loop that reruns changes for specified
* variables.
*
* The generation of graphs is no longer handled within this program.
* It is now done by 'plot error results.cpp'.
*
* changes that need to be made to make it a sensitivity program
* need to rerun the model three times with the variable that needs
    to
* be changed each time.  The changes mainly have to do with output
    file
* handling and graph file handling
*
* To follow was completed on 11/05/09
* The program was split from the 'Common-Rail model-Find
    coefficients
```

```
* .cpp" program so that error analysis can be done on variables.
*
* Fixed the location of the legends on the plots
*
* To follow was completed on 07/05/09
*
* Fixed the labels on the x and y axis, corrected plot labels to
    read
* simulation or experiment, changed the values of the axis to be in
* ms, MPa, mm^3 and mm^3/ms
*
* made it possible to output png files and eps files by changing a
* single command.
*
* To follow was completed on 06/05/09
*
* Included functions that calculate the discharge coefficients using
* best curve fits from empirical comparison.
*
* Changed the way the discharge coefficient was handled, each flow
    area
* now has a unique discharge coefficient that if required can be
    varied
*
* To follow was completed on 05/05/09
*
* made it possible to output the files to eps format in a results
* folder
*
* To follow was completed on 02/05/09
*
* made it possible to print only one experimental plot at a time
    based
* on a desired duration that needs to be tested.  the duration only
* needs to be set once to set it everywhere in the program
*
* To follow was completed on 26/03/09
*
* The Akribis works, a constant with a velocity_chamber term was
    wrong
```

```
* It requires a big damping constant however, but because the fuel
    and
* nitrogen act as springs in compression and therefore would
    oscillate
* forever.Thus a damping constant is required
*
* The correct Akribis dimensions are included into the model.  These
* were taken from the Akribis help file.
*
* The varying volume in the pressure equation was included
* See "Modelling and injection rate estimation of common-rail
    injectors
*  for direct-injection diesel engines" paper
*
* To follow was completed on 09/03/09
*
* Found two errors, 1) in the flow rate transfer out of the injector
* the wrong flow area was used. 2) the wrong constants used in the
* chamber velocity and displacement.
*
* To follow was completed on 27/02/09
*
* Runge kutta now works, works in an inefficient way because it
* calculates flow rates in and out twice.
*
* The motion of the needle is constrained now by a spring damper
    system
* unlike earlier versions that use the resetting of the velocity,
    lift
* and acceleration via differentiating functions.  This is because
    the
* RK4 method would require these constrains on the calculation of
    the
* constants in addition to the check at the end of the calculation.
*
* To Follow was completed on 23/02/09
*
* fixed flow rate function so division of doubles by double (2.00)
    and
* not int (2).
```

```
*
* To follow was completed on 21/02/09
*
* The acceleration function was broken down so that the pressure
    force
* is calculated by another function called P_force.  This was done
    as
* part of breaking the acceleration equation down into core
    components
* so that Runge-Kutta integration can be used included later
*
* A bool control variable has been included so that the program can
* be run with a constant Prail pressure or with and input pressure
* trace with full interpolation.  This has been done so that one
* program can run both conditions so that updates do not need to be
* included in two programs that are essentially the same
*
* The main control "for" loop was fixed so that it terminated at the
* final specified time.  Previously the loop would continue and if
    and
* nan errors would occur.
*
* To follow was completed on 19/02/09
*
* Program works with file input.
*
* The interpolation function was included
*
* The program can read from a source pressure file and use that as
* the rail pressure.  The interpolation function means that
    intermediate
* points can be calculated
*
* included the #include <iomanip> library so that the precision of
    the
* input and output files could be set
*
* To follow was completed on 18/02/09
*
* Some minor errors were corrected with the calculation of dP_1/dt
```

```
* the area term was set to zero as the velocity components was
    removed
* Q_12 was used as a second input instead of Q_1control
*
* add the close(file) at the end of the program
*
* To follow was completed on 17/02/09
*
* Variation in density has been included.  This has an effect on
    k_l1
* and k_rl which are no longer the same
* because of any fluctuation in density that may occur.
*
* To follow was completed on 16/02/09
*
* The vol_1 which ran from the rail all the way to vol_2 (see below)
* has been split further into two parts.
* The volume is now split into the line volume and the volume within
* the injector to volume 2.
*
* NOTE: the value k_rl and k_l1 are the same because they both based
* on the line diameter.  * That is why two values are used in both
* the rail-line and line to  * vol_1 calculations.
*
* P2 a second volume with in the injector between the rail and the
* sac has been included.  This means that the old P1
* has been broken into two volumes.
*
* P2 has been changed to PS and all associated calculations included
    .
*  This is supposed to represent the sac volume.
*
* The sac through the orifice flow is Q_o with k_o
*
* P3 is now Pcontrol so that more volumes can be added and  their
* numbers incremented.
*
* The differentiate function is included and can adjust the needle
* heights at limits of motion, * this means that there are no
* artificial spring constants that act
```

```
 * on the model.
 *
 * The model works and predicts the same results as the scilab model.
 * Further change is purely for improvement.
 *
 * There is recommendations to watch out for aliasing and test that
 * the model is independent of it.
 *
 * The bulk modulus is computed for each volume based on the pressure
 * in that volume.
 */

#include <cstdlib>
#include <iostream>
#include <fstream>
#include <sstream>
#include <string>
#include <stdio.h>
#include <string.h>
#include <math.h>
#define PI 3.14159265E0
#include <vector>

//This is required for setting the precision of the output
#include <iomanip>

//F_ means its a variable in a function.  The F_ separates this
//variable from the global variable

double interpolated_point(double next_point,double last_point,
    double next_time, double last_time, double required_time)
{
    return((next_point-last_point)*(required_time-last_time)/(
        next_time-last_time)+last_point);
}

double density_vs_pressure (double F_pressure,double F_den_fact)
{
  double dummy=0;
```

```
  if (F_pressure >0) dummy=1/(7.61905e-19*F_pressure*F_pressure
      -6.78571e-10*F_pressure+1.22167);
  return (dummy*1000*F_den_fact);
//  return (840);
}

double area(double F_radius)
// area calculation from the radius
{
  double var_area=PI*F_radius*F_radius;
  return(var_area);
}

double integrate(double F_val_f,double F_val_i,double t,double
    Initial_val)
/* an integration function that returns the integral of the last two
 * points added to the
 * result of all previous integrations ( provided that the correct
 * parameters are passed
 * This function uses trapezoidal integration as an approximation
 */
{
  return((F_val_f+F_val_i)/2*t+Initial_val);
}

double differentiate (double final,double initial,double F_time)
// calculated the derivative of two points
{
  return ((final-initial)/F_time);
}

double k_inverseDIVrho (double F_area_flow,double F_density,double
    F_dischargeC,double F_num_holes)
/* k_inverse (1/k) calculates the k for the flow rate equation
 * It has been left as 1/k so that if areas are zero, division by
    zero is avoided
 */
{
  double dummy=00.00;
  if (F_area_flow == 0)
```

```
    dummy=0.00;
  else
    dummy=1/(1.0 / 2.00 / F_area_flow / F_area_flow /
      F_dischargeC / F_dischargeC/F_num_holes/F_num_holes);
  return(dummy);
}

double k_inverse (double F_area_flow,double F_density,double
   F_dischargeC,double F_num_holes)
/* k_inverse (1/k) calculates the k for the flow rate equation
 * It has been left as 1/k so that if areas are zero, division by
    zero is avoided
 */
{
  double dummy=00.00;
  if (F_area_flow == 0)
    dummy=0.00;
  else
    dummy=1/(F_density / 2.00 / F_area_flow / F_area_flow /
      F_dischargeC / F_dischargeC/F_num_holes/F_num_holes);
  return(dummy);
}

double bulk_vs_pressure(double pressure,double F_bulk_fact)
/*This function calculates the local bulk modulus according to the
   equation
 */
{
  return(35/3*pressure+1.4e9*F_bulk_fact);
}

double flow_rate_out (double P_here, double P_there,double F_k)
/*This function calculated the flow rate from the current volume into
    the next volume
 * NOTE that this function can handle revere flow despite the
    negetive square root that would occur
 */
//P_here is the pressure in the current volume
//P_there is the pressure in the next volume to which the flow would
   flow
```

```
{
  double F_temp=0.0;
  double multi=0.0;
  double dP=P_here-P_there;
  if (dP>0.0)
    multi=1.0;
  else
   {
     if (dP<0.0)
     {
        dP=P_there-P_here;
        multi=-1.0;
    }
    else
    {
      multi = 0;
      dP=0;
    }
    }
  F_temp=multi*sqrt(dP*F_k);
  return(F_temp);
}

double dp_dt (

    double F_bulk_fact1,
    double F_den_fact1,
    double F_vol,
    double F_Pm,
    double F_Pn,
    double F_Po,
    double F_Pp,
    double Area_in,
    double F_vel,
    double F_n_mn,
    double F_n_no,
    double F_n_np,
    double a_mn,
    double a_no,
    double a_np,
```

```
    double F_dischargeC_mn,
    double F_dischargeC_no,
    double F_dischargeC_np,
    double F_x
    )

/*This function calculated dP/dt
 * This function only uses the flow rates in and out and does not
 * perform these calculation in function
 */
{
  double F_bulk=bulk_vs_pressure(F_Pn,F_bulk_fact1);
  double F_density=density_vs_pressure(F_Pn,F_den_fact1);

  //calculate the flow in or Q_mn
  double k_mn=k_inverse(a_mn,F_density,F_dischargeC_mn,F_n_mn);
  double F_Qmn=flow_rate_out(F_Pm,F_Pn,k_mn);
  //calculate the flow rate out the volume:

  double F_Qno;
  if (a_no==0.0) F_Qno=0.0;
  else
  {
    double k_no=k_inverse(a_no,F_density,F_dischargeC_no,F_n_no);
    F_Qno=flow_rate_out(F_Pn,F_Po,k_no);  //flow rate from line to
        vol1
  }
  double F_Qnp=0.0;

  //Q_np calculation:
  //the second flow rate is only used once with vol1,therefore check
  //it needs to be done:
  if (a_np==0.0) F_Qnp=0.0;
  else
  {
      double k_np=k_inverse(a_np,F_density,F_dischargeC_np,F_n_np);
      F_Qnp=flow_rate_out(F_Pn,F_Pp,k_np);  //flow rate from line to
          vol1
  }
```

```
  //Calculate Q_in times the sqrt of the local density to convert
      from
  //mass flow rate to volumetric flow rate
   double dummy =F_bulk/(F_vol-F_x*Area_in)*(F_Qmn-F_Qno-F_Qnp-
       Area_in*F_vel);
  //remember that the variable passed out of the function have to be
  //in terms of mass rate and not volumetric flow rate.
  return(dummy);
}

double dp_dt_opt (
    double F_bulk,
    double F_vol,
    double Q_in,
    double Q_out1,
    double Q_out2,
    double Area_in,
    double F_vel,
    //double F_dischargeC_mn,
    double F_x
  //  double& F_temp
    )
{
  double dummy =F_bulk/(F_vol-F_x*Area_in)*(Q_in-Q_out1-Q_out2-
      Area_in*F_vel);
  //remember that the variable passed out of the function have to be
  //in terms of mass rate and not volumetric flow rate.
  return(dummy);
}

double dp_dt_TEST (
    double F_bulk_fact1,
    double F_den_fact1,
    double F_vol,
    double F_Pm,
    double F_Pn,
    double F_Po,
    double F_Pp,
    double Area_in,
    double F_vel,
```

```
    double F_n_mn,
    double F_n_no,
    double F_n_np,
    double a_mn,
    double a_no,
    double a_np,
    double F_dischargeC,
    double F_x,
    double& F_temp
    )

/*This function calculated dP/dt
 * This function only uses the flow rates in and out and does not
 * perform these calculation in function
 */
{
  double F_bulk=bulk_vs_pressure(F_Pn,F_bulk_fact1);
  double F_density=density_vs_pressure(F_Pn,F_den_fact1);

  //calculate the flow in or Q_mn
  double k_mn=k_inverse(a_mn,F_density,F_dischargeC,F_n_mn);
  double F_Qmn=flow_rate_out(F_Pm,F_Pn,k_mn);
  //calculate the flow rate out the volume:
  double F_Qno;
  if (a_no==0.0) F_Qno=0.0;
  else
  {
    double k_no=k_inverse(a_no,F_density,F_dischargeC,F_n_no);
    F_Qno=flow_rate_out(F_Pn,F_Po,k_no);  //flow rate from line to
        vol1
  }
  double F_Qnp=0.0;

  //Q_np calculation:
  //the second flow rate is only used once with vol1,therefore check
  //it needs to be done:
  if (a_np==0.0) F_Qnp=0.0;
  else
  {
      double k_np=k_inverse(a_np,F_density,F_dischargeC,F_n_np);
```

```
    F_Qnp=flow_rate_out(F_Pn,F_Pp,k_np);  //flow rate from line to
        vol1
  }
  //Calculate Q_in times the sqrt of the local density to convert
     from
  //mass flow rate to volumetric flow rate
  double dummy =F_bulk/(F_vol-F_x*Area_in)*(F_Qmn-F_Qno-F_Qnp-Area_in
     *F_vel);
  //remember that the variable passed out of the function have to be
  //in terms of mass rate and not volumetric flow rate.
  F_temp = F_Qmn;
  return(dummy);
}
double dp_dt_n2 (double F_vol,double Area_in,double F_vel)

/*This function calculated dP/dt
 * This function only uses the flow rates in and out and does not
 * perform these calculation in function
 */
{
  double F_bulk=7.85e6; //constant BM
  double dummy =F_bulk/F_vol*(0.0-Area_in*F_vel);
  //remember that the variable passed out of the function have to be
  //in terms of mass rate and not volumetric flow rate.
  return(dummy);
}

double P_force (double F_p1,double F_p2,double F_p3,double F_a_1,
    double F_a_2,double F_a_3,double F_a_cv)
//This function calulates the pressure force
{
  return (F_p1*(F_a_1-F_a_3)  +  F_p2*F_a_3  -  F_p3*F_a_cv);
}

double acceleration (double F_force,double F_mass,double F_k_spring,
    double F_x,double F_k_sac,double F_v,double f_x_limit)
/*_cv is the Control Volume area
 * This function calculates the acceleration of the needle.
 * The interaction force has been made obselete by the inclusion of
    the limits on the the needle motion that are take into
```

```
 * account in the main program.
 * The reason that its taken into account there and not here is
    because of the intergrals that are calculated.
 */
{
  double c=0;
  //F_k_sac=0;
  if (F_x<0.0)
  {
    c=5e4;
  }
  else
  if (F_x>f_x_limit)
  {
    c=5e4;
    F_x=F_x-f_x_limit;
  }
  else
  {
    F_k_sac=0.0;
    c=0.0;
  }
  double force_T;  //force Total
  force_T= F_force -  F_x*F_k_spring-c*F_v-F_k_sac*F_x-0.0000000*F_v-
     F_k_spring*0.0000;//-bob*F_x;
  double dummy = 1/F_mass*force_T;
  return(dummy);
}

double area_lift(double lift, double F_r_1)
/* This function calculated the area through which the fuel can flow
    that is created when the needle lifts
 * Thus this area is a function of the needle lift, i.e. a(X).
 * This area is assumed to be for a needle point that is at 45
    degrees.
 */
{
  double F_temp=0;

  if (lift > 0.0)
```

```
  {
     F_temp=(2*sqrt(2)*PI*(((4*F_r_1+lift)/2)*((4*F_r_1+lift)/2)/2-
         F_r_1*((4*F_r_1+lift)/2)));
    }
   else F_temp=0;
     return F_temp;
}

using namespace std;
int main()

  {string path="";
    bool file_place=1;
    if (file_place ==1)
    {//this goes to the find coefficients part
      path = "/home/thomas/Documents/Masters/Real_Testing/Results/
          Find_Coefficients/";
    }
    else
    {//this goes to sensitivity analysis part
      path = "/home/thomas/Documents/Masters/Real_Testing/Results/
          error/";
    }
    string outfile_RK="";
    int cc=1;
  string tempy;
  string test_duration1="";
  for (int var_counter=1; var_counter<=1; var_counter++)
  {
    for (int sen_counter = 2 ; sen_counter<=2;sen_counter++)
      {
      double change_by;
      string change;
      string sen="";
      switch (sen_counter)
          {
              case 0:
               sen = "+20";
               change_by=1.2;
               break;
```

```
        case 1:
         sen = "+10";
         change_by=1.1;
         break;
        case 2:
         sen = "+00";
         change_by=1.0;
         break;
        case 3:
         sen = "-10";
         change_by=0.9;
         break;
        case 4:
         sen = "-20";
         change_by=0.8;
         break;
       default : {};
      }
int test_counter = 1;// this is used to pick which test to
    model out
//of the "list of test" list below
//Declarations
double dischargeC =0.64;  //discharge coefficient
double density = 840;  //kg/m^3   //the density of the fuel
double k_spring = 30e3; //N/m  //the spring in the needle
    plunger assembly
double k_sac_interaction=1e9;  //N/m   //This is the
    interaction spring constant // now obselete
double r_r1=1e-3;  //m  pipe radius to voll from rail
double line_length = 0.15; // m //the line length
double r_cv=2.13e-3;  //m   //the radius of the top of the
    plunger that is inside the control volume
double r_i1=1e-3;  //m // radius if the injector line i.e.
    within the injector
double r_1=2e-3;  //m  //the largest radius of the needle
double r_s=0.6e-3;  //m  //the radius of the needle that is by
    the sac
double r_3=1.07e-3;  //m  //further subdivision of the needle
    //obsolete
```

```
double r_f=0.15e-3;//dischargeC/dischargeC*.4700;  //m feed
    radius
double r_b=0.275e-3;//dischargeC/dischargeC*.2500; //m bleed
    radius
double r_o=0.170e-3/2; //m orifice radius
int list_of_tests[20];
list_of_tests[0]=400;
list_of_tests[1]=500;
list_of_tests[2]=600;
list_of_tests[3]=700;
list_of_tests[4]=800;
list_of_tests[5]=900;
list_of_tests[6]=1000;
list_of_tests[7]=425;
list_of_tests[8]=450;
list_of_tests[9]=475;
list_of_tests[10]=525;
list_of_tests[11]=550;
list_of_tests[12]=575;
list_of_tests[13]=1500;
list_of_tests[14]=2000;
list_of_tests[15]=625;
list_of_tests[16]=650;
list_of_tests[17]=675;
list_of_tests[18]=725;
list_of_tests[19]=750;
list_of_tests[20]=775;
//string test_duration = itos"1000";
double Sinj(1.0e-3);double Einj;
const char *test_time;// creating the string that will be
    passed to the pipe
double P_rail=140e6; //Pa rail pressure
double P_c=2.85e6; // Pa atmospheric pressure
double vol_1=4.398229716e-7; //m^3
double vol_2=4.523893422e-7; //m^3
double vol_s=1.767e-8; //m^3
double vol_out=3.168610351e-8;
double vol_control=1.382e-8/2; //m^3
double mass=0.015; //kg  //this is the mass of the needle,
    plunger and spacer.  Essentially the part of the injector
```

```
    that moves
double n_holes=6.0;  //  This is the number of holes that the
    injector has
double x_limit=0.24e-3; //m  //this is the maximum travel that
    the needle and plunger may lift
double P_chamber=28e5;//the pressure of the chamber being
    injected
double mass_chamber=0.01;//kg mass of the akribis piston
double vol_chamber=0.208e-7;//m^3 //
double vol_n2=.50;//m^3 //guesed
double r_Ak=5.5e-3;//m radius of the Akribis piston
double cd_b=0.24;
double cd_f=0.78;
cd_f=feed_coefficient(list_of_tests[test_counter]);
cd_b=bleed_coefficient(list_of_tests[test_counter]);
//Preliminary Calculations for area for the above radii
double a_r1=area(r_r1);  //m2  pipe area to vol1 from rail
double a_cv=area(r_cv);  //m2
double a_il=area(r_il);//m2
double a_1=area(r_1);  //m2  //this is a "one" as in area_one (
    not L(l))
double a_s=area(r_s);  //m2
double a_3=area(r_3);  //m2
double a_f=area(r_f);  //m2  feed area
double a_b=area(r_b); //m2 bleed area
double a_o=area(r_o); //discharfe orifice
double a_12=a_1-a_s;
double a_Ak=area(r_Ak);
double den_fact = 1.0;
double bulk_fact = 1.0;
double vol_l = a_r1*line_length;
switch (var_counter)
    {
        case 0: //limit
         x_limit=x_limit*change_by;
         change = "lift-limit_";
         break;
        case 1: //bleed orifice
         cd_b=cd_b*change_by;
         change = "cd-b_";
```

```
        break;
      case 2: //feed orifice
        cd_f=cd_f*change_by;
        change = "cd-f_";
        break;
      case 3://dischargeC
        dischargeC=dischargeC*change_by;
        change="dischargeC_";
        break;
      case 4:  //line length
        line_length =line_length*change_by;
        change="line_length_";
        break;
      case 5:  //mass
        mass =mass*change_by;
        change="mass_";
        break;
      case 6:  //P_rail
        P_rail =P_rail*change_by;
        change="P_rail_";
        break;
      case 7:  //density
        den_fact =den_fact*change_by;
        change="density_";
        break;
      case 8:  //vol_1
        vol_1 =vol_1*change_by;
        change="vol_1_";
        break;
      case 9:  //vol_2
        vol_2 =vol_2*change_by;
        change="vol_2_";
        break;
     case 10:  //r_o
       r_o =r_o*change_by;
       change="r_o_";
       break;
     case 11:  //bulk modulus
       bulk_fact =bulk_fact*change_by;
       change="bulk_";
```

```
            break;
          default : {};
        }
    cout<<bulk_fact<<"    "<<den_fact<<endl;
    double t_f=0.005;  //final time for the simulation
    double time_step_size = 10e-8;  //amount to increment the time
       for the simulation;
    //Array definitions
    vector <double> time_T;
    vector <double> Q_12;
    vector <double> Q_2s;
    vector <double> Q_1control;
    vector <double> Q_o;
    vector <double> Q_controlb;
    vector <double> Pl; //the line pressure
    vector <double> P1;
    vector <double> P2;
    vector <double> Ps;
    vector <double> Pcontrol;
    vector <double> X; //displacement
    vector <double> V; //velocity
    vector <double> A; //acceleration
    vector <double> Prail;
    vector <double> Pchamber;
    vector <double> Pn2;
    vector <double> X_chamber; //displacement
    vector <double> V_chamber; //velocity
    vector <double> A_chamber; //acceleration
    vector <double> Pout; //pressure above the control volume
    vector <double> Mass;//mass delivered
    //Array initialisations zero time definitions
    Q_12.push_back(0);
    Q_2s.push_back(0);
    Q_1control.push_back(0);
    Q_o.push_back(0);
    Q_controlb.push_back(0);
    Mass.push_back(0);
    V.push_back(0); //velocity
    A.push_back(0);
    X_chamber.push_back(0); //displacement
```

```
V_chamber.push_back(0); //velocity
A_chamber.push_back(0); //acceleration
time_T.push_back(0);
double a_2s=0.0;
//one time calculations
std::string test_duration;
std::stringstream out;
out << list_of_tests[test_counter];
test_duration = out.str();
test_duration1=test_duration;
Einj=Sinj+list_of_tests[test_counter]/1e6;    //this adds the
    converted integer to the start time
bool var_input_P=1; //if var_input ==0 then use the variable
    input
if (var_input_P==0)
{
ifstream Input_pressure ("/home/thomas/Desktop/CompletePress_(
    bar).txt");
vector <double> File_time;
vector <double> File_pressure;
double x;

/*this part of the program reads in the input from the source
    file
* The multiplication values are because the file used is from
    the
* Akribus which outputs time in ms and pressure in bars.
*/
while (!Input_pressure.eof())
{
     Input_pressure>>setprecision(10)>>x;
     File_time.push_back(x*1e-3);
     Input_pressure>>setprecision(10)>>x;
     File_pressure.push_back(x*1e5);
}
Input_pressure.close();
/* The next part of the program interpolates to get the
    required
 * resolution file that the model is solved for.  It is done
 * prior to actually solving the problem so that interpolation
```

```
 * is not done during the main part of the program
 */
int count1=0;
for (double i =0.0;i<=t_f; i=i+time_step_size)
{
  if ( i==File_time[count1])
  {
    Prail.push_back(File_pressure[count1]);
  }
  else
  {
    while (File_time[count1] <i)
    {
      count1++;
    }
    Prail.push_back(interpolated_point(File_pressure[count1],
        File_pressure[count1-1],File_time[count1],File_time[
        count1-1],i));
  }
}
//     cout << Prail[1]<<endl;
P_rail=Prail[0];
}
else
{
Prail.push_back(P_rail);
for (double t=time_step_size;t<=t_f;t=t+time_step_size)
  Prail.push_back(P_rail);
}
//initialisations
double P_1=P_rail; //Pa
double P_1=P_1; //Pa
double P_2=P_1; //Pa
double P_s=4e6;  //Pa
double P_control=P_1; //Pa
double P_n2=P_chamber;
double P_out = P_c;
X.push_back(P_force(P_2,P_s,P_control,a_1,a_s,a_3,a_cv)/
    k_sac_interaction); //displacement;
```

```
double i[5],j[5],k[5],l[5],m[5],n[5],o[5],p[5],q[5],r[5],s[5],u
    [5],z[5];
for (int bob=0;bob<6;bob++)
{
i[bob]=0.0;   //pl
j[bob]=0.0; //p1
k[bob]=0.0; //p2
l[bob]=0.0; //ps
m[bob]=0.0; //pcontrol
n[bob]=0.0; //acc
o[bob]=0.0; //vel
p[bob]=0.0;   //chamber
q[bob]=0.0;   //nitrogen
r[bob]=0.0; //akribis piston acc
s[bob]=0.0; //akribis piston vel
u[bob]=0.0; //vol above control
z[bob]=0.0; //mass delivered
}
double PF=0;
P1.push_back(P_1);
P1.push_back(P_1);
P2.push_back(P_2);
Ps.push_back(P_s);
Pcontrol.push_back(P_control);
Pchamber.push_back(P_chamber);
Pn2.push_back(P_n2);
Pout.push_back(P_out);
int location =P1.size();
double Q1,Q2,Q3,k1,k2,k3;
double Qin,Qout1,Qout2,Qtemp;
for (double t=time_step_size;t<=t_f;t=t+time_step_size)
{
location =P1.size()-1;
P_rail=Prail[location];
P_1=P1[location];
P_1=P1[location];
P_2=P2[location];
P_s=Ps[location];
P_control=Pcontrol[location];
P_n2=Pn2[location];
```

```
P_chamber=Pchamber[location];
P_out=Pout[location];
for (int bob=0;bob<5;bob++)
{
  i[bob]=0.0;   //pl
  j[bob]=0.0; //p1
  k[bob]=0.0; //p2
  l[bob]=0.0; //ps
  m[bob]=0.0; //pcontrol
  n[bob]=0.0; //acc
  o[bob]=0.0; //vel
  p[bob]=0.0;   //chamber
  q[bob]=0.0;   //nitrogen
  r[bob]=0.0; //akribis piston acc
  s[bob]=0.0; //akribis piston vel
  u[bob]=0.0; //vol above control
  z[bob]=0.0; //mass delivered
}
for (int constant_count=1;constant_count<=4;constant_count++)
{
  double h=0.0;
  switch ( constant_count )
  {
    case 1:
      h=0.0;
      break;
    case 2:
      h=1.0/2.00*time_step_size;
      break;
    case 3:
      h=1.0/2.00*time_step_size;
      break;
    case 4:
      h=1.0*time_step_size;
      break;
    default:{};
  }
//Line
double bulk, density;
bulk=bulk_vs_pressure(P_l+i[constant_count-1]*h,bulk_fact);
```

```
density=density_vs_pressure(P_1+i[constant_count-1]*h,den_fact)
    ;
k1=k_inverse(a_r1,density,dischargeC,1);
Q1=flow_rate_out(P_rail,P_1+i[constant_count-1]*h,k1);
k2=k_inverse(a_r1,density,dischargeC,1);
Q2=flow_rate_out(P_1+i[constant_count-1]*h,P_1+j[constant_count
    -1]*h,k2);
k3=k_inverse(0,density,dischargeC,1);
Q3=flow_rate_out(P_1+i[constant_count-1]*h,0,k3);
Qin=Q1;
Qout1=Q2;
Qout2=Q3;
i[constant_count]=dp_dt_opt ( bulk, vol_1,Qin,Qout1,Qout2
    ,0.0,0.0,0);
bulk=bulk_vs_pressure(P_1+j[constant_count-1]*h,bulk_fact);
density=density_vs_pressure(P_1+j[constant_count-1]*h,den_fact)
    ;
k1=k_inverse(a_r1,density,dischargeC,1);
Q1=flow_rate_out(P_1+i[constant_count-1]*h,P_1+j[constant_count
    -1]*h,k1);
k2=k_inverse(a_f,density,cd_f,1);
Q2=flow_rate_out(P_1+j[constant_count-1]*h,P_control+1[
    constant_count-1]*h,k2);
k3=k_inverse(a_il,density,dischargeC,1);
Q3=flow_rate_out(P_1+j[constant_count-1]*h,P_2+k[constant_count
    -1]*h,k3);
Qin=Q1;
Qout1=Q2;
Qout2=Q3;
j[constant_count]=dp_dt_opt ( bulk, vol_1,Qin,Qout1,Qout2
    ,0.0,0.0,0); vol_1,P_1+i[constant_count-1]*h,P_1+j[
    constant_count-1]*h,P_control+1[constant_count-1]*h,P_2+k[
    constant_count-1]*h,0.0,0.0,1.0,1.0,1.0,,dischargeC,cd_f,
    dischargeC,0);
//vol_2
if ((X[location]+o[constant_count-1]*h)>0.0) a_2s=area_lift((X[
    location]+o[constant_count-1]*h),r_s);
else a_2s=0.0;
bulk=bulk_vs_pressure(P_2+k[constant_count-1]*h,bulk_fact);
```

```
density=density_vs_pressure(P_2+k[constant_count-1]*h,den_fact)
    ;
k1=k_inverse(a_il,density,dischargeC,1);
Q1=flow_rate_out(P_1+j[constant_count-1]*h,P_2+k[constant_count
    -1]*h,k1);
k2=k_inverse(a_2s,density,dischargeC,1);
Q2=flow_rate_out(P_2+k[constant_count-1]*h,P_s+m[constant_count
    -1]*h,k2);
k3=k_inverse(0,density,dischargeC,1);
Q3=flow_rate_out(P_2+k[constant_count-1]*h,0,k3);
Qin=Q1;
Qout1=Q2;
Qout2=Q3;
k[constant_count]=dp_dt_opt (bulk, vol_2,Qin,Qout1,Qout2,a_12,
    V[location]+n[constant_count-1]*h,1.0*(X[location]+o[
    constant_count-1]*h));
//vol_control
if ((time_T[location]>Sinj) & (time_T[location] < Einj)) //
    Sinj(1.0e-3),Einj(1.8e-3);
{
  a_b=area(r_b);
}
else
  {a_b=0;}
 if ((X[location]+o[constant_count-1]*h)>=x_limit) a_b=0.0;
//   a_b=0;
bulk=bulk_vs_pressure(P_control+l[constant_count-1]*h,bulk_fact
    );
density=density_vs_pressure(P_control+l[constant_count-1]*h,
    den_fact);
k1=k_inverse(a_f,density,cd_f,1);
Q1=flow_rate_out(P_1+j[constant_count-1]*h,P_control+l[
    constant_count-1]*h,k1);
k2=k_inverse(a_b,density,cd_b,1);
Q2=flow_rate_out(P_control+l[constant_count-1]*h,P_out+u[
    constant_count-1]*h,k2);
k3=k_inverse(0,density,dischargeC,1);
Q3=flow_rate_out(0,0,k3);
Qin=Q1;
Qout1=Q2;
```

```
Qout2=Q3;
l[constant_count]=dp_dt_opt ( bulk, vol_control,Qin,Qout1,Qout2
    ,a_cv,-1.0*(V[location]+n[constant_count-1]*h),1.0*(X[
    location]+o[constant_count-1]*h));
//vol out
bulk=bulk_vs_pressure(P_out+u[constant_count-1]*h,bulk_fact);
density=density_vs_pressure(P_out+u[constant_count-1]*h,
    den_fact);
k1=k_inverse(a_b,density,cd_b,1);
Q1=flow_rate_out(P_control+l[constant_count-1]*h,P_out+u[
    constant_count-1]*h,k1);
k2=k_inverse(a_il,density,dischargeC,1);
Q2=flow_rate_out(P_out+u[constant_count-1]*h,P_c,k2);
k3=k_inverse(0,density,dischargeC,1);
Q3=flow_rate_out(0,0,k3);
Qin=Q1;
Qout1=Q2;
Qout2=Q3;
u[constant_count]=dp_dt_opt ( bulk, vol_out,Qin,Qout1,Qout2
    ,0,0,0);
//vol_s
if ((X[location]+o[constant_count-1]*h)>0) a_o=area(r_o);
else a_o=0.0;
bulk=bulk_vs_pressure(P_out+u[constant_count-1]*h,bulk_fact);
density=density_vs_pressure(P_out+u[constant_count-1]*h,
    den_fact);
k1=k_inverse(a_2s,density,dischargeC,1);
Q1=flow_rate_out(P_2+k[constant_count-1]*h,P_s+m[constant_count
    -1]*h,k1);
k2=k_inverse(a_o,density,dischargeC,n_holes);
Q2=flow_rate_out(P_s+m[constant_count-1]*h,P_chamber+p[
    constant_count-1]*h,k2);
k3=k_inverse(0,density,dischargeC,1);
Q3=flow_rate_out(0,0,k3);
Qin=Q1;
Qout1=Q2;
Qout2=Q3;
z[constant_count] =(Q2*density+z[constant_count-1]*h);
m[constant_count]=dp_dt_opt ( bulk, vol_s,Qin,Qout1,Qout2,a_s,V
    [location]+n[constant_count-1]*h,-1.0*(X[location]+o[
```

```
    constant_count-1]*h));
//cout<<Q2<<endl;
//Needle Velocity
PF=P_force(P_2+k[constant_count-1]*h,P_s+m[constant_count-1]*h,
    P_control+l[constant_count-1]*h,a_1,a_s,a_3,a_cv);
n[constant_count]=acceleration(PF,mass,k_spring,X[location-1]+o
    [constant_count-1]*h,k_sac_interaction,(V[location]+n[
    constant_count-1]*h),x_limit);
//Displacement
o[constant_count]=(V[location]+n[constant_count-1]*h);
//pchamber
double temp1;
p[constant_count]=dp_dt ( bulk_fact, den_fact, vol_chamber,P_s+
    m[constant_count-1]*h,P_chamber+p[constant_count-1]*h
    ,0.0,0.0,a_Ak,-1.0*(V_chamber[location]+r[constant_count
    -1]*h),n_holes,0.0,0.0,a_o,0.0,0.0,dischargeC,dischargeC,
    dischargeC,1.0*(X_chamber[location]+s[constant_count-1]*h))
    ;
//n2 chamber
q[constant_count]=dp_dt_n2(vol_n2,a_Ak,1.0*(V_chamber[location
    ]+r[constant_count-1]*h));
//chamber Velocity
r[constant_count]=1.0/mass_chamber*(((P_chamber+p[
    constant_count-1]*h)-(P_n2+q[constant_count-1]*h))*(-1.0)*
    a_Ak-(V_chamber[location]+r[constant_count-1]*h)*100);
//the minus one term after the pressure forces is to use the
//correct directions
//chamber Displacement
s[constant_count]=(V_chamber[location]+r[constant_count-1]*h);
}
P1.push_back(P_1+1.0/6.0*time_step_size*(i[1]+2.0*i[2]+2.0*i
    [3]+i[4]));
P1.push_back(P_1+1.0/6.0*time_step_size*(j[1]+2.0*j[2]+2.0*j
    [3]+j[4]));
P2.push_back(P_2+1.0/6.0*time_step_size*(k[1]+2.0*k[2]+2.0*k
    [3]+k[4]));
Pcontrol.push_back(P_control+1.0/6.0*time_step_size*(l[1]+2.0*l
    [2]+2.0*l[3]+l[4]));
Pout.push_back(P_out+1.0/6.0*time_step_size*(u[1]+2.0*u[2]+2.0*
    u[3]+u[4]));
```

```
Ps.push_back(P_s+1.0/6.0*time_step_size*(m[1]+2.0*m[2]+2.0*m
    [3]+m[4]));
V.push_back(V[location]+1.0/6.0*time_step_size*(n[1]+2.0*n
    [2]+2.0*n[3]+n[4]));
X.push_back  (X[location]+1.0/6.0*time_step_size*(o[1]+2.0*o
    [2]+2.0*o[3]+o[4]));
density=density_vs_pressure(P_chamber,den_fact);
double k_so=k_inverse(a_o,density,dischargeC,n_holes);
Q_o.push_back(flow_rate_out(Ps[location],Pchamber[location],
    k_so));
Pchamber.push_back(P_chamber+1.0/6.0*time_step_size*(p[1]+2.0*p
    [2]+2.0*p[3]+p[4]));
Pn2.push_back(P_n2+1.0/6.0*time_step_size*(q[1]+2.0*q[2]+2.0*q
    [3]+q[4]));
V_chamber.push_back(V_chamber[location]+1.0/6.0*time_step_size
    *(r[1]+2.0*r[2]+2.0*r[3]+r[4]));
X_chamber.push_back(X_chamber[location]+1.0/6.0*time_step_size
    *(s[1]+2.0*s[2]+2.0*s[3]+s[4]));
Mass.push_back(Mass[location]+1.0/6.0*time_step_size*(z[1]+2.0*
    z[2]+2.0*z[3]+z[4]));
time_T.push_back(time_T[location]+time_step_size);
}
string path = "/home/thomas/Documents/Masters/Real␣Testing/
    Results/Find␣Coefficients/";
string outfile_cplus=path +"Model-output-ConstntCD-"+
    test_duration+".txt";
outfile_RK=outfile_cplus;
const char *outfile_c;
ofstream outfileA (outfile_cplus.c_str());
for(int temp = 0; (temp != time_T.size()-1); temp++ )
{
outfileA<< setprecision(10) <<time_T[temp] <<"␣"<<Pcontrol[temp
    ]<<
"␣"<<P1[temp]<< "␣" << P2[temp]<<"␣"<< X[temp]<<"␣"<< V[temp]<<
"␣"<<Prail[temp]<< "␣" <<P1[temp]<<"␣"<<Ps[temp]<<"␣"<< Q_o[
    temp]<<
"␣" <<1.0*X_chamber[temp]*a_Ak<<"␣" <<Pn2[temp]<<"␣"<<Pchamber[
    temp]<<
"␣"<< V_chamber[temp]*-1.0*a_Ak<<"␣" << X_chamber[temp]*-1.0*
    a_Ak << "␣" <<Pout[temp] <<"␣"<<Mass[temp]
```

```
        <<endl;
        }
        outfile_cplus = path+"collated-Model-outputconstantcds"+
            test_duration+".txt" ;
        if (sen_counter==0) //creates an empty file
        {
          ofstream outfile(outfile_cplus.c_str());
          outfile.close();
        }
        ofstream outfile;
        outfile.open(outfile_cplus.c_str(),ios::app);
        outfile << setprecision(10) << sen<<" "<<X_chamber[X_chamber.
            size()-1]*-1.0*a_Ak<<" "<< Mass[Mass.size()-1]<< endl;
        outfile.close();
        outfileA.close();
        tempy="plot \"Model-output-ConstntCD-"+test_duration+change+sen
            +".txt\" using 1:17 with lines\n";
        }
    }
    return 0;
}
```

Appendix D

Testscope output file sorting program

```
 #include <cstdlib>
#include <iostream>
#include <fstream>
#include <sstream>
#include <string>
#include <stdio.h>
#include <string.h>

using namespace std;

string CreateFileName (string path, string meas, int inj_num,int
    test_speed,int test_pressure)

//This is the file that is exported from testscope
{
  string temp="";
  std::string fspeed,num,fpressure;
  std::stringstream out;
  std::stringstream out1;
  std::stringstream out2;
  out << inj_num;
  num = out.str();

  out1 << test_speed;
  fspeed =out1.str();

  out2 << test_pressure;
```

```
  fpressure =out2.str();

  temp=path+fpressure+"_bar/"+fspeed+"ms/data "+fpressure+"bar " +
      fspeed+"micros_"+num+"_"+meas+".txt";
//  temp=path+fpressure+" bar\\"+fspeed+" ms\\Data "+fpressure+" bar
    " + fspeed+" micros_"+num+"_"+meas+".txt";
  return (temp);
}
string CreateFileNameOut (string path, string meas, int test_speed,
    int test_pressure)  //this function creates the output file
//This creates the file that you will export data to
{
  string temp="";
  std::string fspeed,num,fpressure;

  std::stringstream out1;
  std::stringstream out2;


  out1 << test_speed;
  fspeed =out1.str();

  out2 << test_pressure;
  fpressure =out2.str();

  temp=path+fpressure+"_bar/"+fspeed+"ms/Complete"+meas+".txt"; //
      Linux
//  temp=path+fpressure+" bar\\"+fspeed+" ms\\Complete"+meas+".txt";
    //Windows

  return (temp);
}

int main()
{
  string meas_property="";
  string temp_file="c:\\";
  for (int pressure = 1400; pressure <=1400; pressure =pressure +200)
  {
```

```
    for (int speed =2000;speed <=2000; speed =speed+250)//here i'm
        using speed as duration
    {

      for (int control = 0; control <5 ;control++)
      {
        switch (control)
        {
           case 0:
            meas_property="Rate";
            break;
           case 1:
            meas_property="Delivery";
            break;
           case 2:
            meas_property="Press (bar)";
            break;
           case 3:
              meas_property="Firing Pulse";
              break;
           case 4:
              meas_property="Windows";
              break;
          default : {};
         }
        string file_path;

        //************************************************
        //ENTER IN THE PATH
        //************************************************

        file_path= "/home/thomas/Documents/Masters/Real_Testing/
            Collated/";//linux
//          file_path= "c:\\My Documents...\\";//windows   // REMEMBER
    double backspace
        string file_name="";
        string temp;
        int num_files=30;  //change this number if its not reading
            all files properly
        float** a = NULL;    // Pointer to int, initialize to nothing.
```

```
float initial,inc_size;
int num_inc;
for (int j = 1; j<=num_files ; j++)
{
  temp=CreateFileName(file_path,meas_property,j,speed,
      pressure);
  ifstream infile ;
  infile.open(temp.c_str());
  while (temp != "ms")
  {
    infile >> temp;
  }
  infile >> initial;
  infile >>inc_size;
  infile >>num_inc;
  if (j == 1)  //this is to check that the array is
      initialised only once
    {
      float** b = new float*[num_inc];  //these lines create
          the 2d array
      for(int i = 0; i < num_inc; i++)
      b[i] = new float[num_files+1];
      for (int i=0; i<num_inc; i++)
        {
          for (int k = 0; k<num_files+1;k++)
            {
              b[i][k] = 0; // Initialize all elements to zero
                  .
            }
        }
        a = b;
    }
for (int i = initial; i< num_inc ;i++)  //this loop reads the
    interesting data from the file
  {
    float temp(0);
  //  cout <<i<<endl;
    infile >> temp;
//    cout <<temp<<endl;
```

```
            a[i][j-1]=a[i][j-1]+temp;  //this stores each of the data
                 in each of the files into the matrix
            a[i][num_files]=a[i][num_files]+temp;  //This stors the
                adds each of the data in the files together and saves
                 it in the last col of the array
          }
        infile.close();
        }
         // When done, free memory pointed to by a.
         // Clear a to prevent using invalid memory reference.
         temp=CreateFileNameOut( file_path, meas_property,speed,
             pressure);
        ofstream outfile(temp.c_str());
        for (int i = 1; i<num_inc;i++)    //this loop steps through
           the array to save the data in the files outfile
        {
          outfile << i*inc_size<<" ";  //this saves the time that the
               data occurs
          for (int j=0;j<num_files-1;j++)  //this is stepping through
               the data
          {
            outfile << a[i][j] << " ";
          }
          float temp_num=num_files-1;
          outfile <<a[i][num_files]/(temp_num+1)<<endl;  //this loop
              adds the final col of the array and averages it here
        }

        for(int i = 0; i < num_files; i++)
          delete[] a[i];
        delete [] a;
        a = NULL;
        outfile.close();
      }
    }
  }

  return 0;
}
```

Appendix E

Sample output files

Table E.1: A sample of the data from the output file from the Scilab program.

Time [s]	Flow rate [m^3/s]	Needle lift [m]	Pressure P_1 [Pa]	Pressure P_2 [Pa]
0.450000000E-05	0.385549536E-08	0.112062695E-07	0.800010562E+07	0.850006510E+05
0.500000000E-05	0.421482834E-08	0.134486843E-07	0.800012675E+07	0.850007780E+05
0.550000000E-05	0.457365120E-08	0.158776423E-07	0.800014964E+07	0.850009162E+05
0.600000000E-05	0.494127708E-08	0.184843258E-07	0.800017421E+07	0.850010694E+05
0.650000000E-05	0.533588356E-08	0.212480551E-07	0.800020026E+07	0.850012470E+05
0.700000000E-05	0.573700360E-08	0.241854631E-07	0.800022794E+07	0.850014415E+05
0.750000000E-05	0.614336147E-08	0.272965499E-07	0.800025726E+07	0.850016529E+05
0.800000000E-05	0.655398297E-08	0.305813153E-07	0.800028822E+07	0.850018813E+05
0.850000000E-05	0.699368279E-08	0.339647190E-07	0.800032011E+07	0.850021422E+05
0.900000000E-05	0.744471377E-08	0.374862478E-07	0.800035330E+07	0.850024274E+05

Table E.2: A sample of the data from the output file from the C++ program for the common rail model. Only the first seven columns have been shown.

Time [s]	P_{cv} [Pa]	P_1 [Pa]	P_2 [Pa]	Needle lift [m]	Needle velocity [m/s]	P_{rail} [Pa]	
5.320E-04	140001590.6	139998319.6	140000758.8	-7.25E-007	7.38E-008	140000000	...
5.321E-04	140001590.6	139998319.6	140000758.8	-7.25E-007	7.38E-008	140000000	...
5.322E-04	140001590.6	139998319.6	140000758.8	-7.25E-007	7.38E-008	140000000	...
5.323E-04	140001590.6	139998319.6	140000758.8	-7.25E-007	7.38E-008	140000000	...
5.324E-04	140001590.6	139998319.6	140000758.8	-7.25E-007	7.38E-008	140000000	...
5.325E-04	140001590.6	139998319.6	140000758.8	-7.25E-007	7.38E-008	140000000	...
5.326E-04	140001590.6	139998319.6	140000758.8	-7.25E-007	7.38E-008	140000000	...
5.327E-04	140001590.6	139998319.6	140000758.8	-7.25E-007	7.38E-008	140000000	...

Table E.3: A sample of the data from the output file from the C++ program for the common rail model. The next seven columns have been shown.

	P_{line} [Pa]	P_3 [Pa]	Q [m^3/s]	Akribis piston displacement [m]	P_{n_2} [Pa]	$P_{chamber}$ [Pa]	Akribis flow rate [mm^3/s]	
...	140001358.2	3999997.76	0	0	2800000	2800000	0	...
...	140001358.2	3999997.76	0	0	2800000	2800000	0	...
...	140001358.2	3999997.76	0	0	2800000	2800000	0	...
...	140001358.2	3999997.76	0	0	2800000	2800000	0	...
...	140001358.2	3999997.76	0	0	2800000	2800000	0	...
...	140001358.2	3999997.76	0	0	2800000	2800000	0	...
...	140001358.2	3999997.76	0	0	2800000	2800000	0	...
...	140001358.2	3999997.76	0	0	2800000	2800000	0	...

Table E.4: A sample of the data from the output file from the C++ program for the common rail model. The last seven columns have been shown.

	-1*Akribis piston displacement [m]	P$_o ut$ [Pa]	$\dot{Mass}$ [kg/s]
...	0	2850000	0
...	0	2850000	0
...	0	2850000	0
...	0	2850000	0
...	0	2850000	0
...	0	2850000	0
...	0	2850000	0
...	0	2850000	0

Appendix F

Discharge coefficient approximation

A method of approximating the discharge coefficient is presented here. The discharge coefficient calculated here can only be used as a guideline as it does not account for transient flow, the different geometry of the injector and the difficulty in accurately measuring the geometry of the injector.

F.1 Analysis

Figure F.1 shows the discharge coefficient versus the Reynolds number for the flow through an orifice with diameter. The discharge coefficient is given for different ratios of the orifice diameter d_o and the pipe diameter D_p. The Reynolds number is given as

$$Re = \frac{VD_p}{\upsilon}.$$

by Munson et al. [23], where V is the velocity of the fuel and υ is the dynamic viscosity.

Letting V = 300 m/s, D_n = 1 mm which is an approximate of what may actually occur since the geometry is varying in time, and υ = 2.0×10^{-6} ms^2/s, then the Reynolds number, Re = 17×10^3. This means the flow definitely turbulent.

Figure F.1 requires that the d_o/D_p ratio is known. In the injector, due to the difficulty in measuring the internal injector geometry and its variation with time, this value D_p is difficult to ascertain. However, since d_o is very small (= 0.173 mm), it is likely that the d_o/D_p value will tend to zero. Thus, for a Reynolds number of Re = 17×10^3,

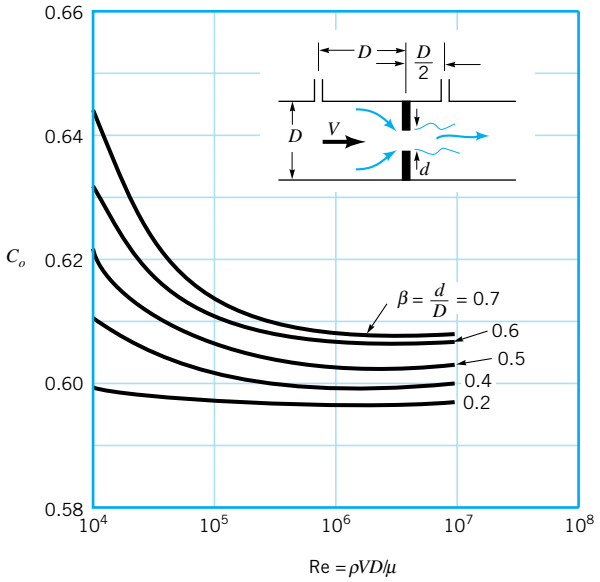


Figure F.1: Discharge coefficient versus Reynolds number greater than 10^4 for flow through an orifice in a pipe with different ratios of the orifice and pipe diameter [23].

it is reasonable to assume, based on this figure, that a value of 0.6 for the discharge coefficient is reasonable.